博　士　論　文

The structural changes and water behaviors in hydrous amorphous silica materials under high pressure and temperature

(和題：高圧力および高温下での含水非晶質珪酸塩物質の構造変化と水の挙動)

金沢大学大学院自然科学研究科
環境科学専攻
自然計測講座

学　籍　番　号　1123142402
氏　　名　荒砂　茜
主任指導教員名　奥野　正幸

The structural changes and water behaviors in hydrous amorphous silica materials under high pressure and temperature

(和題：高圧力および高温下での含水非晶質珪酸塩物質の構造変化と水の挙動)

荒砂　　茜

平成 26 年　1 月

Contents

Chapter 1
Background and the purpose of this study

1.1 Background

Hydrous amorphous silica materials including water molecules and silanols (Si-OH) in the structure are easily found on the earth surface and the sea floor. Until now, many hydrous minerals have been found and their structures and physical properties also investigated. For example, chalcedony, agate and opal are famous hydrous silica minerals. In these minerals, the water contents generally increases with decreasing their crystallinities (Graetsch, 1994). Opals are classified based on their structure into opal-C, opal-CT and opal-A. The crystallinity of the opal decreases in order of the above (Jones and Segnit, 1971). Opal-A is composed of highly disordered or almost amorphous SiO_2 (Jones and Segnit, 1971). Graetsch (1994) reported that water content of opal-C, opal-CT and opal-A are 1-3, 3-10 and 4-8 wt%, respectively. Hydrous silica amorphous minerals such as opal-A containing high water content includes both the water molecules and silanol.

Not only the study of the structural feature and water species in opal but also the transformation of its structure during diagenesis is interesting. As the burial depth of the sediment including opal-A increases, this material finally transforms to thermodynamically stable quartz via opal-C. However, this structural transformation of opal-A still includes many indistinct points about the structural evolution and water behavior in opal.

On the other hand, it is well known that hydrous amorphous silica mineral such as opal-A forms the body of algae and plankton. External skeletons of diatom and radiolarian are made of hydrous amorphous silica, and therefore these are referred to as “biogenic silica”. Gendron-Badou et al. (2003) reported that infrared spectra for the fossil diatom skeletons and the marine sponge spicules indicate that these materials contain silanol and water molecules. Besides, silica gel, which is synthetic hydrous amorphous silica material, shows an infrared spectrum similar to that of materials described above and contains also silanol and water molecules in the structure (Kamiya et al., 2000; Arasuna et al., 2013a). These biogenic silicas, especially the external skeleton of diatom, transform to diatomite and chart by deposition on the sea floor and

successive metamorphism. Moreover, the water in these materials may be transported to the subduction zone. Therefore, high pressure and temperature experiments for these materials may be useful to elucidate the transformation mechanisms and the water transportation capabilities for these materials. However, to get an enough quantity of these hydrous materials for the high pressure and temperature experiments is difficult. Consequently, the structural change and water behavior in biogenic silicas under high pressure and temperature are not well known even now, although the knowledge of these behaviors is important for the studies of subduction zone and diagenesis of hydrous mineral and biogenic silicas.

Whipple (1950, 1951) suggested that the comet nucleus contains water ice. After this pioneering report, Greenberg (1998) suggested that the comet is formed by the silicate, complex organic refractory and H_2O. Recently, Elsila et al. (2009) revealed that a returned cometary sample from the coma of comet 81P/wild2 by NASA's stardust spacecraft includes glycine which is one of amino acids. Numerous comets fallen into the primitive earth. Therefore, it was possible to the comet brought amino acids on the earth which were materials for the primitive life of the earth. Furthermore, water in meteorite and comet may be related with the formation of early ocean. The shock-wave compression experiment of material including H_2O (ice), silicate and amino acid performs as the analog experiment for compression behaviors of comet during the impact event and provide much important information on these materials. At the beginning of this analog experiment, I pay attention to behaviors of silicate material and water under the shock compression, because possibly the silicate material and water in the comets may contribute to the stability of the amino acids.

Several scientists already investigated the structural evolution of silicate minerals such as quartz, cristobalite and feldspars and some silicate glasses by shock compression (see chapter 4). However, the shock compression study for hydrous mineral and material is only one case of synthetic opal reported by Inoue et al. (2010). The obtained results from the study of shock compression for hydrous materials are important in the field of astrophysics as well as earth sciences. On the shock event of the comet, the high temperature generated by shock compression may also give large influence on the structure of silicate and the water in comet. Therefore, high temperature experiment for hydrous silica materials is important to understand shock impact effect on them.

As noted above, the high pressure and temperature experiments for hydrous silica,

especially hydrous amorphous silica, is very important for the earth science and astrophysics. In order to obtain the basic data of high pressure and temperature behaviors for hydrous silica minerals and materials, the synthetic material is desirable for these experiments because of its homogeneity and reproducibility. In this study, silica gel is used as a model material for the external skeleton of the diatom and comet nucleolus. Synthetic opal is used as a model material for the natural opal-A and other natural hydrous silica minerals.

1.2 The purpose of this study

In the present study, the pressure-induced structural changes have been examined for a silica gel by the static compression and shock compression. Furthermore, structural changes of a synthetic opal and the silica gel by thermal treatment are examined.

In chapter 2, the details of synthesis procedure for silica gel and opal used in this study are described. The review of the typical sol-gel method and the stöbor method are also described on this chapter.

In chapter 3, static compression experiments up to 10 GPa at 300 and 373 K were performed for the synthetic silica gel. The mechanism of structural change of silica gel under high pressure and temperature was discussed and compared with the structural evolutions of silica glass reported by previous studies. Water behavior in the compressed sample is also discussed.

In chapter 4, shock-recovery experiments up to 31 GPa were performed for the silica gel. The structural changes of silica gel by shock compressions were discussed precisely. The specific features of pressure induced water behavior in silica gel were also discussed.

In chapter 5, the structural changes of synthetic opal by thermal treatment up to 1673 K are discussed and compared with that of thermal treated silica gel. The changes of intermediate order range structure in thermal treated opal and silica gel were discussed.

The dehydration mechanism of water molecules and silanol (Si-OH) under high temperature in opal and silica gel was revealed.

In chapter 6, the general conclusion of the above chapters is provided.

Chapter 2
Sample preparations

2.1 Synthesis of silica gel

2.1.1 The sol-gel method

Silica gel samples used in this study were synthesized by typical sol-gel method. Therefore, I review the sol-gel method firstly. The sol-gel method has been widely used for preparation of inorganic oxides by wet chemical procedures. This technique includes following many advantages. The sol-gel method enables the syntheses of glass and poly-crystalline ceramics at relatively low temperature. Moreover, the synthesized material has high homogeneity.

Generally, precursor compounds for sol-gel method are metallic alkoxide, e.g., Si $(OC_2H_5)_4$, Al $(OC_3H_7)_3$ etc. In sol-gel method, the metal alkoxide is hydrated and polymerized in a solvent with addition of catalyst. Alcohol solution, e.g., methanol, ethanol, propanol, is usually used for the solvent. The catalyst, which is chosen from among the hydrochloric, acetic, sulfuric and nitric acid and ammonia, is added to make a homogeneous solution.

The partial hydrolysis reaction is generally represented as following.

$$M(OR)_n + mH_2O \rightarrow M(OR)_{n-m}(OH)_m + mROH \qquad (2.1)$$

This reaction is followed by condensation as next reaction,

$$2M(OR)_{n-m}(OH)_m \rightarrow (RO)_{n-m}(OH)_{m-1}M\text{-}O\text{-}M(OR)_{n-m}(OH)_{m-1} + H_2O \qquad (2.2)$$

where M is a metallic element and R is alkyl (C_nH_{2n+1}) group.

Three-dimensional siloxane bonds are formed by further condensation in sol-solution as follows:

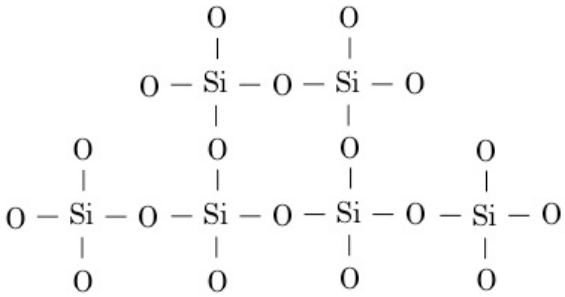

and generated a spherical particle in the solution.

The sol-solution is solidified by a further reaction and drying at suitable temperature, and the monolith gel is obtained finally.

The generated spherical silica particle has a secondary structure (Orcel et al., 1988). At first, the tiny silica particle with a diameter in several nm is formed, and it is usually regarded as a primary sphere. This tiny sphere agglomerates and becomes larger particles which referred as a secondary sphere. Moreover, the micro-gaps are formed when the primary and secondaly particles agglomerate, so that the synthesized silica gel usually has a micro porous structure.

Generally obtained silica gel is amorphous substance. Furthermore, by a thermal treatment at suitable temperature for this monolith gel, the more densified glass and poly-crystalline ceramics are obtained. The gel – glass conversion process by thermal treatments has been investigated based on the intermediate range structure and discussed the relationship between its structure and the water dehydration. Bertoluzza et al. (1982) reported that TEOS-derived silica gel could transform to glass through a hydrolytic polycondensation process by thermal treatment at 800 °C completely. Kamiya and Nasu (1998) indicated that the intermediate range structure of silica gel might be compact than that of silica glass based on the X-ray distribution analysis and reconstructed to that of silica glass at 200-500 °C.

2.1.2 Synthesis procedure of silica gel used in this study

The sample used in this study was synthesized by modifying the synthesis procedure reported by Kamiya and Sakka (1980). The flow chart in figure 2.1 illustrates the sample preparation procedure. It was typical sol-gel method mentioned in 2.1.1. TEOS [$Si(OC_2H_5)_4$] (Wako Chemicals Co., Japan), ethanol (dehydrated more than twice with a

molecular sieve) and acetic anhydride (97 %; Wako Chemicals Co., Japan) are used for the precursor compound, alcohol solution and catalyst, respectively. TEOS, H_2O, CH_3COOH, and C_2H_5OH used in this study were in the molar ratio 0.200 : 10.0 : 0.002 : 1.400. Firstly, dehydrated ethanol was added to a TEOS solution in a glove box filled with the nitrogen gas. H_2O, acetic acid and dehydrated ethanol were mixed in a draft chamber. Then, this mixed solution was added to the solution of TEOS and dehydrated ethanol under stirring at 25 °C. The solution was stirring for 1h and then heated at 40 °C for 1 month, and the silica gel was obtained finally (Fig. 2.2).

2.2 Synthesis procedure of opal

2.2.1 The Stöber's process

Stöber et al. (1968) succeeded the produce of tetraalkylsilicate derived spherical silica particle with uniform size in various alcohol solvents. They used methanol, ethanol, n-propanol and n-butanol as solvents. The alcohol solvent is effective to particle size and reaction rate, e.g., the reaction rate is fastest and the particle size is smallest in methanol solution. In contrast, the slowest reaction rate and the biggest particle size are obtained in n-butanol solution (Stöber et al., 1968). A similar correlation was observed when comparing the result with different alkyl silicates (Stöber et al., 1968). Depending on the used alkyl silicate and alcohol solvents, the generated particle size provided from less than 0.05 μm to 2μm in diameter (Stöber et al., 1968).

2.2.2 Synthesis procedure of opal

A synthetic opal used in this study was prepared based on the procedure reported in Okudera and Hozumi (2003) which produced the silica nanoparticle and thin film on flat substrate by modifying Stöber's process. This synthesis procedure includes the hydrolysis, dehydration, and condensation of TEOS in a solution of ethanol solvent with ammonia as a catalyst. Figure 2.3 illustrates the flow chart of sample preparation procedure for synthetic opal. TEOS [$Si(OC_2H_5)_4$] (Wako Chemicals Co., Japan), ethanol (dehydrated more than twice with a molecular sieve) and NH_3 (28 % aqueous

solution; Wako Chemicals Co., Japan) are used. Firstly, dehydrated ethanol was added to TEOS solution in a glove box filled with the nitrogen gas. Then, the aqueous solution of H_2O and 28% NH_3 poured in TEOS-ethanol solution and the mixed solution was stirring at 20 °C for 1hr. Silica nanospheres are generated by hydrolysis, dehydration and condensation of TEOS in this mixed solution. These spheres precipitated gradually and stacked in the bottom of a beaker. After drying supernatant solution, the synthetic opal is obtained. The ordered stacking of silica spheres collapses easily by a concussion. If the spheres become disorderly, the obtained opal shows only opaque white without opalescence. Therefore, it is desirable to be careful handling of this solution. After drying the suspension for more than one month, synthetic opal with beautiful opalescence such as a natural gem-opal is obtained (Fig. 2.4).

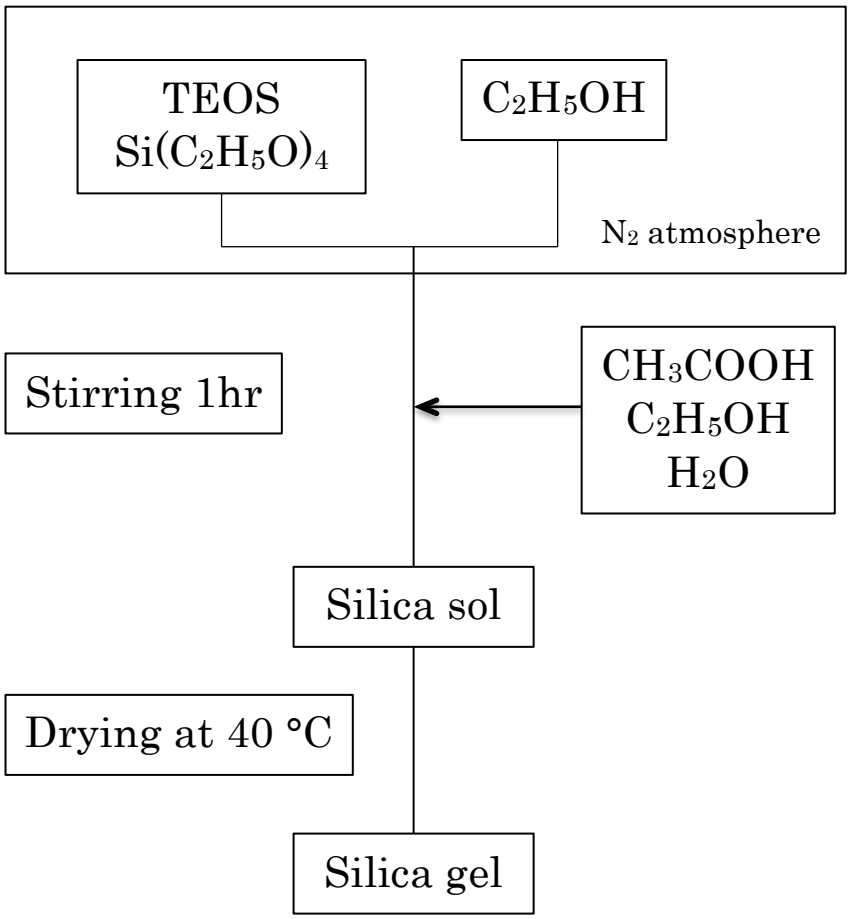

Fig. 2.1 The flowchart of silica gel preparation procedure

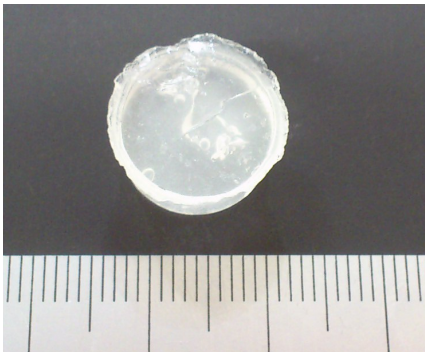

Fig. 2.2 As-synthesized silica gel

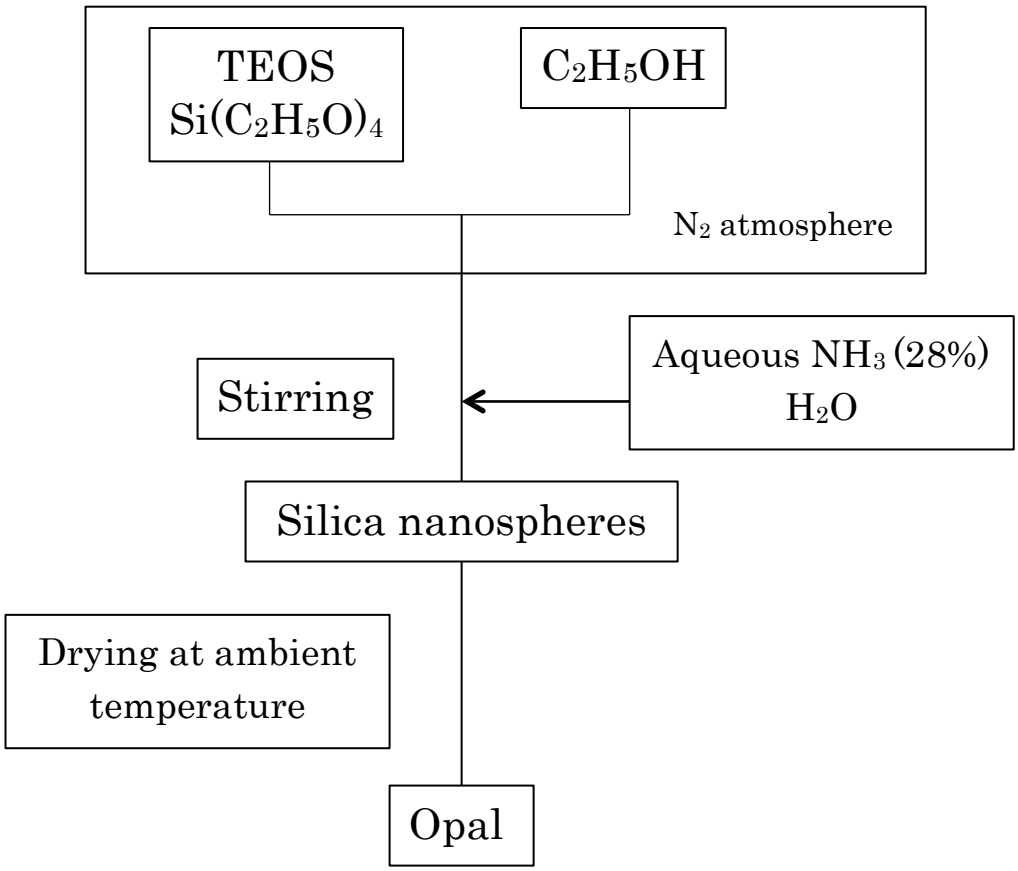

Fig. 2.3 The flowchart of opal synthesis procedure

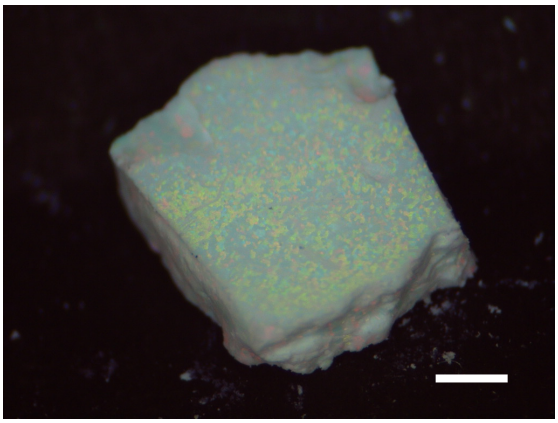

Fig. 2.4 As-synthesized opal. Scale bar is 1mm

Chapter 3
The structural change of silica gel by compression up to 10 GPa under 100 °C

3.1 Introduction

Studies on the structural change and the water behavior in hydrous amorphous silica during static compression provide the important information to the studies of the burial diagenesis of hydrous minerals and physical properties for subduction zone.

The static compression experiments for silica glass at room temperature have been performed by several researchers (Walrafen and Krishnan, 1981; Hemley et al., 1986 etc). *In-situ* measurement of Raman spectrum for silica glass under high pressure (~8GPa) showed a sharpening of the band at ν = ~440 cm^{-1} and the band position shifted toward higher frequency due to a densification of network structure by compression (Hemley et al., 1986). They also reported that the sharpening of the Raman band was reversible up to compression of 8 GPa, resulting in the structural change of silica glass without a collapse of ring structure (Hemley et al., 1986).

On the other hand, study on the compression behavior in silica gel under 4.5 GPa at room temperature was only reported by Costa et al. (1997). They revealed that the reduction up to 60 % in water content, the dehydration and condensation of silanol, the formation of very small pores due to the compression of tiny amorphous silica spheres, and the presence of the trapped water in the small pores after the compression (Costa et al.,1997). Therefore, unlike compressed silica glass, it is presumed that the irreversible structural change occurs in compressed silica gel at relatively lower pressure range (<8GPa). However, Costa et al. (1997) didn't mention about the structural feature of compressed silica gel in contrast to that of as-synthesized one.

On the other hand, the amorphous silica could be transformed to quartz and high-pressure SiO_2 phase such as coesite and stishovite by compression. Coes (1953) firstly experimentally synthesized coesite crystals by compression under 3.5 GPa over 500 °C for 15 hr. After this pioneering report, several authors reported the synthesis of coesite from amorphous silica, especially hydrous amorphous silica, at relatively low temperatures and pressures in short duration (Naka et al., 1974; Kato et al., 1975; Zhang et al., 2009). Kato et al. (1975) reported that ultrafine particles of amorphous silica

could be transformed to coesite in 30 min at 450 °C and 5 GPa. Recently, Zhang et al. (2009) succeeded in the synthesis of coesite from hydrous amorphous silica powder at 4.2 GPa and 190 °C for 30 min. They demonstrated that the hydroxyl in amorphous silica gave a considerable influence on the transformation to coesite at relatively low temperature and pressure (Zhang et al., 2009). However, the effect of water on coesite formation has still indistinct points.

In this chapter, TEOS-derived silica gel compressed up to 10 GPa at room temperature and 100 °C were investigated by scanning electron microscopy (SEM), X-ray diffraction (XRD) measurement, Raman, Fourier transform infrared (FTIR) and nuclear magnetic resonance (NMR) spectroscopies, and thermogravimetric-DTA (TG-DTA) measurement. The results are compared with those of previous studies on silica glass and silica gel, and provide new insights into the structural change of compressed silica gel, the variation of silanol (Si-OH) contents, and the effects of water in these matters.

3.2 Experimental

3.2.1 High pressure experiments and SEM observation

The synthetic silica gel samples were compressed up to 10 GPa at room temperature and up to 5 GPa at 100 °C for 1 hr using a 6-8 Kawai-type multi anvil apparatus at Gakushuin University. For the high pressure experiments, the synthetic silica gels were shaped into a cylinder with the diameter and length both equal to 3.8 mm. Tungsten carbide anvils with the edge of 8.0 mm and pressure medium of a MgO octahedron of 14.0 mm on edge were used. Each silica gel sample was encased into a cylindrical Pt capsule. For the experiment at 100 °C, the Pt capsule also was used as a furnace. The heating temperature was measured using a 0.1mm-diameter Pt-13%RhPt thermocouple located on the outer surface of the central part of the Pt furnace. All the recovered samples were then investigated. On the other hand, to compare with the sample recovered after the compression at 5 GPa at 100 °C, coesite sample was synthesized by Prof. Akaogi of Gakushuin University using the 6-8 Kawai-type multi anvil apparatus at Gakushuin University. A reagent grade low-quartz was compressed under 5.5 GPa at 1200 °C for 2 hr in Au capsule.

SEM observation of as-synthesized silica gel was performed using HITACHI S-5200 at JAIST. SEM observation was conducted with accelerating voltage in the range of 10 kV.

3.2.2 X-ray diffraction measurement

XRD measurements for all samples were performed using Rigaku RINT 2200 with Cu Kα radiation. The θ/2θ scanning technique was adopted over the 2θ = 2-100° with a scan step of 0.02° and 0.05° for the compressed sample at room temperature and 100 °C, respectively. The applied acceleration voltage and current used were 40 kV and 30 mA, respectively.

3.2.3 Raman spectroscopy

Raman spectra for all of the samples were recorded using micro-Raman spectrometers (Jovin Yvon Ramanor T-6400). The 514.5 nm line of Ar^+ laser (MELLES GRIOT, 43 SERIES ION LASER, 543-GS-A02) was used to excite Raman scattering. A grating with 600 lines/nm was used to give a wavenumber resolution of 1.4-1.8 cm^{-1} and a spectral resolution of approximately ±1.6cm^{-1} in the spectral range. All observed Raman spectra were corrected for background.

3.2.4 FTIR spectroscopy

FTIR absorption measurements were recorded using FTIR spectrometer (JASCO FT/IR 610 V) with KBr micro-pellet transmission method. Spectra for all of the samples were recorded in the range of ν = 400 - 4000 cm^{-1} with a band pass of 4 cm^{-1}.

3.2.5 NMR spectroscopies

^1H MAS NMR, ^1H-^{29}Si CP MAS, and ^{29}Si MAS NMR spectra measurements for the as-synthesized silica gel and the samples compressed at room temperature were performed using a Varian Unity-Inova 400 NMR spectrometer and a 2.5 CP-MAS probe at ISEI, at Okayama University. Resonance frequencies were 400.3 MHz for ^1H

MAS NMR and 79.5 MHz for ^{29}Si NMR. For all NMR spectra measurements, 20 kHz of spinning rate was adopted. 0.02 s of acquisition time and 3s of d1 (recycle delay time) were adopted for the measurements of ^{1}H MAS NMR. For the measurements of ^{1}H-^{29}Si CP-MAS NMR, 0.005 s of acquisition time were adopted and the contact times were 2, 8, 20 ms for all the samples. ^{29}Si MAS NMR measurements were performed with 0.005 s of acquisition time. 1.8 s and 1.7 s of pulse width (pwx) were used for the as-synthesized silica gel and the recovered samples, respectively. Both ^{29}Si and ^{1}H chemical shifts were referred to tetramethylsilane (TMS).

3.2.6 TG-DTA measurement

TG-DTA measurements were performed using a Rigaku Thermo Plus 2 Tg 8120. The as-synthesized silica gel and the sample compressed at 5 GPa and 100 °C were ground, and then 10 mg of the silica gel and 5 mg of the compressed sample were placed into a Pt pan. The samples were heated to 1400 °C at a heating rate of 10 °C min^{-1} in a nitrogen atmosphere.

3.3 Results

3.3.1 SEM observation for as-synthesized silica gel

SEM micrograph indicates that the microstructure of as-synthesized silica gel may consist of an agglomeration of tiny amorphous silica spheres, although most of silica spheres are unified (Fig. 3.1). A diameter of the sphere is about several tens of nanometer.

3.3.2 X-ray diffraction analysis

The XRD patterns for the as-synthesized silica gel and the samples compressed up to 10 GPa at room temperature are shown in figure 3.2. As-synthesized silica gel has a diffuse scattering maximum centered at $2\theta = 23.2°$ with no crystalline peaks. By compression at 5 GPa, the position of the scattering maximum shows a positive shift of

about 0.6° and seems to be constant above this pressure. Furthermore, the intensity of small angle scattering at around 2θ = 2° decreases by about 48 % after the compression at 5 GPa. The intensity is roughly constant above 5 GPa.

The XRD patterns for the samples compressed under 100 °C, as-synthesized silica gel, and synthetic coesite are presented in figure 3.3. After the compression at 2 GPa and 100 °C, the scattering maximum shows the positive shift about 0.6 ° without typical crystalline peaks. XRD pattern of the sample compressed at 5 GPa under 100 °C shows distinct crystalline peaks, with the maximum intensity peak located at 2θ = 28.7°. All of crystalline peaks are consistent with the diffraction peaks of well-crystallized synthetic coesite.

3.3.3 Raman spectroscopic analysis

Raman spectra of the as-synthesized silica gel and the samples compressed at room temperature are shown in figure 3.4. Raman spectrum of the as-synthesized silica gel exhibits a broad band centered at around ν = 450 cm^{-1} attributed to a symmetrical Si-O-Si stretching mode and a band at ν = 483 cm^{-1} attributed to the oxygen-breathing mode of the four-membered ring of SiO_4 tetrahedra, denoted as D_1 band (Galeener, 1982a and b; Galeener and Geissberger, 1983; Sharma et al., 1984). The band around ν = 795 cm^{-1} is attributed to the oxygen vibrations perpendicular to the Si-Si line (McMillan and Wolf, 1995), and the band at around ν = 978 cm^{-1} is corresponding to Si-O stretching of the silanol (Stolen and Walrafen, 1976; Murray and Greytak, 1979). For the samples compressed up to 10 GPa at room temperature, the broad band loses its intensity in region below ν = 480 cm^{-1} and becomes much sharper than that before compression, whereas the position of the peak maximum shows a negligible change. Furthermore, the band of silanol shows the negative shift about 8 cm^{-1} by compressions above 5 GPa.

In the higher frequency region, a broad band centered at ν = 3400 cm^{-1} is observed in the spectrum of the as-synthesized silica gel (Fig. 3.5). This broad band seems to be composed of peaks located around ν = 2900, 3250, and 3430 cm^{-1} with the shoulders around ν = 3600 and 3640 cm^{-1}. The lower weak component around ν = 2900 cm^{-1} may be attributed to the CH absorption of residual starting TESO solution (Innocenzi, 2003). The bands around ν = 3250 and 3430 cm^{-1} can be attributed to the O-H stretching of

adsorbed water molecules (Krol and Van Lierop, 1984). Moreover, the weak shoulders around ν = 3600 and 3640 cm^{-1} may be largely attributed to the O-H stretching of silanol (Walrafen and Samanta, 1978; Krol and Van Lierop, 1984; Davis and Tomozawa, 1996). After the compressions at 10 GPa and room temperature, the broad band remains with a little spectral change (Fig. 3.5). The bands around ν = 3250 and 3430 cm^{-1} only attributed to water molecule become less intense in comparison with the bands of silanol presented above ν = 3600 cm^{-1}.

On the other hand, after the compressions at 2 and 5 GPa under 100 °C, each compressed sample shows crystalline peaks (Fig. 3.6-3.7). The sample compressed at 2 GPa shows various Raman spectra by the measurement point (Fig. 3.6 a-c). A sharp crystalline band around ν = 458 cm^{-1} with a weak band around ν = 495 cm^{-1} is observed in some part of the compressed sample (Fig. 3.6 a). However, other part may indicate that the crystallinity of the compressed sample may be not so high (Fig. 3.6 b). On the other hand, some parts of 2 GPa sample show the Raman spectrum similar to that of silica gel (Fig. 3.6 c). It may indicate that a part of compressed sample keeps the feature of silica gel after the compression at 2 GPa.

The sample compressed at 5 GPa and 100 °C shows the sharp crystalline bands (Fig. 3.7). These bands basically correspond to that of well-crystallized coesite, whereas some bands are broad or not clear below ν = 400 cm^{-1}. The spectrum shows the intense band at around ν = 518 cm^{-1} attributed to four-membered ring of SiO_4 tetrahedra of coesite (Sharma et al., 1981; Kingma and Hemley, 1994). Moreover, the weak bands at ν = 1070 and 1160 cm^{-1} appear after the compression. These bands may be attributed to asymmetric Si-O stretching vibration within a fully-polymerized tetrahedral network (McMillan, 1984).

The broad band around ν = 3400 cm^{-1} due to the water molecules and silanol groups remains even after compressions up to 5 GPa and 100 °C (Fig. 3.8-3.9). As with the result of the sample compressed at room temperature, the bands below ν = 3430 cm^{-1} attributed to water molecule become less intense in comparison with those of silanol located above ν = 3600 cm^{-1}. Moreover, the band around ν = 3550 cm^{-1} becomes prominent in the sample compressed at 5 GPa and 100 °C (Fig. 3.9). Well-crystallized synthetic coesite does not contain the bands due to the water molecules and silanol groups in all measurement range.

3.3.4 Infrared spectroscopic analysis

FTIR spectrum of the as-synthesized silica gel shows three distinct bands at ν = 1090, 798, 467 cm^{-1} which are characteristic for the silica glass and crystalline silica polymorph (Fig. 3.10). These bands are attributed to the mode of Si-O anti-symmetric stretching, bending, rocking, respectively (Handke and Mozgawa, 1993). The spectrum also shows another distinct band around ν = 954 cm^{-1} attributed to Si-O stretching mode of silanol (Orcel et al., 1986) and the weak band around ν = 1653 cm^{-1} attributed to the H-O-H bending mode of adsorbed molecular water at the surface of the sample (Benesi and Jones, 1959).

After compressions up to 10 GPa at room temperature, the Si-O anti-symmetric stretching band may become broad and the position of the silanol band around ν = 954 cm^{-1} shifts toward lower frequency by about 15 cm^{-1} (Fig. 3.11).

In the region of ν = 2500-4000 cm^{-1}, the FTIR spectra for the as-synthesized silica gel and the samples compressed at room temperature are shown in figure 3.12. The spectrum for the silica gel has a broad band centered at ν = 3500 cm^{-1}, which is a superposition of the bands for several O-H stretching modes of molecular water and silanol groups (Davis and Tomozawa, 1996). After the compression at 10 GPa and room temperature, the broad band is still observed clearly without significant spectral change.

The FTIR spectrum of the sample compressed at 2 GPa and 100 °C shows some changes in comparison with that of as-synthesized silica gel (Fig. 3.13). The broadening of the Si-O stretching band around ν = 1100 cm^{-1} is observed, and it may induce the obscureness of the Si-OH band at around ν = 954 cm^{-1}. Moreover, the weak band at ν = 555cm^{-1} becomes intense. The assignment of this band will be discussed later. The sample compressed at 5 GPa and 100 °C has new bands at ν = 683, 600, and 571 cm^{-1} that can be attributed to the band due to coesite structure (Lippincott et al., 1958; Williams et al., 1993). The former band may be attributed to the Si-O-Si bending vibrations (Williams et al., 1993) and the latter two bands may be attributed to either O-Si-O or Si-O-Si vibrations (Lippincott et al., 1958). The spectrum of the 5 GPa sample shows an obvious sharpening of the broad band attributed to the Si-O stretching mode around ν = 1090 cm^{-1}. Furthermore, a broadening of the silanol band at around ν = 954 cm^{-1} and the disappearance of the band of water molecules at around ν = 1653

cm^{-1} are observed. Synthetic coesite has main band at around ν = 1090 cm^{-1} and weak bands at ν = 1038, 1157 and 1227 cm^{-1} (Fig. 3. 13). These bands are not distinct in the 5 GPa. The bands of silanol and molecular water are not observed in the spectrum of synthetic coesite.

The broad band centered at ν = 3500 cm^{-1} is still observed after the compression at 5 GPa and 100 °C (Fig. 3.14). After the compression at 2 GPa, the weak band around ν = 3630 cm^{-1} shifts toward higher frequency by about 20 cm^{-1}. Consistent with the result of Raman spectroscopy, FTIR spectrum for the 5 GPa sample shows the prominent new band at around ν = 3555 cm^{-1}.

3.3.5 NMR Spectroscopic analysis

The ^{1}H MAS NMR spectra for the as-synthesized silica gel and the samples compressed up to10 GPa at room temperature are presented in figure 3.15. ^{1}H NMR spectrum of as-synthesized silica gel shows a prominent peak around 4.9 ppm attributed to relatively mobile molecular water and a very weak tail to higher frequency attributed to strongly hydrogen-bonded silanol or water molecule. By compressions up to 10 GPa at room temperature, the peak around 4.9 ppm becomes less intense. However, the weak tail extended to about 10 ppm becomes prominent. The total water content for each samples estimated from the ^{1}H NMR spectra is listed in Table 3.1. With increasing pressure, the water content of sample decreases gradually.

^{1}H-^{29}Si CP-MAS NMR spectra for the as-synthesized silica gel and the compressed samples at room temperature are presented in figures 3.16-3.18. These NMR spectra are deconvoluted to obtain the detailed information on Q_n species by means of gaussian peak fittings using IGOR pro 6.3 program. The spectrum of the as-synthesized silica gel has peaks around -111, -101, and -92 ppm, attributed to Q_4 (Si bonded to 0 OH), Q_3 (Si bonded to 1 OH), and Q_2 (Si bonded 2 OH), respectively. The positions of these peaks in the spectra for the compressed samples are similar to those of as-synthesized silica gel, whereas each peaks becomes significant broader than that of silica gel (Table 3.2).

^{29}Si MAS NMR spectra for samples are presented together with gaussian peak fitting results of these spectra in figures 3.19-3.21. The used parameters for peak fitting, the position and FWHM of Q_n peaks, are obtained by ^{1}H-^{29}Si CP-MAS analysis (Table 3.2). ^{29}Si MAS NMR spectra for the as-synthesized silica gel show similar absolute

intensities among Q_1, Q_2 and Q_3 above 60 s of recycle delay time (d1). However, the compressed samples need a longer d1, e.g. d1≥480, than silica gel. For the as-synthesized silica gel, the calculated relative intensities of Qn species based on the result of deconvoluton peaks are 57, 37, and 6 % for Q_4, Q_3, and Q_2, respectively (table 3.3). After the compressions up to 10 GPa, the relative intensities of Q_n species are almost unchanged within the calculation error of 3%.

3.3.6 TG-DTA analysis

The TG and DTA curves measured for the as-synthesized silica gel are present in figure 3.22. The TG curve of silica gel shows that large weight loss (17.5 wt%) up to 160 °C, and then the gradual weight loss (4.7 wt%) up to 1400 °C. Observed total weight loss is about 22.2 wt%. DTA curve for silica gel has a broad endothermic band at around 82 °C and an exothermic band at around 1350 °C.

The TG curve for the sample compressed at 5 GPa and 100 °C shows the similar weight loss as observed in silica gel (Fig 3.23). A first weight loss (2.6 wt%) is observed up to 130 °C, and then second weight loss (6.6 wt%) is observed up to 1000 °C. A small continuous weight loss (0.1 wt%) is also observed. The total weight loss up to 1400 °C is about 9.3 wt %. The detailed analysis of the DTA curve for the recovered sample cannot be carried out due to the low S/N ratio. The sample recovered after TG-DTA measurements were checked by XRD technique. The silica gel and the sample compressed at 5 GPa and 100 °C transformed to low-cristobalite and well-crystallized coesite, respectively by heating up to 1400 ºC.

3.4 Discussion

3.4.1 The structure of as-synthesized silica gel

According to previous reports (Orcel et al., 1988; Hench and West, 1990), the tiny silica sphere in as-synthesized silica gel detected by SEM observation is also likely to be composed of agglomerates for smaller silica spheres, although the SEM results could not show the evidence of the presence of this small sphere. However, XRD pattern of

the as-synthesized silica gel shows that the intense small-angle scattering at $2\theta = 2°$. It is probably related to this spherical nanostructure.

Raman spectrum of the as-synthesized silica gel shows the broad band around $\nu = 450$ cm^{-1} and sharp D_1 band at $\nu = 483$ cm^{-1}, suggesting that silica gel may contain various types of ring structures. On the other hand, XRD pattern of the as-synthesized silica gel has the diffuse scattering maximum centered at 23.2 ° called as first sharp diffraction peak (FSDP). The analysis of FSDP positions ($S_1 = 4\pi\sin\theta/\lambda$) is known to be useful to evaluate the size of the intermediate range order structure. Based on the concept of "quasi-lattice", S_1 can be associated with the averaged cell dimension d_m (where $d_m = 2\pi/S_1$) of intermediate range structural units (Tan and Arndt, 1999). The estimated FSDP position for as-synthesized silica gel is S_1 =1.64 $Å^{-1}$ and is very similar to that of previously reported silica gel (S_1 =1.60-1.67 $Å^{-1}$, Kamiya and Nasu, 1998). Kamiya and Nasu (1998) revealed that the intermediate structure of silica gel was mainly composed of four-membered ring of SiO_4 tetrahedra based on the X-ray radial distribution analysis. Therefore, silica gel used in this study may contain a large amount of four-membered ring in the structure. This is supported by the distinct D_1 band in the Raman spectrum for as-synthesized silica gel.

Besides, the Raman and FTIR spectra for the as-synthesized silica gel show the prominent band attributed to Si-O stretching of silanol at around $\nu = 980$ cm^{-1} and $\nu = 955$ cm^{-1}, respectively. Moreover, quantitative ^{29}Si MAS NMR analysis reveals high abundance of Q_3 and Q_2 in the silica gel. Consequently, silica gel used in this study has lower polymerized network structure, which is terminated by OH.

3.4.2 Water species of as-synthesized silica gel and their behavior under pressure

In higher wavenumber region above $\nu = 3000$ cm^{-1} of both Raman and FTIR spectra for the as-synthesized silica gel, the strong broad band due to the water molecules and silanol groups is observed. In consonance with these results, the ^1H MAS NMR shows that as-synthesized silica gel contains the water of about 19.6 wt%. This water content is somewhat smaller than that obtained by TG analysis. It seems to be explained by the sample condition, *i.e.*, the powder sample and bulk sample are used for the TG-DTA analysis and ^1H MAS NMR spectroscopy, respectively. The powder sample easily

adsorbs water molecules in atmosphere.

In the TG curve for the as-synthesized silica gel, the considerable weight loss (17.5 wt %) is shown up to 160 °C. According to the report of Graetsch et al. (1985), this may be responsible for the release of the adsorbed water molecules. The strong peak at 4.9 ppm in ^{1}H NMR spectrum for the as-synthesized silica gel also indicates that the presence of surface-adsorbed water molecules. TG analysis shows that the continuous weight loss of 4.7 wt% above 160 °C. In this temperature region, silanol groups are dehydrated (Graetsch et al., 1985). Raman, FTIR, and ^{29}Si MAS NMR spectra for as-synthesized silica gel ensure the presence of silanol. In the Raman spectrum, the band of silanol at $\nu = 980cm^{-1}$ has the weak tail to around $\nu = 900\ cm^{-1}$. Krol and Van Lierop (1984) only assigned this band to Q_2 as called germinal silanol. The assignment of this band in Raman spectrum was uncertain, because no other previous report on this band. However, the result of ^{29}Si MAS NMR indicates the obvious presence of Q_2 in silica gel.

After compressions up to 10 GPa at room temperature, the both Raman and FTIR spectra show the intense broad bands corresponding to water molecules and silanol above $\nu = 3000\ cm^{-1}$. However, the relative intensity of the bands attributed to water molecules is weak in contrast to that of silanol. This is supported by the presence of strong Raman band of silanol around $\nu = 980\ cm^{-1}$ with the weak shoulder around $\nu = 900\ cm^{-1}$ even after the compression at 10 GPa. This may indicate that the water molecules may be released easily than silanol.

The results of ^{1}H and ^{29}Si MAS NMR analyses provide more detailed water behavior under compressions. With increasing pressure, ^{1}H MAS NMR spectra for compressed samples show that the band at 4.9 ppm becomes less intense. It may indicate that the loss of a large number of water molecules by compressions. Moreover, the ^{1}H NMR spectra of the samples show that the shoulder which is extended to 10 ppm becomes prominent above compression of 5 GPa. Xue and Kanzaki (2007) reported that the correlation of between ^{1}H chemical shift and O-H···O distance. Below 2.8 Å of R(O-H···O), the shortening of bond distance is linearly related with positive ^{1}H chemical shift. Therefore, the development of the band at around 7.5 ppm may indicate the increase for proportion of strongly hydrogen-bonded SiOH or H_2O groups.

For the sample compressed at 2 GPa under 100 °C, Raman and FTIR spectra show that a large amount of water molecules and silanol groups still remain even after

compression. However, these analyses indicate that the water molecules may be released easily than silanol, as observed in the sample compressed up to 10 GPa at room temperature. In the FTIR spectrum, small spectral change by compression is observed, e.g., the band around ν = 3450 cm^{-1} becomes prominent. However, it may be caused by the water molecules adsorbed in the KBr pellet.

Even after compression at 5 GPa under 100 °C, the compressed sample shows the broad band of water molecules and silanol above ν = 3000 cm^{-1} in both Raman and FTIR spectra. Moreover, the band at around ν = 3550 cm^{-1} becomes prominent in both FTIR and Raman spectra. Koch-Müller et al. (2001) reported that the incorporation of hydrogen into the coesite structure above 5.0 GPa and 1100 °C. For this OH bearing coesite, FTIR spectrum shows strong bands at ν = 3460, 3520 and 3572 cm^{-1} attributed to OH stretching. Therefore, this report may suggest that the crystalline part in the sample of 5 GPa in this study also could keep silanol in the structure. Moreover, the result of TG measurement reveals that the 5 GPa sample contains about 9.3 wt% water. The amounts of remaining adsorbed water molecules and silanol groups in 5 GPa sample estimated from the TG analysis are about 2.6 wt% and 6.6 wt%, respectively. Moreover, a small weight loss about 0.1 wt% above 1000 °C may be corresponding to the silanol located at the structural site (Graetsch et al., 1985). It is thus this silanol is considered as the OH which is located in the coesite structure.

3.4.3 The pressure variation of first sharp diffraction peak (FSDP) position

FSDP positions of as-synthesized silica gel and the samples compressed at room temperature are shown in figure 3.24. For 5 GPa sample, the S_1 value of FSDP position increases by 0.06. A positive shift of FSDP position means that the intermediate range order structure may become compact by compression in contrast to that of as-synthesized silica gel. Above 5 GPa, the FSDP position seems to be constant. Therefore, the considerable change of intermediate range structure may not occur above this pressure. The sample compressed at 2 GPa and 100 °C also shows the positive shift about 0.06 of FSDP position. It indicates that the intermediate rang order structure of the 2 GPa sample also becomes compact than that before compression.

3.4.4 The Raman and FTIR spectroscopic analysis

Based on Raman spectroscopy, ring configurations of SiO_4 tetrahedra in silica polymorphs have been investigated in many previous studies (Sharma et al., 1981; Matson et al., 1986; Kingma and Hemley, 1994). According to these reports, the band attributed to the four-membered ring structure in coesite and moganite is observed at around ν = 500 cm^{-1}. The band for six-membered ring in quartz, cristobalite and trydimite is presented in the frequency region of ν = 380-480 cm^{-1}, whereas Miehe and Graetsch (1992) reported that moganite has the band of eight-membered ring at ν = 449 cm^{-1}. The Raman band corresponding to larger ring structure locates at lower wavenumber region. Silica glass, which has various ring structure, shows that the broad band at around ν = 450 cm^{-1}, D_1 and D_2 bands similar with that of silica gel. Probably, the network structure of silica gel has the various rings structure of SiO_4 tetrahedra, although the four-membered ring is dominant in the structure as described in chapter 3.4.3.

The sample compressed at 5 GPa and room temperature shows the narrowing of the Raman band around ν = 450 cm^{-1}. It may be related to the structural change of larger rings such as eight- or six-membered rings in the compressed sample. Besides, Hemley et al. (1986) observed the similar narrowing of the broad Raman band below ν = 490 cm^{-1} for compressed silica glass under the compression up to 8 GPa, and they concluded that this narrowing band was caused by the buckling of network structure under the compression. However, these features were unquenchable and the spectrum returned to that of the original SiO_2 glass after pressure release (Hemley et al., 1986). It should be noted here, the narrowing of the Raman band below ν = 480cm^{-1} observed in the compressed silica gel is maintained after compression (Fig. 3.25). It may indicate that compressed silica gel samples may keep the features of high-pressure phase. The significant difference of structural feature between silica glass and silica gel is that silica gel can include the water molecule and silanol. Therefore, the irreversible band narrowing in the compressed silica gel may be concerned with the presence of the water.

FTIR spectra of the samples compressed at room temperature show a broadening of the band corresponding to Si-O stretching around ν =1090 cm^{-1} in contrast to that of as-synthesized silica gel. Innocezi (2003) reported that FTIR spectrum of silica gel has

the broad band of the Si-O stretching mode (LO, TO) in the frequency region of ν = 1000-1300 cm^{-1}, and this band can be deconvoluted to at least four bands at ν = 1254, 1200, 1170 and 1082 cm^{-1}. Based on the results of his study, the bands in the frequency ν = 850-1350 cm^{-1} of as-synthesized silica gel and the compressed samples are deconvoluted (Fig. 3.26). The result indicates that the Si-O stretching band in the FTIR spectrum of as-synthesized silica gel is formed by four bands at ν = 1039, 1089 1160, 1200 cm^{-1}. Unlike the report of the Innocezi (2003), our sample has no trace around ν = 1250 cm^{-1}. After the compression at 5 GPa, all bands included in the Si-O stretching band shift toward lower frequency (Fig. 3.26). Especially, the bands at ν = 1039 and 1089 cm^{-1} show a significant negative shift of about 10 cm^{-1}. It is thus considered that these considerable negative band shifts may induce the broadening of the Si-O stretching band in the spectra for the compressed samples. Moreover, the negative shift of these bands indicates a lengthening of the Si-O bond distance, which implies the reduction of mean Si-O-Si angle (Lasaga and Gibbs, 1988; Murray and Ching, 1989).

The sample compressed at 2 GPa and 100 °C, which is the stable pressure and temperature field of low-quartz, shows the various Raman spectra. Some parts of the compressed sample show the crystalline bands at around ν = 458 cm^{-1} and ν = 494 cm^{-1} (Fig. 3.6 a). The former band may be attributed to the six-membered ring observed in low-quartz and the latter to the four-membered ring in Moganaite (Kingma and Hemley, 1994). It may indicate that the four-membered ring as observed in the silica gel remains stably and becomes order by compression, despite in the low-quartz stable field. This may be supported by the development of the FTIR band at around ν = 555 cm^{-1}. Miehe and Graetsch (1992) observed the FTIR band of ordered four-membered ring in Moganite around ν = 555 cm^{-1}. Therefore, this band may be evidence of the development of ordered four-membered ring after the compression at 2 GPa and 100 °C. Other part of the compressed sample has the similar Raman spectrum to silica gel, whereas the broad band (< ν = 480cm^{-1}) maximum shifts toward lower frequency region (Fig 3.6 c). The development of the band due to six-membered ring may occur and it may cause the negative shift of the broad band maximum. The Raman spectrum seen in figure 3.6a is not frequent in this compressed sample. This is consistent with the result that the XRD pattern of the 2 GPa sample shows no crystalline peaks. After the compression at 2GPa and 100 °C, the Si-OH Raman band at around ν = 977 cm^{-1} becomes less intense. It is presumed that the dehydration and condensation of silanol

may occur and lead the formation of network structure for the ordered six-membered ring of SiO_4 tetrahedra such as observed in low-quartz. Moreover, this silanol band shifts toward lower wavenumber region by compression. It may be related with the dehydration and condensation of silanol (see chapter 5).

FTIR and Raman spectra of the sample compressed at 5 GPa and 100 °C show the crystallization of silica gel to coesite, although some Raman and FTIR bands of coesite are missing. Moreover, the band attributed to silanol is also observed in both Raman and FTIR spectra. These results may indicate that the sample compressed at 5 GPa and 100 °C keeps the feature of silica gel and the water even after the compression, although it is obvious that most part of the sample crystallizes to coesite structure.

3.4.5 The analyses of ^{29}Si-^{1}H CP MAS and ^{29}Si MAS NMR spectroscopies

^{29}Si-^{1}H CP MAS NMR spectra of the samples show that the peaks of Q_4, Q_3 and Q_2 species at -111, -101 and -92 ppm, respectively. The presence of intense Q_3 peak is good agreement with the result of Raman and FTIR spectroscopies. Moreover, NMR analysis shows the obvious presence of Q_2 which was uncertain in Raman spectroscopic analysis. These three peaks become broad with increasing pressure. It may indicate that the network structure of the compressed sample becomes disorder.

^{29}Si MAS NMR spectra for compressed samples under room temperature show obvious peaks of Q_2, Q_3, and Q_4 species and are similar to that of as-synthesized silica gel. The positional change of Q_n species is also negligible. These may indicate that the considerable structural change of silica gel does not occur under the compressions up to 10 GPa at room temperature.

Q_n peaks in ^{29}Si MAS NMR spectra for as-synthesized silica gel and compressed samples are deconvoluted, and the relative intensities of Q_n peaks are calculated (Table 3.3). After the compressions, the calculated relative intensities of Q_n species change within the range of error (Table 3.3). Almost of germinal and single silanols in compressed samples may be not dehydrated. Furthermore, it is presumed that the polymerization and de-polymerization of network does not occur under the compressions at room temperature.

3.4.6 The structural change of amorphous phase under compression at room temperature

FSDP positions of XRD patterns and the analyses of FTIR spectra for the samples compressed up to 10 GPa at room temperature indicate that the intermediate range order structure of silica gel becomes compact by compression. Raman spectra of the compressed samples show the obvious narrowing of the broad band below $\nu = 480$ cm^{-1}. I supposed that two following spectral changes might cause the narrowing of the Raman band, (1) the positive shift of the bands placed below $\nu = 450$ cm^{-1} as observed in the compressed silica glass and (2) the reduction of the intensity of the band below $\nu = 450$ cm^{-1}. The components at lower wavenumber region in the broad band below $\nu = 480$ cm^{-1} generally correspond to the larger ring structure, e.g., six- or eight-membered ring of SiO_4 tetrahedra. Thus, if the collapse of the larger rings occurs, the intensity of the band located below $\nu = 450$ cm^{-1} decreases and de-polymerization of the network may occur. However, quantitative ^{29}Si MAS NMR spectroscopy reveals that the considerable de-polymerization of the Si-O-Si network does not happen under the compressions. Therefore, it is presumed that the positive shift of the band placed at lower wavenumber region (<450 cm^{-1}) is due to the narrowing the broad band ($<480 cm^{-1}$) as observed by Hemley et al. (1986).

According to the report of Hemley et al. (1986), the narrowing of the broad Raman band may be due to the buckling of network structure without collapse or reconstruction. The buckling of the network structure probably induces the decrease of mean Si-O-Si angle. Silica gel has the lower polymerized structure with silanol $[SiO_x(OH)_{4-x}]$. This feature easily leads the buckling compact network structure under compressions and makes it possible to maintain the buckled structure even after release of pressure.

3.4.7 The crystallization of silica gel to coesite

In the sample compressed at 2 GPa and 100 °C, the four-membered ring as observed in the as-synthesized silica gel can remain and be slightly ordered by compression, although this experimental condition is stability field of quartz. Moreover, the dehydration and condensation of Si-OH may induce the formation of the network structure of SiO_4 tetrahedra, in which six-membered rings may be dominant. Moreover,

the larger ring (> six-membered ring) may be reconstructed to six-membered ring by the compression. FTIR and XRD results for the compressed sample indicate that the intermediate structure becomes compact by compression. In addition to the formation of ordered four- and six-membered ring structure, it is considered that the buckling of the network structure also occurs by compression and induces the compact structure as observed in the sample compressed at room temperature.

After the compression at 5 GPa and 100ºC, the XRD pattern and FTIR and Raman spectroscopies indicate that the compressed sample is crystallized to coesite obviously. However, it is presumed that this sample may retain the feature of as-synthesized silica gel slightly. Nonetheless, it is sure that the crystallization to coesite occurred at relatively low temperature and short duration.

The coesite structure is also composed of four-membered rings of SiO4 tetrahedra such as those found in silica gel (Hemley et al., 1994; Kamiya and Nasu, 1998). However, coesite has well-ordered structure in comparison with that of silica gel, and four-membered rings in coesite are linked at corners to form chains parallel to **c** axis (Hemley et al., 1994). The structurral similarity between coesite and silica gel may be very important for the easy crystallization of silica gel to coesite. The stability of the four-membered ring under compression may also contribute to this crystallization. In this study, Raman spectrum for the sample compressed at 5 GPa and 100ºC shows the development of the Q_4 band around ν = 1070 and 1160 cm^{-1}, which indicates the network polymerization by dehydration of silanol. Moreover, this new network structure may be dominant by the four-membered ring. As with the sample recovered after the compressions up to 10 GPa at room temperature, the buckling of the network structure may also occur in the sample compressed at 5 GPa and 100ºC. The dehydration and polymerization of silanol under the buckling of the structure may promote the formation of the small ring such as four-membered ring.

In previous studies, the synthesis of coesite from amorphous silica material at relatively low temperature and pressure was succeeded only by using powder like materials (*e.g.* Zhang et al., 2009). It is considered that coesite synthesis is largely depends on the sample conditions, namely, powder like or a bulk solid sample. It should be note that the sample used in this study was bulk solid sample. This result shows that bulk solid silica gel can crystalize to coesite by compression at relatively low temperature in short duration. Higher water content (about 20 wt%) of the sample may

allow the crystallization to coesite despite non-powder sample.

3.5 Conclusions

The silica gel shows the irreversible structural change under the compressions up to 10 GPa at room temperature in contrast to silica glass. In these compressed samples, the buckling of the network structure by the compressions may occur without reconstruction. The lower polymerized structure with Si-OH of the as-synthesized silica gel easily leads the compact buckling network structure under compressions. This network feature of silica gel keeps the buckling structure after the compressions. Above compressions of 5 GPa, a large number of adsorbed water molecules are released, although the considerable amount of Si-OH remains after compressions.

On the other hand, the sample compressed up to 5 GPa at 100 °C shows the considerable structural change despite of low temperature.

Under 2 GPa at 100 °C, although it is stable pressure and temperature field of low-quartz, the four-membered ring of SiO_4 tetrahedra in the structure of as-synthesized silica gel is stable and slightly ordered by compression. Moreover, the dehydration and condensation of silanol may lead the formation of the ordered six-membered ring. Under 5 GPa at 100 °C, the silica gel crystallizes to coesite. The network structure of as-synthesized silica gel principally made of four-membered ring of SiO_4 tetrahedra and the stability of four-membered ring under the compression are important factors of easy crystallization to coesite. As well as these features, the presence of silanol is also important for this crystallization. The dehydration and polymerization of silanol under the buckling of the structure may promote the formation of the small ring such as four-membered ring under relatively low pressure and temperature condition.

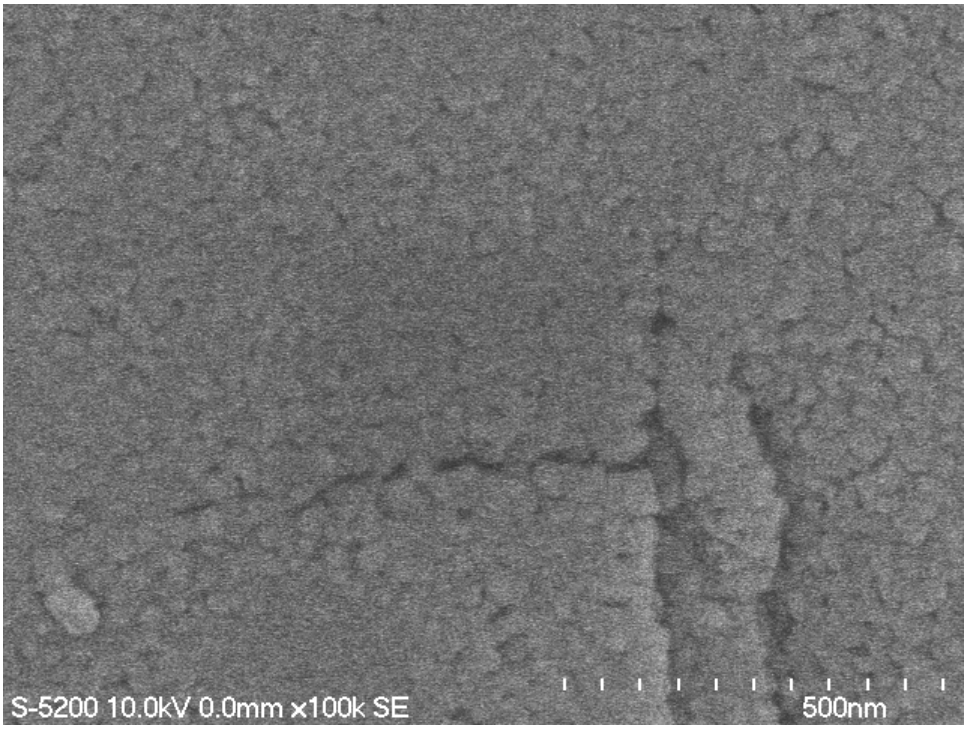

Fig. 3.1 SEM image for as-synthesized silca gel

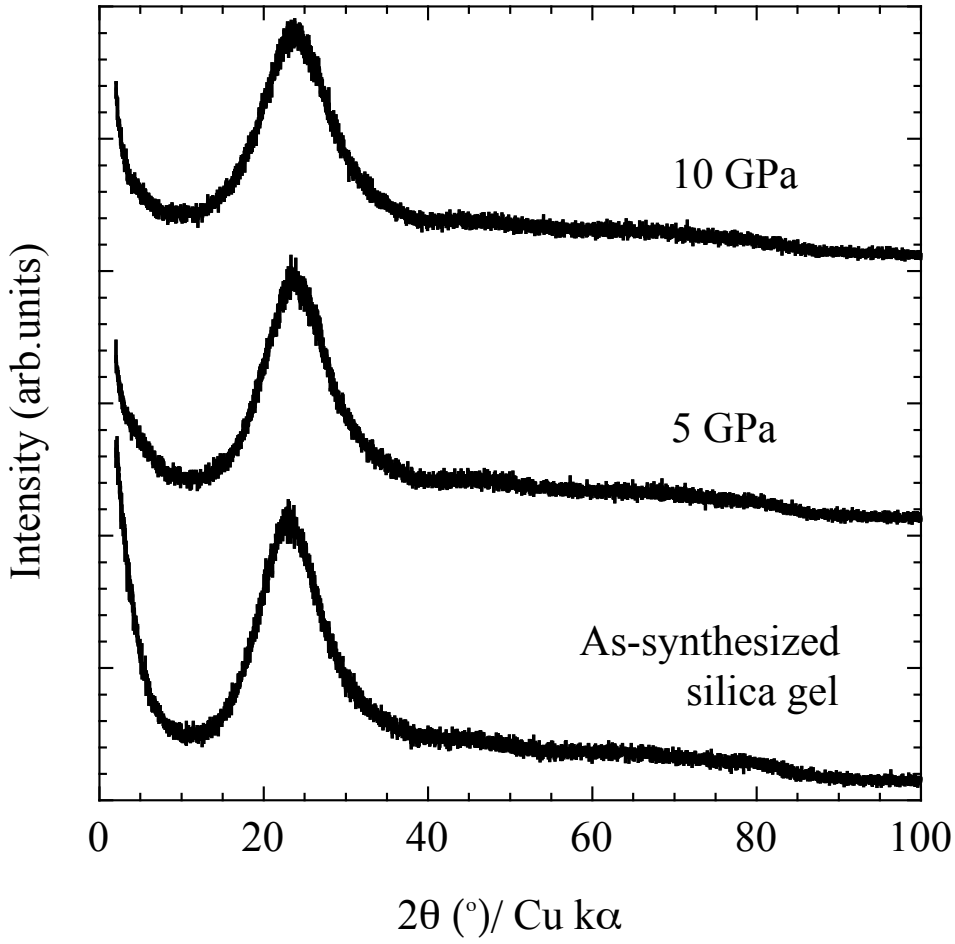

Fig. 3.2 XRD patterns for as-synthesized silica gel and the samples compressed at 5 and 10 GPa under room temperature

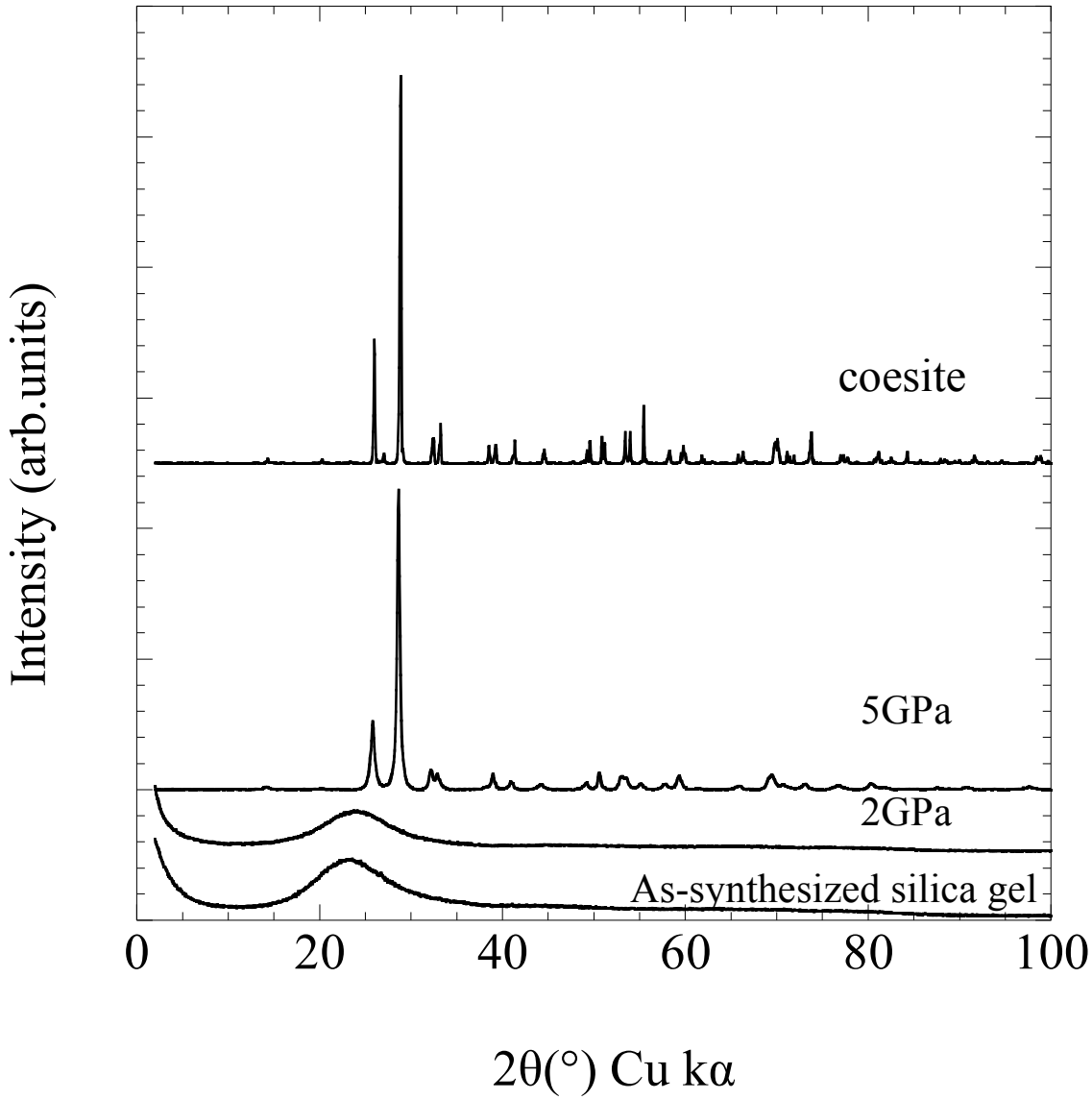

Fig. 3.3 XRD patterns for as-synthesized silica gel, the sample comressed at 2 and 5 GPa under 100 °C, and synthetic coesite. This figure was modified from Arasuna et al. (2013a), © 2013 Shweizebart Science Publishers, http://www.schweizerbart.de

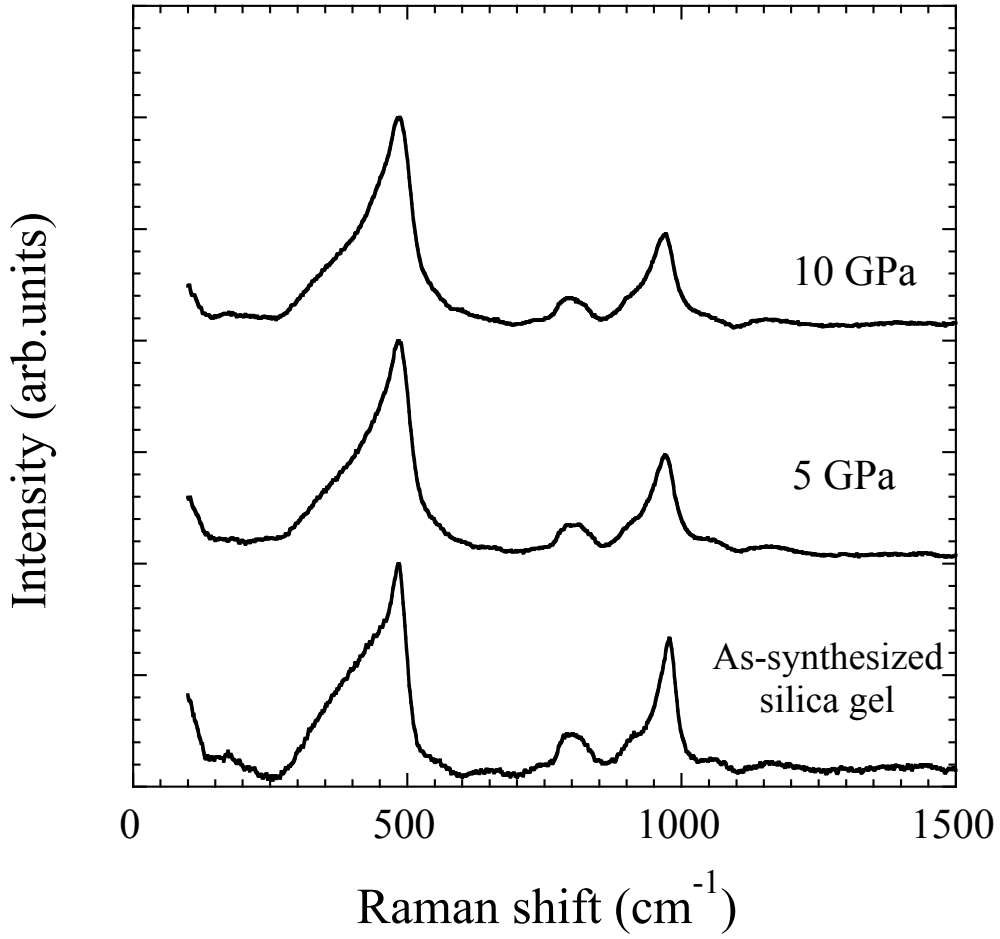

Fig. 3.4 Raman spectra (ν = 100-1500 cm^{-1}) for as-synthesized silica gel and the samples compressed at 5 and 10 GPa under room temperature

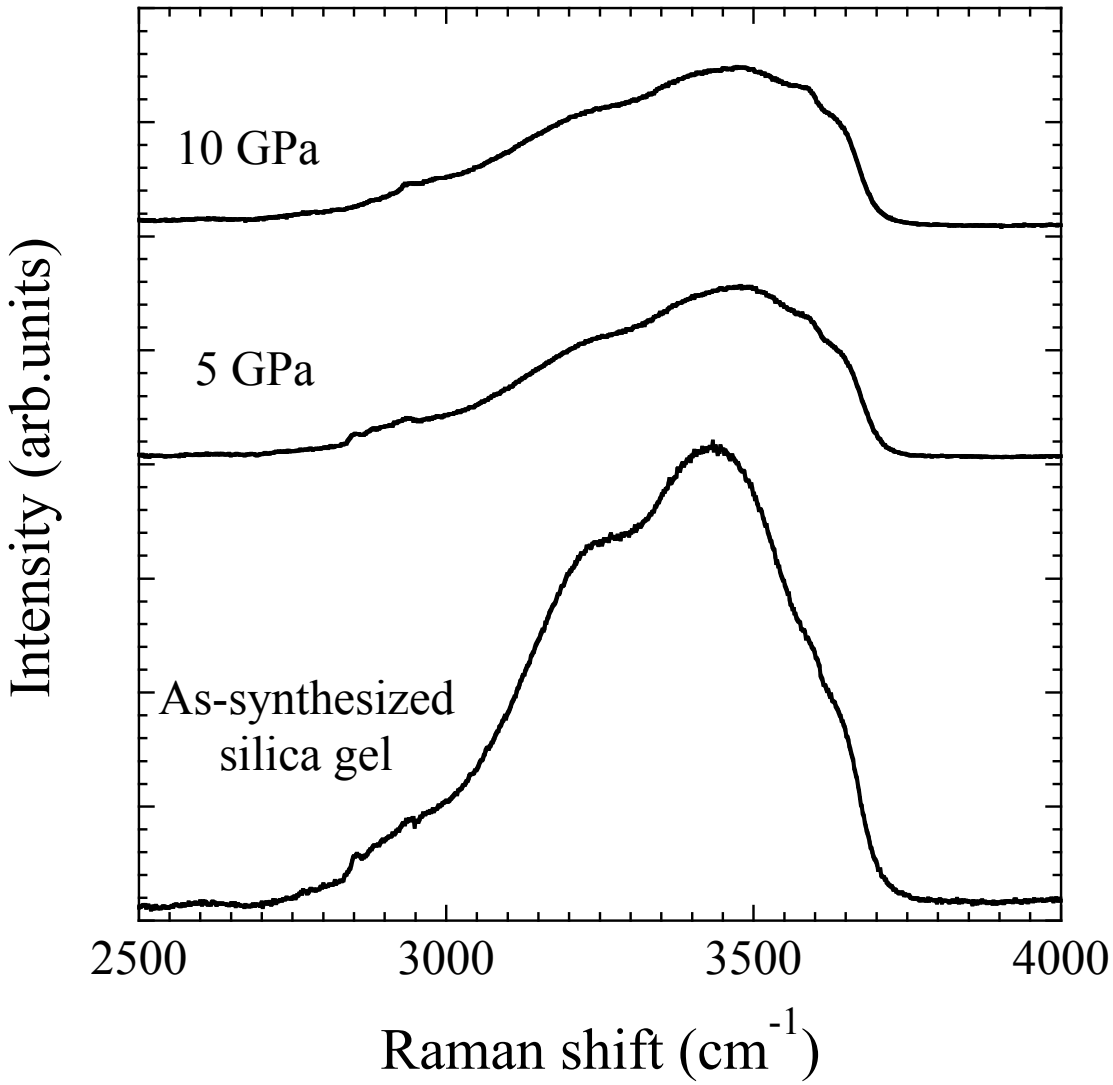

Fig. 3.5 Raman spectra (ν = 2500-4000 cm^{-1}) for as-synthesized silica gel and the samples compressed at 5 and 10 GPa under room temperature

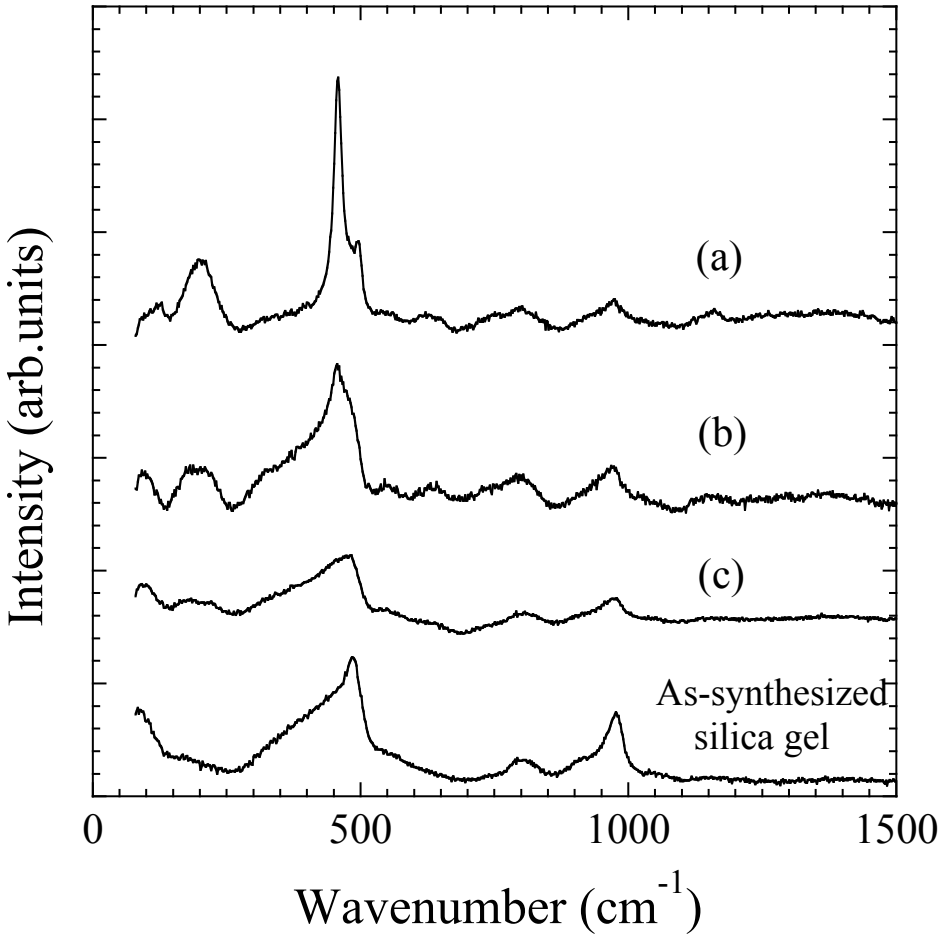

Fig. 3.6 Raman spectra (ν = 100-1500 cm^{-1}) for as-synthesized silica gel and (a)-(c) samples compressed at 2 GPa and 100 °C

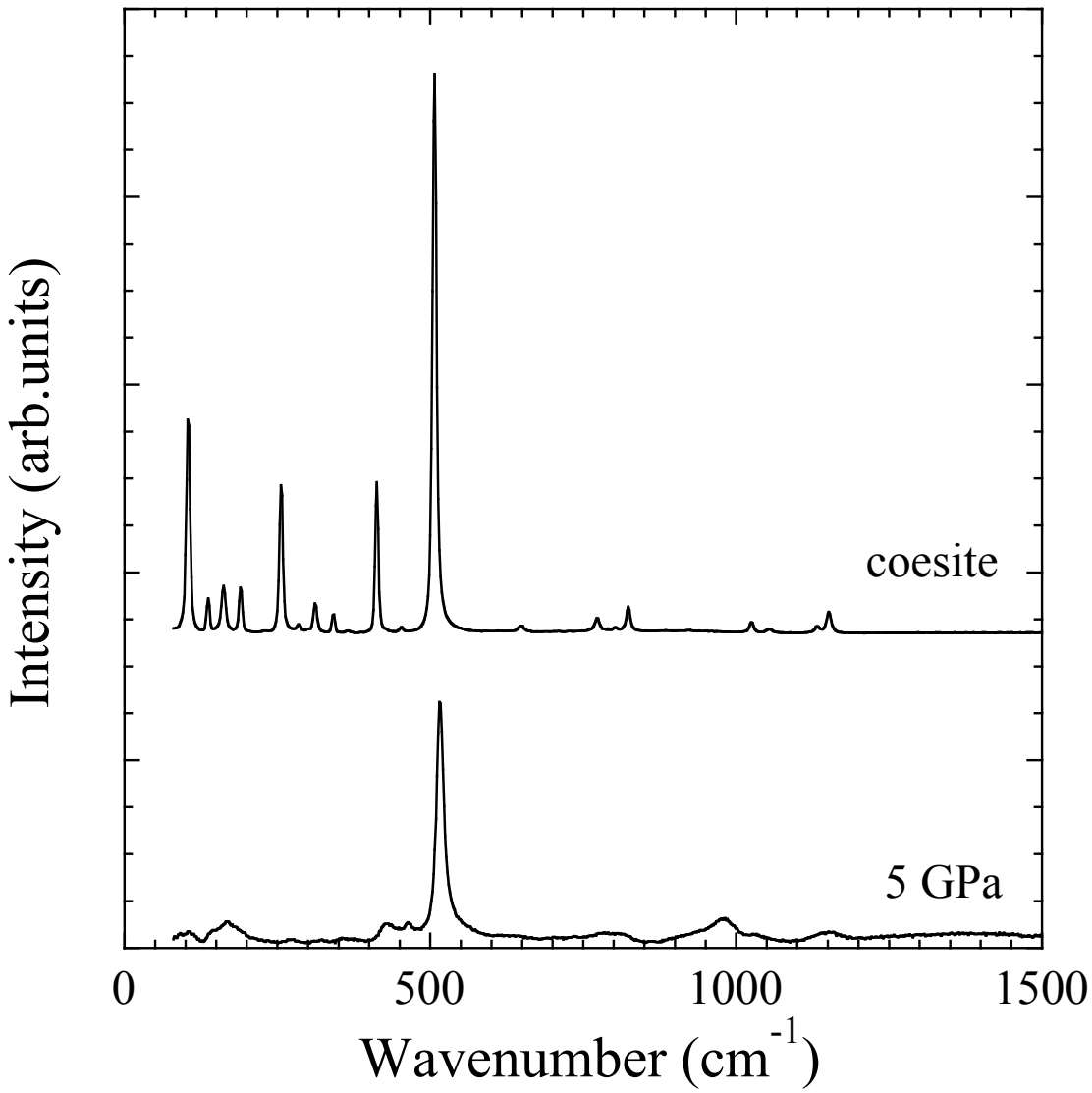

Fig. 3.7 Raman spectra (ν = 100-1500 cm^{-1}) for the sample compressed at 5 GPa and 100 °C and synthetic coesite. This figure was modified from Arasuna et al. (2013a), © 2013 Shweizebart Science Publishers, http://www.schweizerbart.de

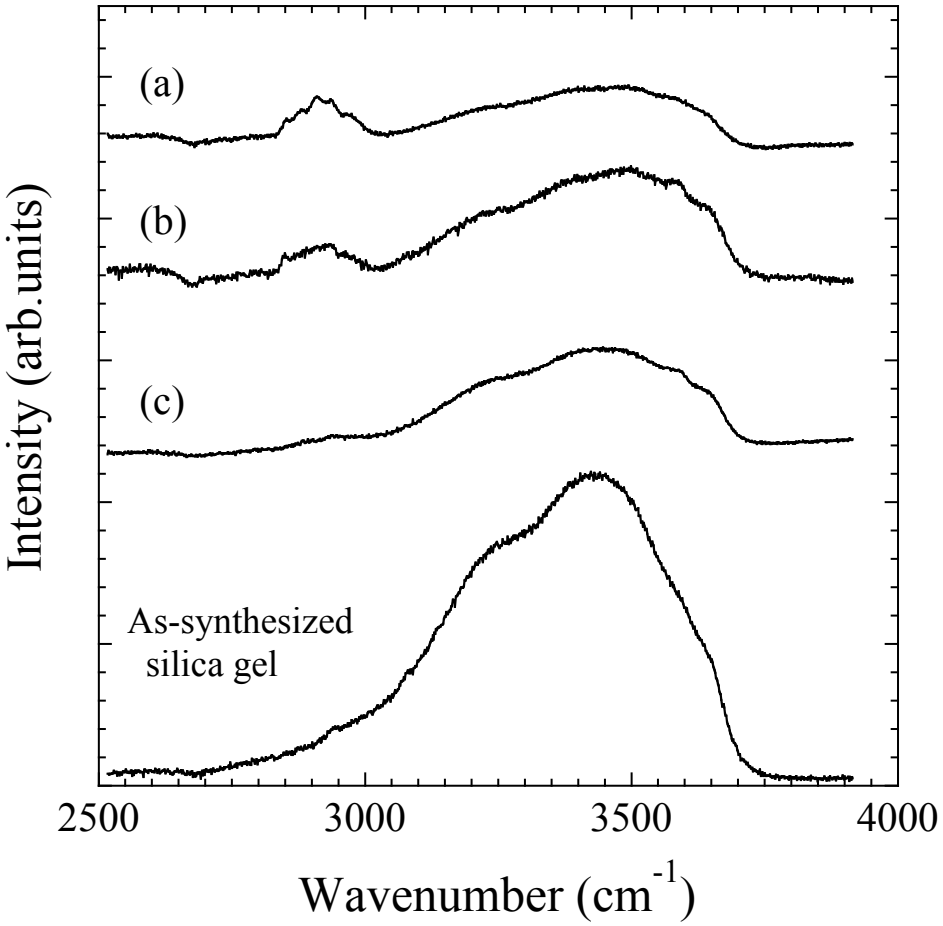

Fig. 3.8 Raman spectra (ν = 2500-4000 cm^{-1}) for as-synthesized silica gel and (a)-(c) sample compressed at 2 GPa and 100 °C

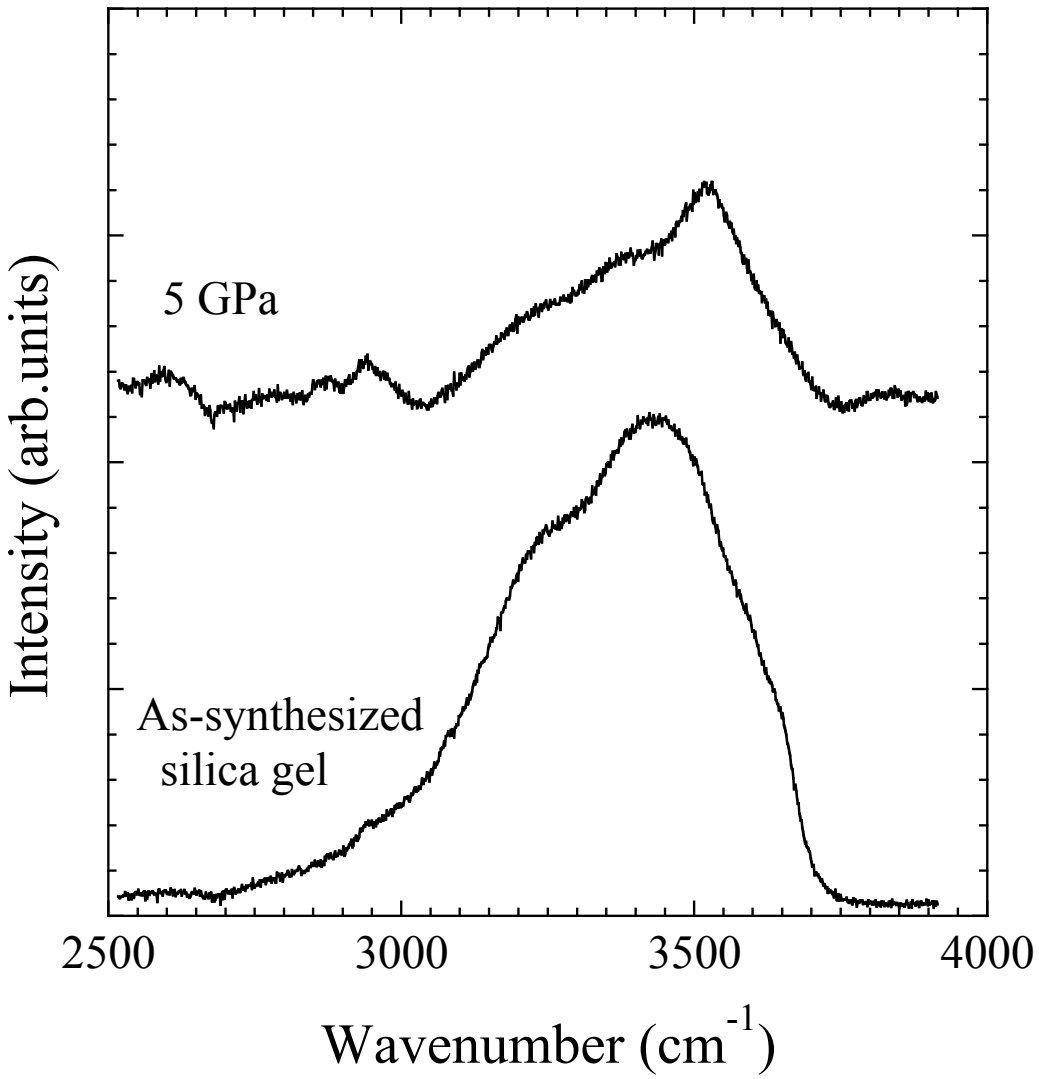

Fig. 3.9 Raman spectra (ν = 2500-4000 cm^{-1}) for as-synthesized silica gel and the sample compressed at 5 GPa and 100 °C. This figure was modified from Arasuna et al. (2013a), © 2013 Shweizebart Science Publishers, http://www.schweizerbart.de

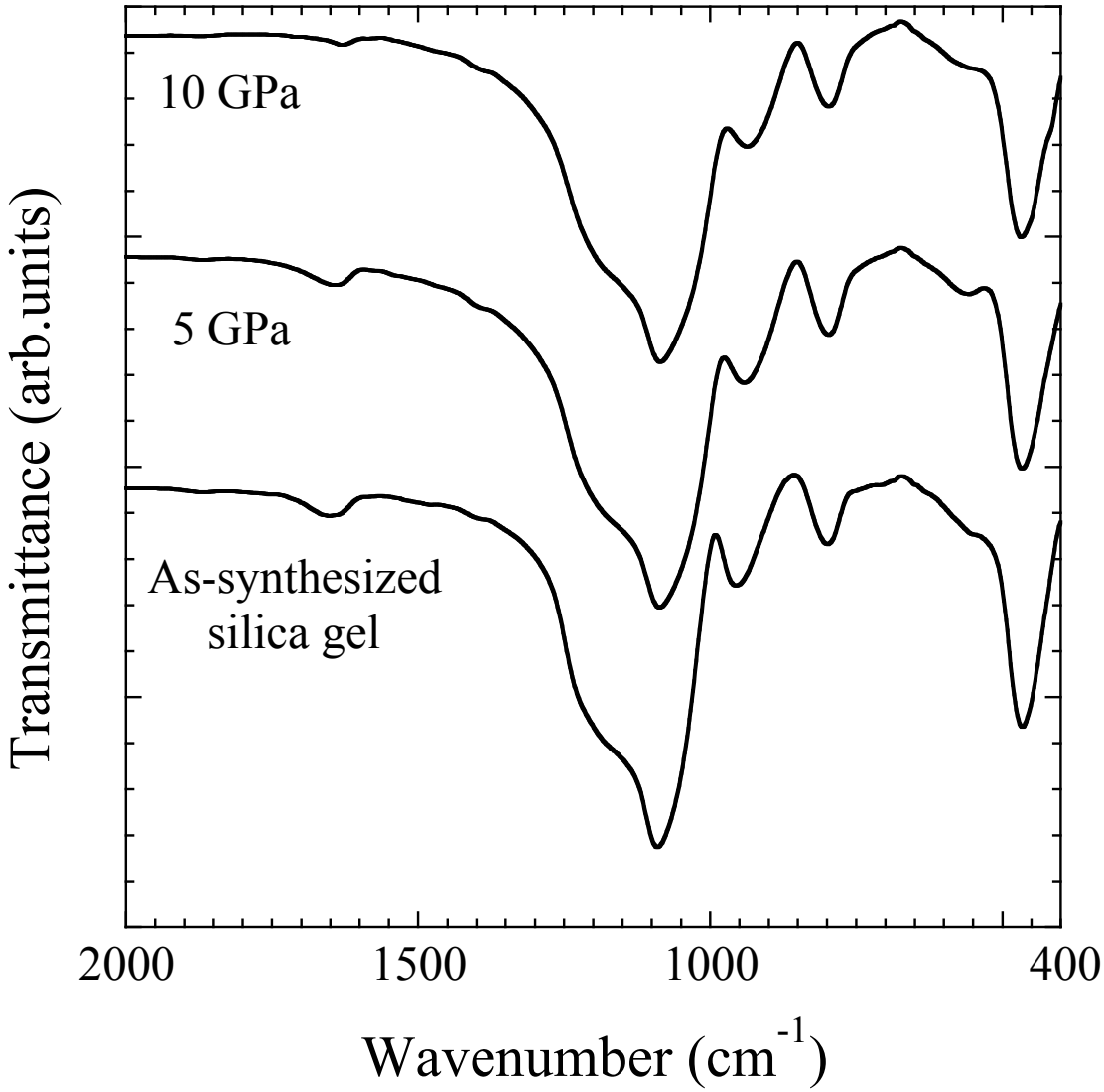

Fig. 3.10 FTIR spectra (ν = 400-2000 cm^{-1}) for as-synthesized silica gel and the samples compressed at 5 and 10 GPa under room temperature

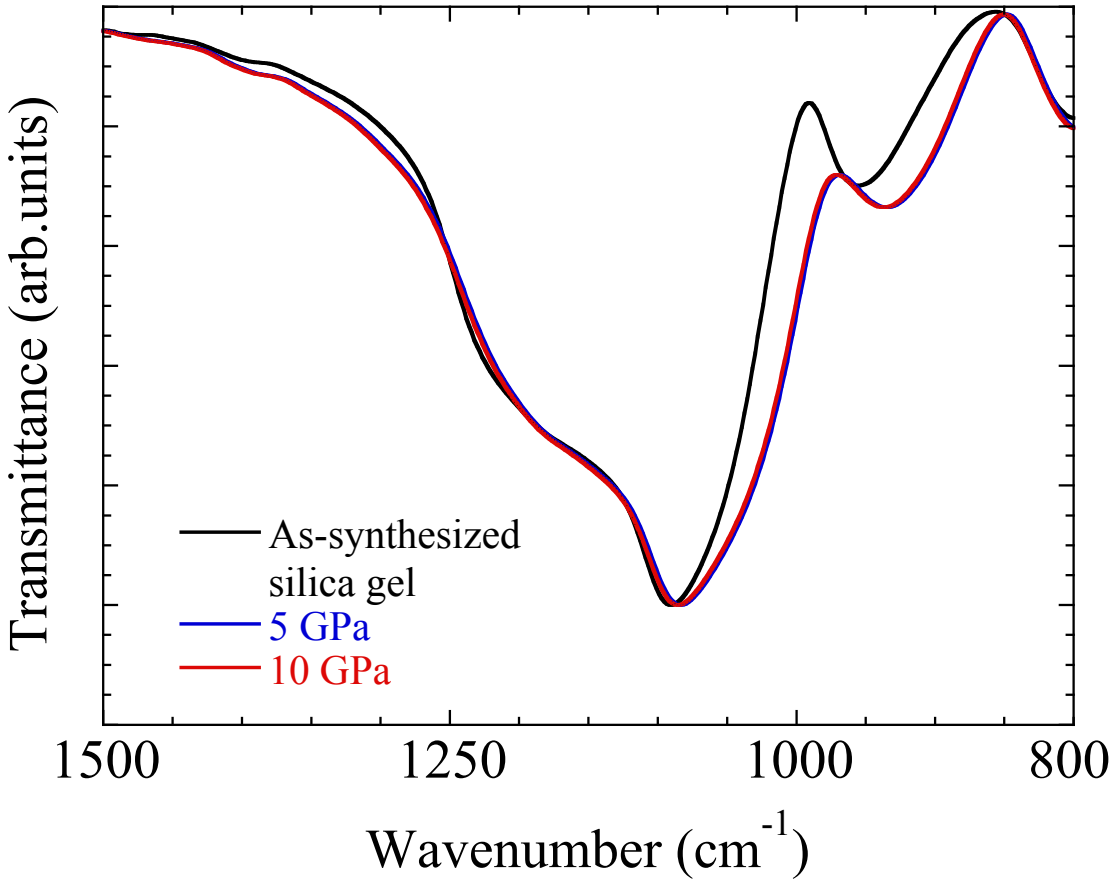

Fig. 3.11 The FTIR spectra in the region of ν = 800-2000 cm^{-1}. All spectra are normalized to the maximum band around ν = 1090 cm^{-1}.

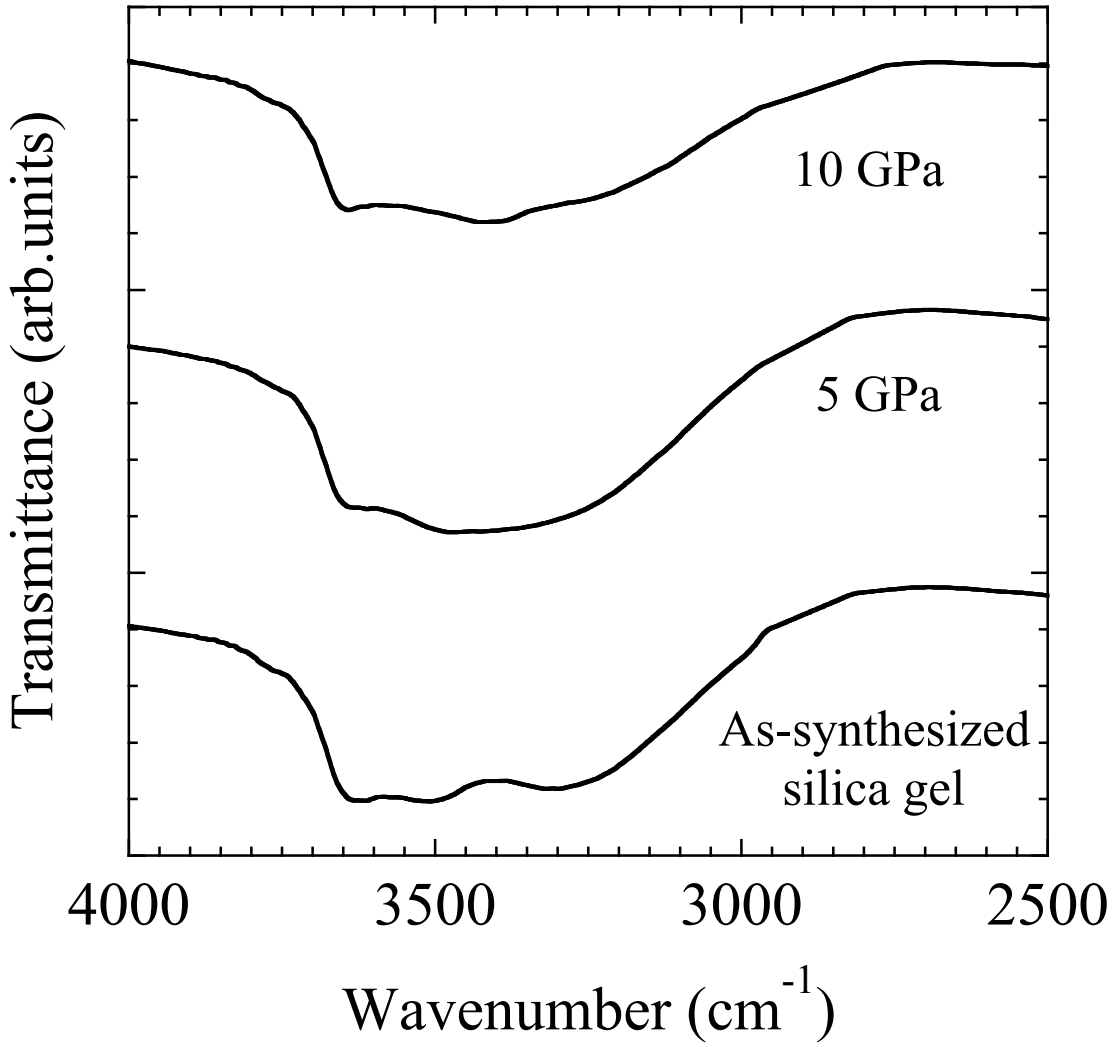

Fig. 3.12 FTIR spectra (ν = 400-2000 cm^{-1}) for as-synthesized silica gel and the samples compressed at 5 and 10 GPa under room temperature

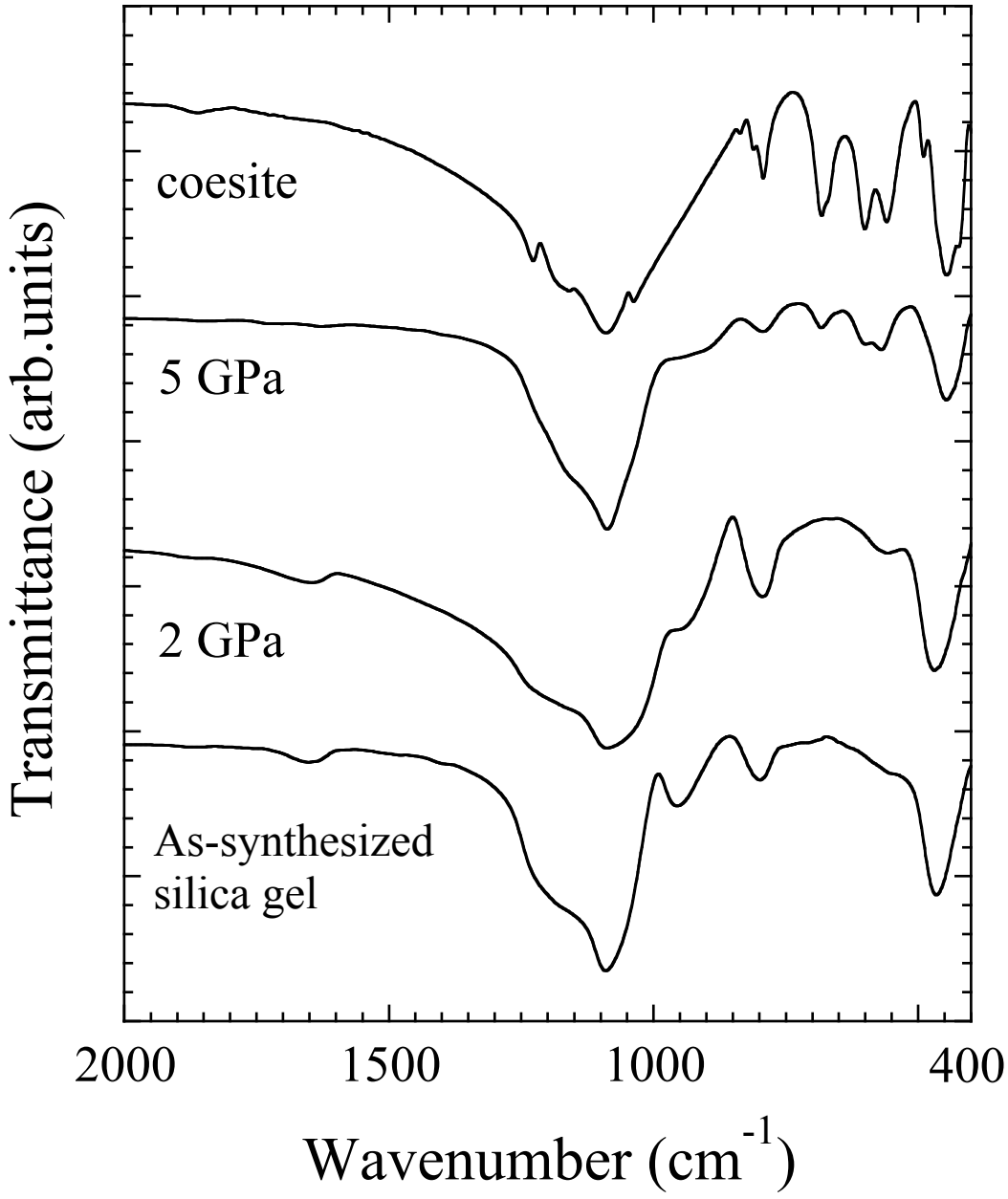

Fig. 3.13 FTIR spectra (ν = 400-2000 cm^{-1}) for as-synthesized silica gel, the samples compressed at 2 and 5 GPa under 100 °C, and synthetic coesite

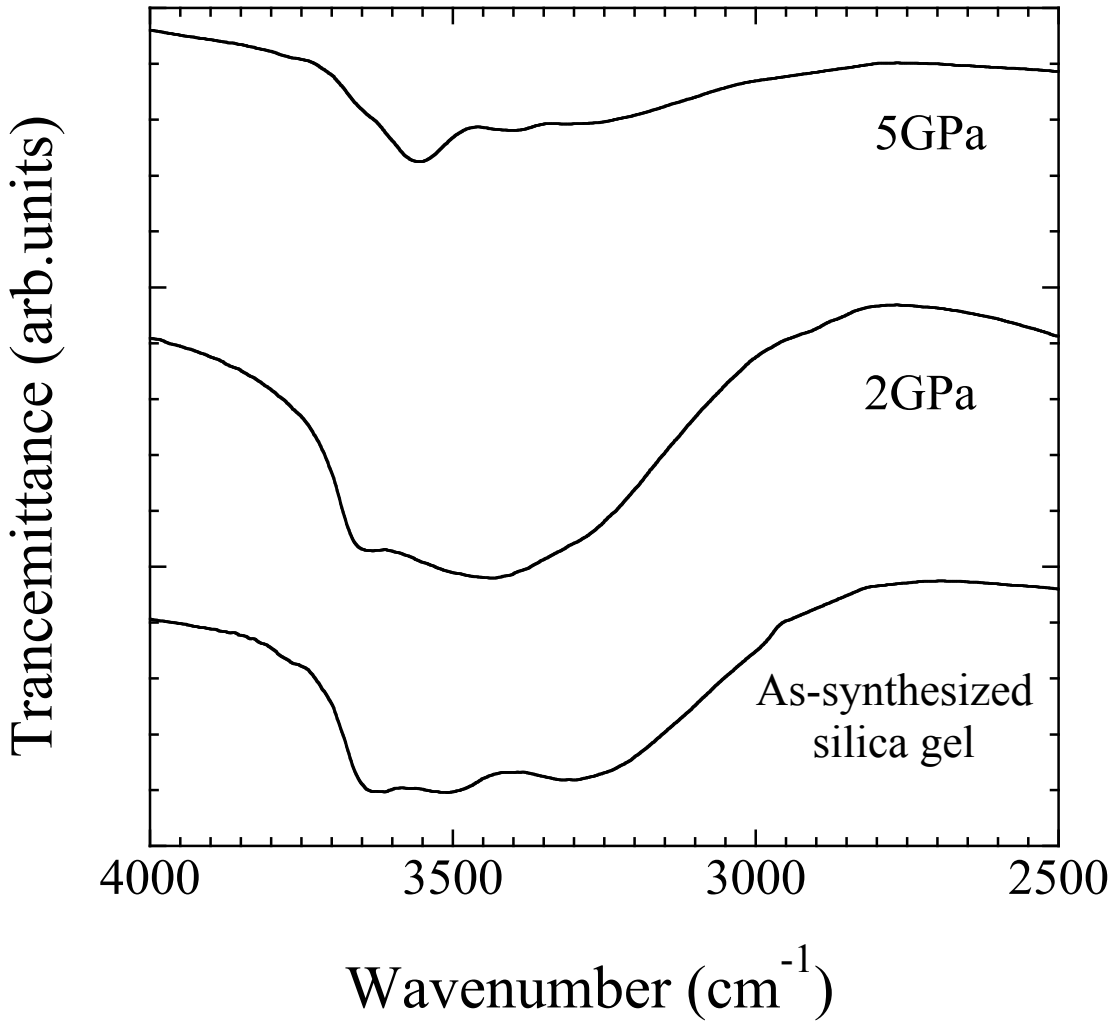

Fig. 3.14 FTIR spectra (ν = 2500-4000 cm^{-1}) for as-synthesized silica gel and the samples compressed at 2 and 5 GPa under 100 °C

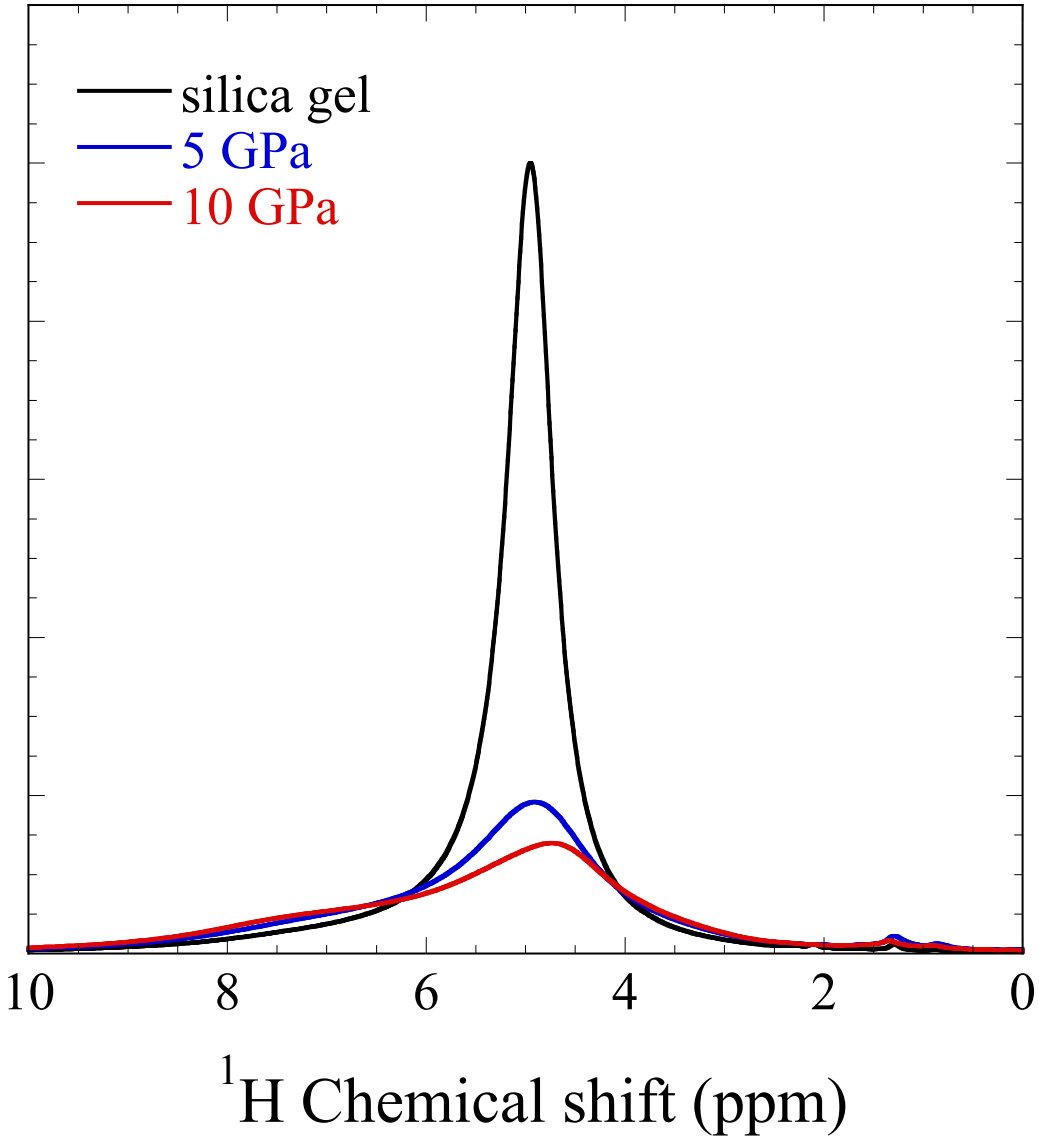

Fig. 3.15 ^{1}H MAS NMR spectra for the as-synthesized silica gel and the samples compressed at 5 and 10 GPa under room temperature

Table 3.1 Total water content in samples measured by ^{1}H MAS NMR

Samples	Water content (wt%)
As-synthesized silica gel	19.6
5 GPa	12.5
10 GPa	10.8

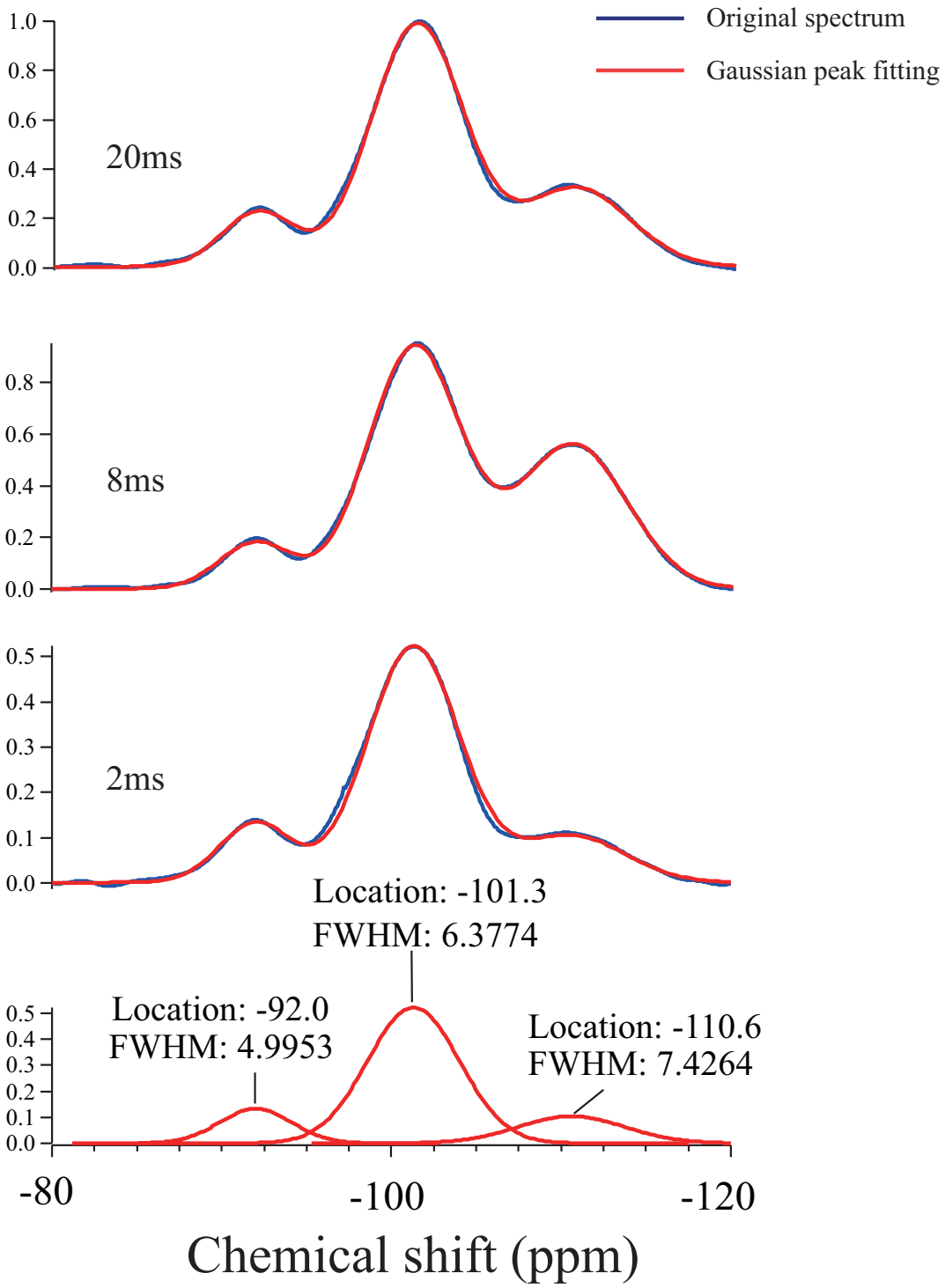

Fig. 3.16 ^{1}H-^{29}Si CP MAS NMR spectra for the as-synthesized silica gel

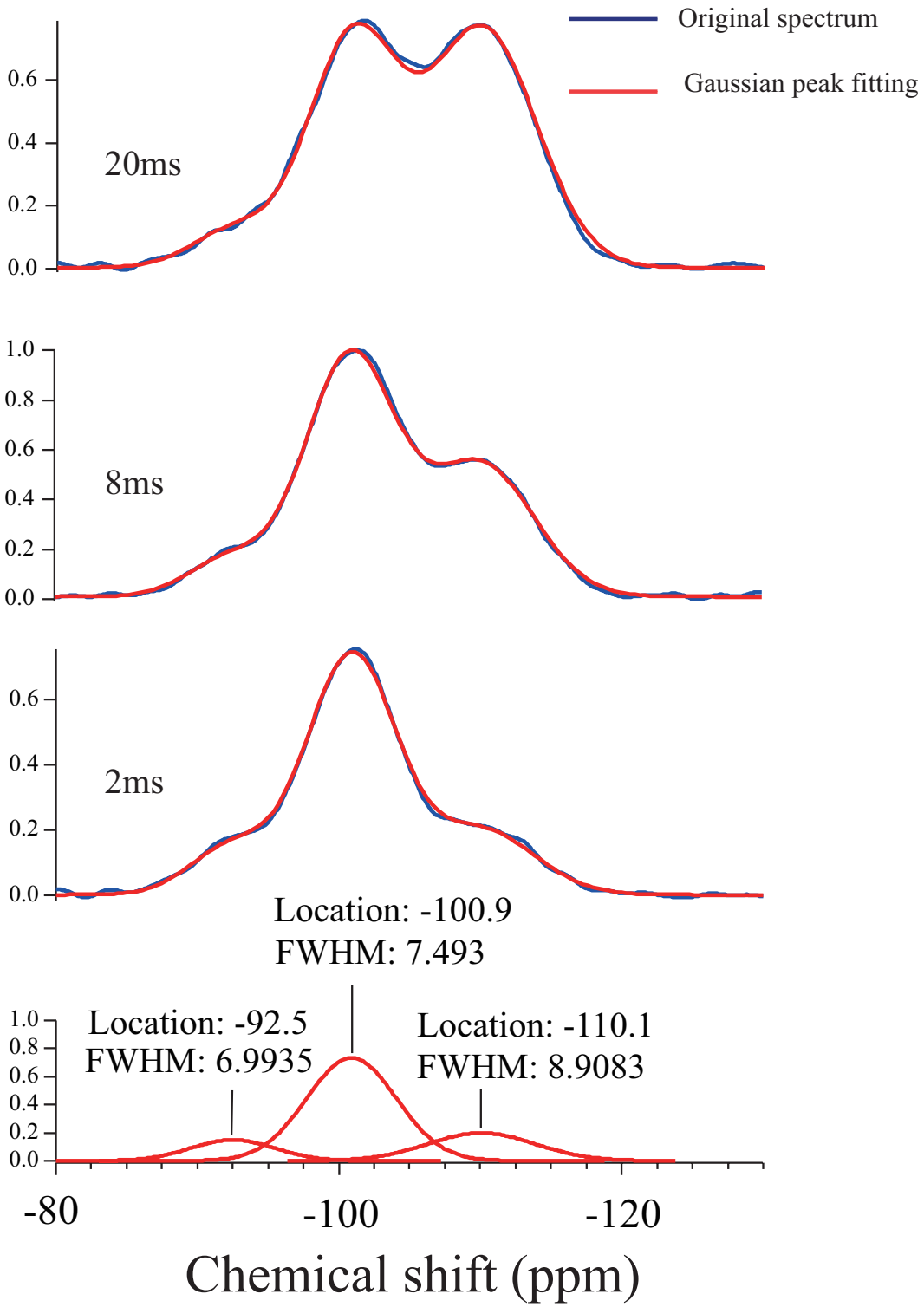

Fig. 3.17 ^{1}H-^{29}Si CP MAS NMR spectra for the sample compressed at 5 GPa under room temperature

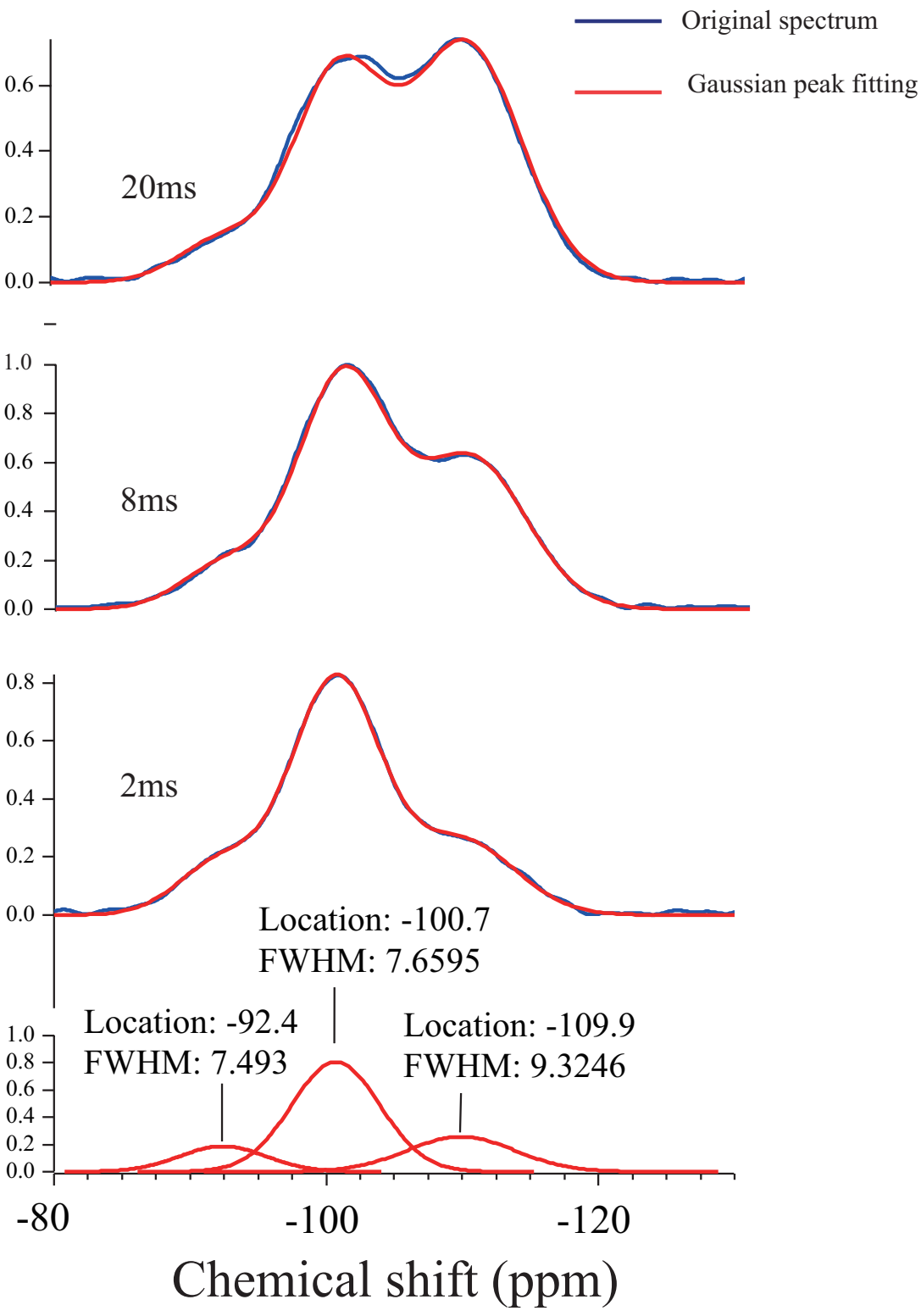

Fig. 3.18 ^{1}H-^{29}Si CP MAS NMR spectra for the sample compressed at 10 GPa under room temperature

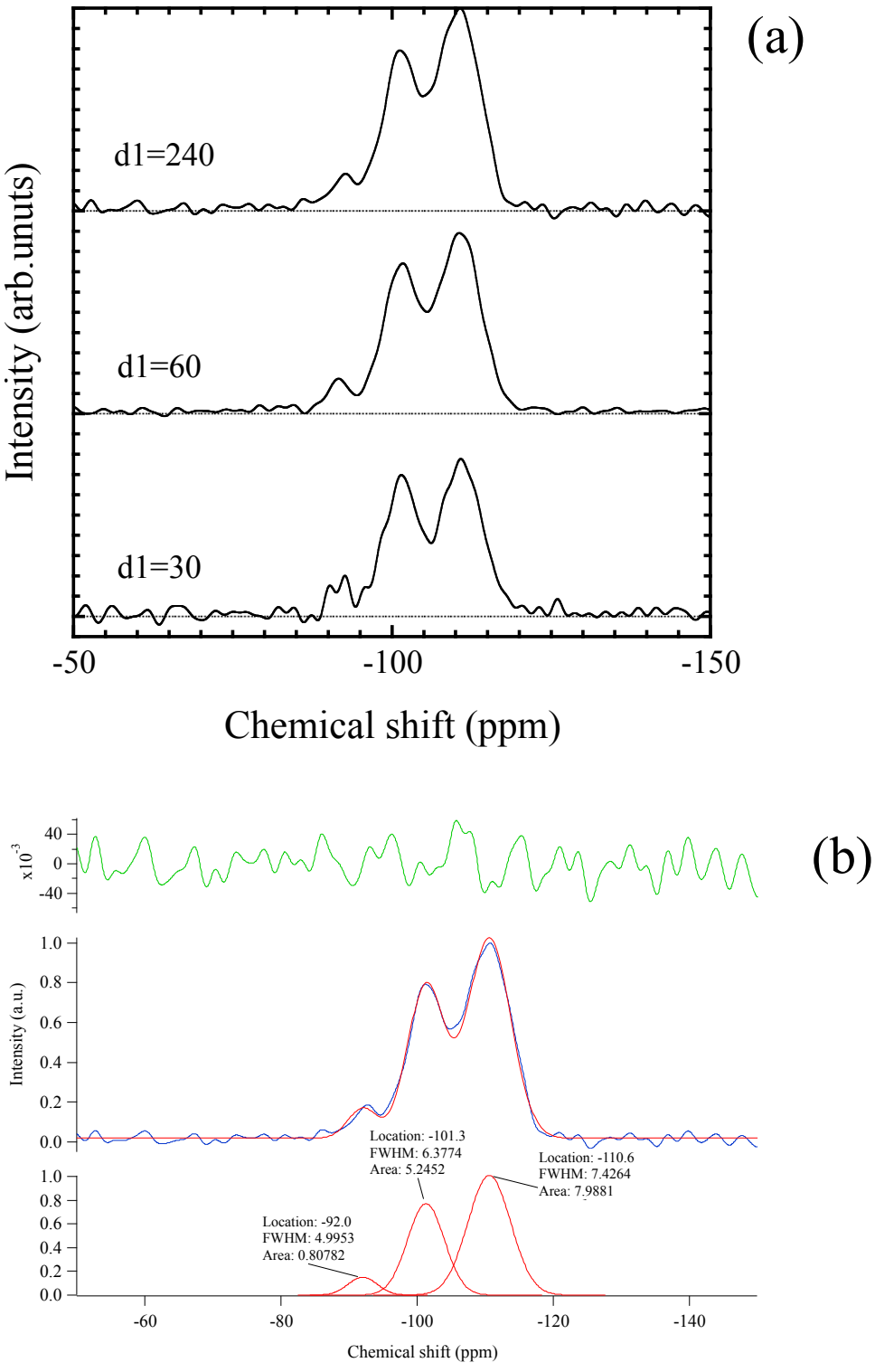

Fig. 3.19 ^{29}Si MAS NMR spectra for the (a) as-synthesized silica gel and (b) result of Gaussian peak fitting of the spectrum of d1=240

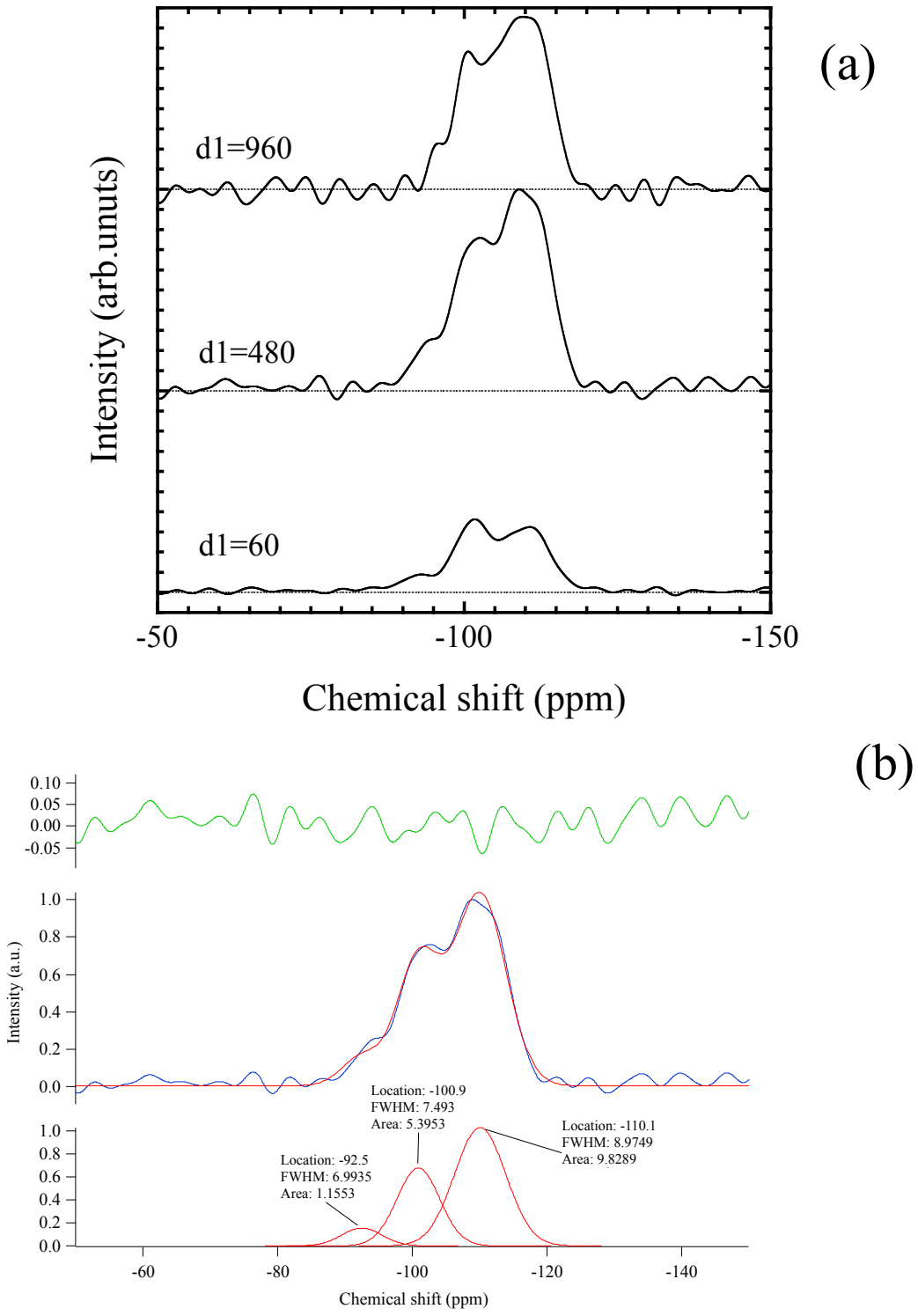

Fig. 3.20 ^{29}Si MAS NMR spectra for the (a) sample compressed at 5 GPa and (b) result of Gaussian peak fitting of the spectrum of d1=480

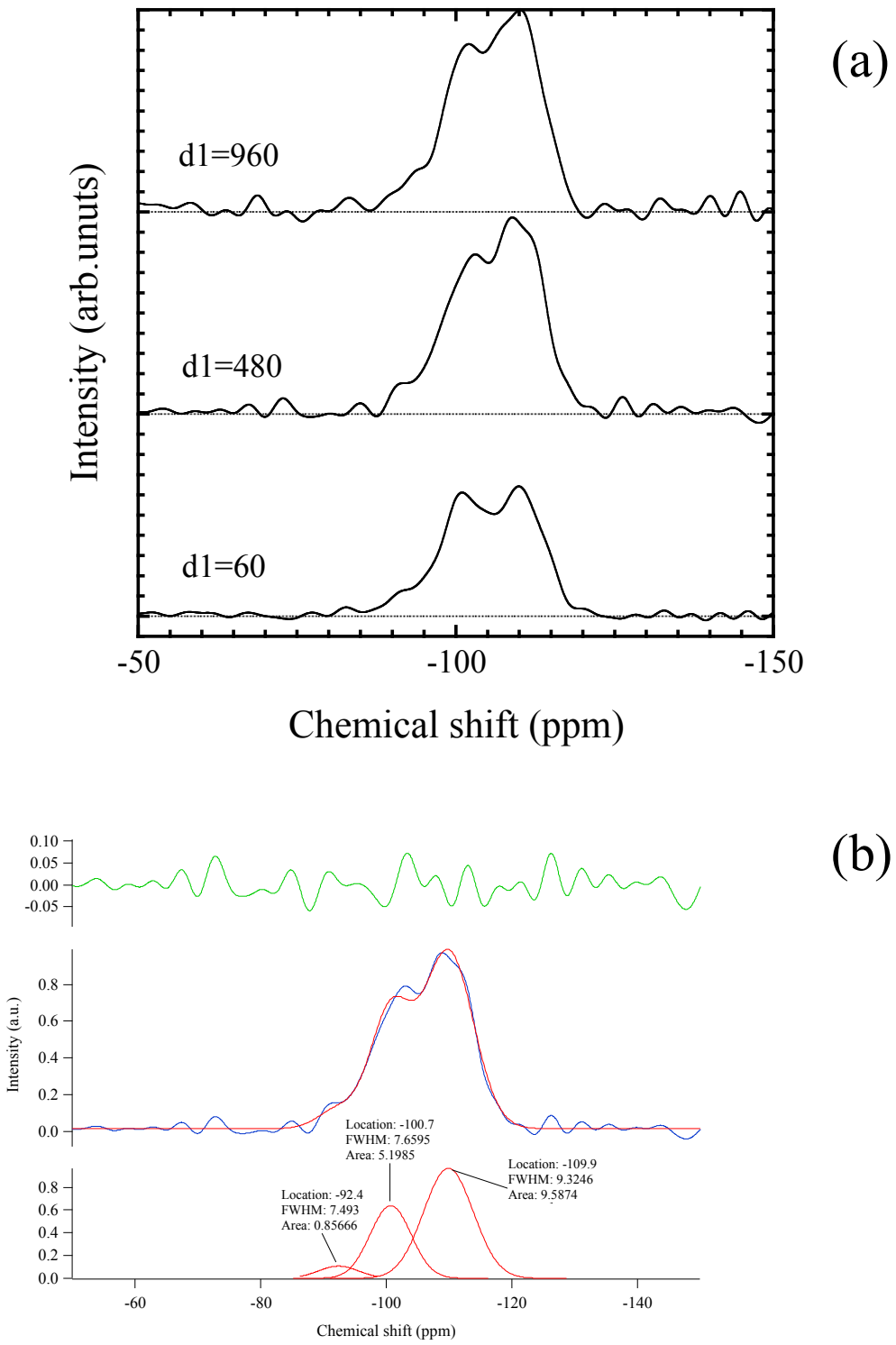

Fig. 3.21 ^{29}Si MAS NMR spectra for the (a) sample compressed at 10 GPa and (b) result of Gaussian peak fitting of the spectrum of d1=480

Table 3.2 Position and FWHM of Q_n peaks by analysis of ^{1}H-^{29}Si CP MAS NMR spectra

Silica gel	Q_4	Q_3	Q_2
Chemical shift (ppm)	-110.6	-101.3	-92.0
FWHM	7.4	6.4	5.0

5GPa	Q_4	Q_3	Q_2
Chemical shift (ppm)	-110.1	-100.9	-92.5
FWHM	9.0	7.5	7.0

10GPa	Q_4	Q_3	Q_2
Chemical shift (ppm)	-109.9	-100.7	-92.4
FWHM	9.3	7.7	7.5

Table 3.3 Relative intensity (%) of Q_n peaks

	Q_4	Q_3	Q_2
Silica gel	57	37	6
5GPa	60	33	7
10GPa	61	33	6

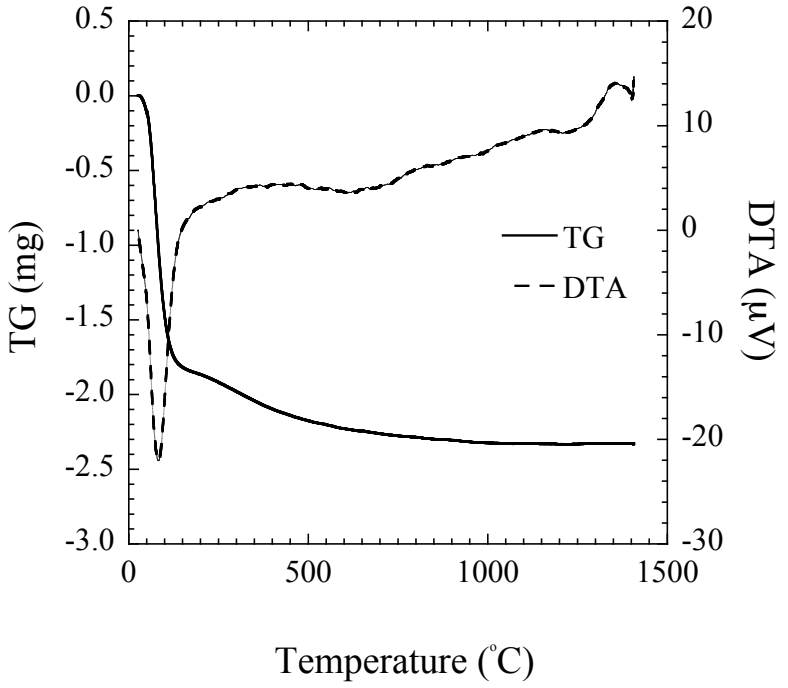

Fig. 3.22 TG-DTA curve for the as-synthesized silica gel

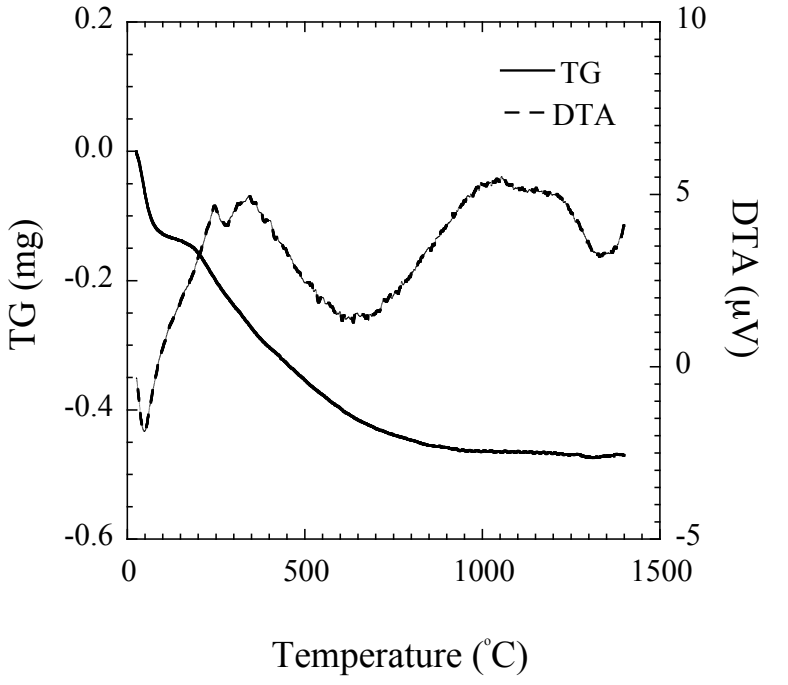

Fig. 3.23 TG-DTA curve for the sample compressed at 5 GPa under 100 °C

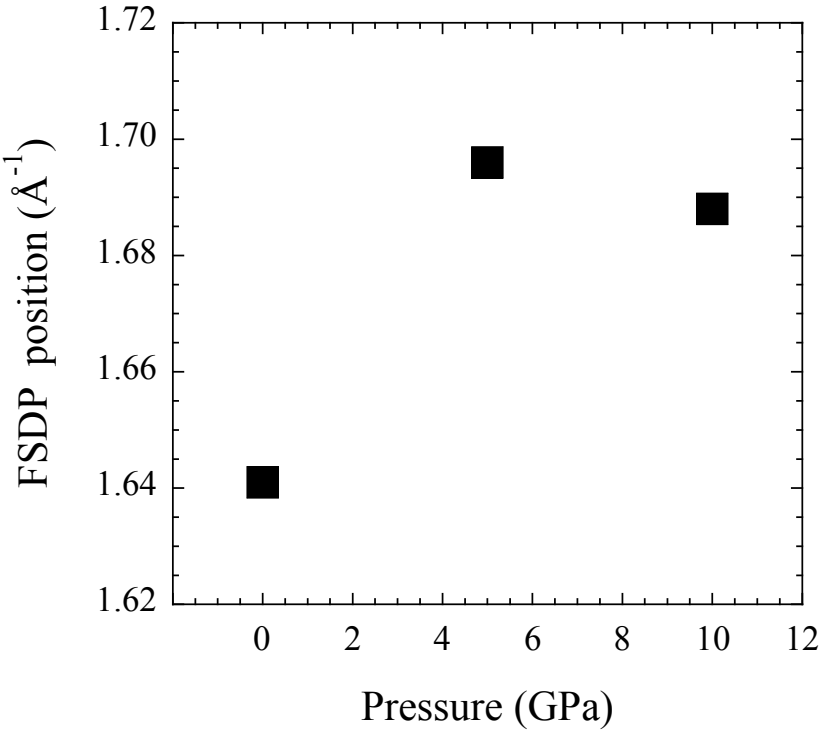

Fig. 3.24 Pressure variation of FSDP for the samples compressed under room temperature

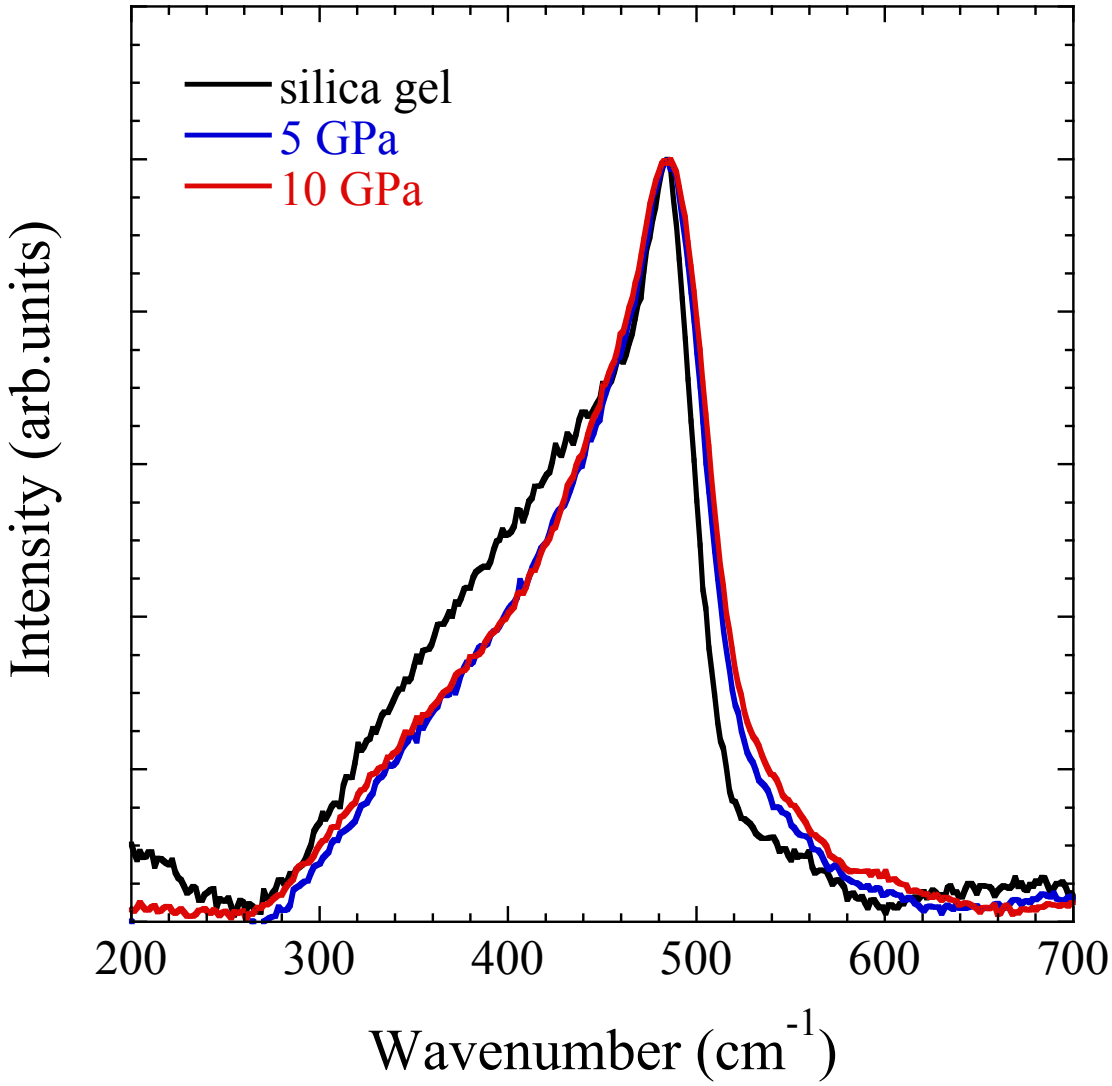

Fig. 3.25 Raman spectra for the as-synthesized silica gel and the samples compressed at 5 and 10 GPa under room temperature.
Spectra are normalized at the band around ν = 480 cm^{-1}.

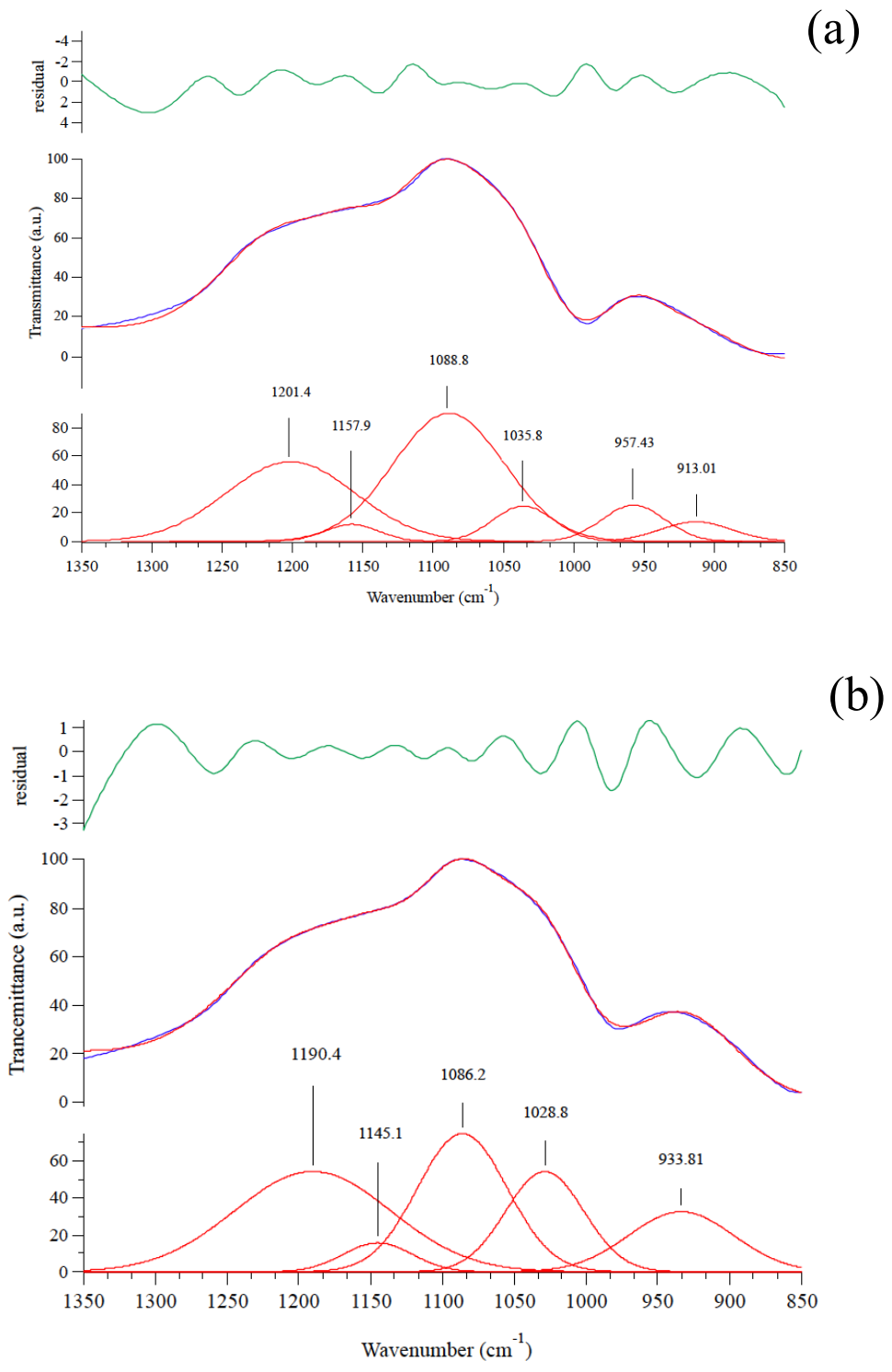

Fig. 3.26 The results of Gaussian peak fittings of the FTIR spectra in the range of ν = 850-1350 cm^{-1} for the (a) as-synthesized silica gel and (b) sample compressed at 5GPa and room temperature

Chapter 4
Structural change of silica gel by shock compressions

4.1 Introduction

Studies on the structural change of silicate crystals and materials by shock-wave compression are important for understanding a meteorite and comet during shock event. The structural evolutions of shock compressed SiO_2 crystals and glasses are investigated by several researchers and are as follows.

DeCarli and Jamienson (1959) performed that the shock compression on natural crystalline quartz and revealed that the shocked quartz transformed to amorphous state over 60 GPa of shock pressure. They reported a temperature of the quartz during shock experiment was calculated to about 1400 K, and the calculated temperature after shock compression was about 1000 K. Stöffler (1994) summarized that the shock behavior of quartz, and reported that compressed quartz above shock compression of 50 GPa has similar feature of fused quartz. Tattevin et al. (1990) reported that a vitrification of quartz by shock compression was strongly influenced by the shock compression without high temperature during and after shock compression.

Study on a structural change of cristobalite by shock compression was reported by Gratz et al. (1993). They reported that cristobalite transformed to amorphous state above 28 GPa. The shock induced diaplectic glass from cristobalite has similar reflective index and density with those of the diaplectic glass made from quartz.

On the other hand, studies on the shock behavior for silicate glasses were reported by several researchers. Okuno et al. (1999) reported that the structure of SiO_2 glass was densified by shock compression of about 26 GPa. In the reference cited above, they concluded that shock-induced densification of silica glass was attributed to the reduction of the average Si-O-Si angle, which was caused by the collapse of the largest ring cavities with the successive formation of small rings of SiO_4 tetrahedra, such as three- and four-membered rings. Above 32 GPa, high after shock residual temperature relax the densified structure of shocked silica glass (Okuno et al., 1999). Pressure variation of FSDP position for shocked samples seems to be influenced by the density of the sample, *e.g.*, the positive shift of FSDP position with the densification of the shocked sample (Shimada et al., 2002). Shock behavior of the albite ($NaAlSi_3O_8$) glass

(Takabatake, 2000) was roughly similar to that of SiO_2 glass. Shimoda et al. (2004) performed the shock-wave experiments for the obsidian and its fused glass, and they reported that the recovered sample from shock compression shows the similar tendency of the densification.

On the other hand, structural change of amorphous silica including water molecules and silanol group by shock compression has not been investigated until the report of the shock compression behavior of synthetic opal (Inoue et al., 2010). Synthetic opal, which is hydrous amorphous silica material, has shown simultaneous change of the dehydration and polymerization of surface silanol and transformation of network structure by shock compression at above 18.4 GPa (Inoue et al., 2010).

In this study, the shock compression experiment for TEOS-derived silica gel including 23 wt% of water was performed as a model experiment for impact event of comet nucleus on the Earth surface. The samples recovered from the shock compression experiments were investigated by means of X-ray diffraction measurement, Raman and FTIR spectroscopies, and TG-DTA analyses.

4.2 Experimental

4.2.1 Shock-wave experiments

Shock wave experiments for TEOS-derived silica gels were performed by using a single stage propellant gun (Mashimo et al., 1984) at Research Institute for Pulse Power Sciences of Kumamoto University, Japan. As-synthesized silica gel was formed to a disk, 12mm in diameter and 2mm in thickness, which was encased in a stainless container. The specimen containers were hit by metal projectiles with velocities of 0.88-1.05 km/s. Shock pressures were estimated from measured projectile velocities, using the impedance matching method. The velocities of metal projectiles and shock pressures are listed in Table 4.1. All recovered samples from shock compressions are shown in figure 4.1. Samples compressed up to 17.0 GPa are transparence. The sample compressed at 20.7 GPa is white block in the center part and transparence in the periphery. Over 27.2 GPa, the samples transformed to white block totally. All shock compressed samples were investigated by XRD, Raman and FTIR spectroscopies, and

TG-DTA measurements. The obtained results were compared to that of commercially available synthetic silica glass.

4.2.2 X-ray diffraction measurement

XRD measurements were performed by using Rigaku RINT 2200 with Cu Kα radiation. The θ-2θ scanning technique was adopted over the range of 2θ = 2-60° with a scan step of 0.05° for the shock compressed samples. The applied acceleration voltage and current used were 40 kV and 30 mA, respectively.

4.2.3 Raman spectroscopy

Raman spectra for samples were recorded by using micro-Raman spectrometers (Lab RAM HR800, Horiba, Jovin Yvon). The 514.5 nm line of Ar^+ laser (MELLES GRIOT, 43 SERIES ION LASER, 543-GS-A02) was used to excite Raman scattering. A grating with 600 lines/nm was used to give a wavenumber resolution of 1.4-1.8 cm^{-1} and a spectral resolution of approximately ± 1.6cm^{-1} in the spectral range. All of the observed Raman spectra were corrected for background.

4.2.4 Infrared spectroscopy

FTIR measurements were performed by using FTIR spectrometer (JASCO FT/IR 610 V) with KBr micro-pellet transmission method. Spectra were recorded in the range of ν = 400 - 4000 cm^{-1} with a band path of 4 cm^{-1} for all of the samples.

Attenuated total reflection (ATR) – IR measurements were recorded using ATR-IR spectrometer (Thermo Scientific Nicolet iS10) equipped with diamond crystal. Spectra of samples were recorded in the range of ν = 2500 - 4000 cm^{-1} with a band path of 4 cm^{-1}.

4.2.5 TG-DTA measurement

TG-DTA measurements were performed by using a Rigaku Thermo Plus 2 Tg 8120. The as-synthesized silica gel and the samples shock compressed at 20.7 and 27.2 GPa

were ground and then each 5 mg sample was put into a Pt pan. The samples were heated to 1400 °C at a heating rate of 10 °C min^{-1} in a nitrogen atmosphere.

4.3 Results

4.3.1 X-ray diffraction analysis

The observed X-ray diffraction patterns for as-synthesized silica gel and all shock compressed samples show the diffuse scattering maximum centered at around $2\theta = 23°$ without any typical sharp peaks (Fig. 4.2). With increasing pressure, the center of this scattering maximum shifts gradually from $2\theta = 23.4°$ in as-synthesized silica gel to 22.0° in the sample compressed at 30.9 GPa. All recovered sample shows no evidence of shock-induced crystallization of silica gel.

The intensity of small angle scattering around $2\theta = 2°$ roughly decreases with increasing shock pressure, whereas somewhat fluctuations of intensity is observed. The reduction rate in intensity at $2\theta = 2°$ is about 47 % after the shock compression at 30.9 GPa.

4.3.2 Raman spectroscopic analysis

Raman spectra for as-synthesized silica gel and the compressed samples are shown in figure 4.3. These spectra are normalized at the intensity of D_1 band at around $\nu = 480cm^{-1}$ and it should be noted that the meaning Raman spectrum for the sample of 30.9 GPa was not obtained because of strong luminescence.

As I noted in the chapter 3.3.3, the Raman spectrum of as-synthesized silica gel shows a broad bands at around $\nu = 450\ cm^{-1}$ due to a symmetrical Si-O-Si stretching mode and D_1 band at $\nu = 480\ cm^{-1}$ (Galeener, 1982a and b; Galeener and Geissberger, 1983; Sharma et al., 1984). The band at around $\nu = 800\ cm^{-1}$ is attributed to the oxygen vibrations perpendicular to the Si-Si line (McMillan and Wolf, 1995) and the sharp band at $\nu = 979\ cm^{-1}$ is due to the silanol (Stolen and Walrafen, 1976; Murray and Greytak, 1979).

The Raman spectrum for the sample compressed at 20.7 GPa shows changes the broad

bands of symmetrical Si-O-Si stretching and silanol. The broad band below ν = 480 cm^{-1} becomes broader and the silanol band may become less intense. The band around ν = 980 cm^{-1} may contain the two bands of differential silanol groups, namely Q_2 and Q_3 bands (see chapter 3.3.3). After the shock compression at 20.7 GPa, the Q3 band may become less intense and the Q_2 band is not distinct in the Raman spectrum (Fig. 4.4). Moreover, Q_3 band shifts toward to lower frequency gradually.

In higher frequency region, Raman spectrum of as-synthesized silica gel shows the broad band centered at ν = 3400 cm^{-1} (Fig. 4.5). This broad band is due to the water molecules and silanol bands and may be composed of peaks located around ν = 3250 and 3430 cm^{-1} with the weak shoulders around ν = 3600 and 3640 cm^{-1}. The lower weak components around ν = 2900 cm^{-1} may be due to the CH absorption of residual starting TESO solution (Innocenzi, 2003). The detailed assignment of bands above ν = 3250 cm^{-1} will be discussed later.

After the shock compression at 27.2 GPa, the broad band due to water molecules and silanol is clearly observed. However, bands at around ν = 3650 and 3600 cm^{-1} becomes prominent after the compression above 20.7 GPa.

4.3.3 Infrared spectroscopic analysis

Figure 4.6 shows that FTIR spectra of as-synthesized silica gel and the compressed samples contain three distinct bands due to the mode of Si-O anti-symmetric stretching, Si-O-Si bending and rocking, which located at around ν = 1090, 800 and 467 cm^{-1}, respectively (Handke and Mozgawa, 1993). The spectrum of silica gel also shows the band corresponding to the silanol at ν = 960 cm^{-1} and the band attributed to water molecules at ν = 1653 cm^{-1} (Orcel et al., 1986; Benesi and Jones, 1959).

With increasing shock pressures, the positive shift of the Si-O stretching band at around ν = 1090 cm^{-1} is observed. Finally, this band position increases by 13 cm^{-1} at 30.9 GPa and approaches to that of silica glass (Fig. 4.7). The band of Si-O-Si bending mode at ν = 798 cm^{-1} shows the pressure variation of its position (Fig. 4.8). Furthermore, the intensity of the band of Si-OH may decrease gradually with increasing shock pressure (Fig. 4.6), and this band position shows the negative shift about 9 cm^{-1} at 30.9 GPa. Above 20.7 GPa, this band presents as a weak shoulder of the band of Si-O stretching. The band of water molecules around ν = 1653 cm^{-1} also shows the decrease

of the intensity with increasing pressure and completely disappears at 30.9 GPa.

In higher frequency region ν = 2500 - 4000 cm^{-1}, the spectrum for as-synthesized silica gel has a broad band centered at ν = 3500 cm^{-1} which should be attributed to the bands of water molecules and silanol groups (Fig. 4.9). This broad band becomes less intense with increasing pressure. At the compression at 30.9 GPa, only the weak band at ν = 3650 cm^{-1} is observed. This band may be attributed to the OH stretching mode of silanol (Walrafen and Samanta, 1978; Stone and Walrafen, 1982; Graetsch et al., 1985). Moreover, in previous study for silica gel (Bergna, 2006 and reference listed herein), the FTIR band around ν = 3660 cm^{-1} in silica gel sample may indicate the presence of vicinal silanol, which means mutually hydrogen bonded silanol groups.

ATR-IR spectra (ν = 2500 - 4000 cm^{-1}) for the samples are measured to examine the presence of the water and silanol in the shock compressed samples (Fig. 4.10). The ATR spectrum for the as-synthesized silica gel shows the broad band centered at ν = 3350 cm^{-1} due to the water molecules and silanol groups. After the compression at 30.9 GPa, the spectrum of compressed sample shows the broad band yet, although the intensity of this band may decrease. Moreover, the weak shoulder around ν = 3655 cm^{-1} is observed.

4.3.4 TG-DTA analysis

TG-DTA curves for as-synthesized silica gel and samples compressed at 17.0 and 27.2 GPa are present in figure 4.11. Other compressed samples were not obtained, because the quantity of samples was not enough to perform the TG-DTA measurements.

The TG curve of roughly grounded as-synthesized silica gel shows that large weight loss (15.8 wt%) up to 160 °C and then the gradual weight loss (4.3 wt%) up to 1400 °C. Observed total weight loss is about 20.1 wt%. DTA curve has a relatively strong endothermic band around 63 °C.

TG curve for the compressed sample at 17.0 GPa shows a similar weight loss with that of silica gel. 13.1 wt% of weight loss is observed up to 160 °C and then 4.9 wt% of small weight loss is observed up to 1400 °C. Total weight loss is about 18.0 wt%. However, the sample of 27.2 GPa shows the considerable small weight loss than other two samples. 3.6 wt% of small first weight loss is observed up to 160 °C and following smaller weight loss (2.5 wt%) is observed up to 1400°C. Total weight loss is about 6.1

wt%. DTA curves of these compressed samples at 18.0 and 27.2 GPa show an endothermic band at 67 and 56 °C, respectively.

4.4 Discussion

4.4.1 Pressure variations of FSDP position in XRD patterns

The analysis of FSDP position ($S_1 = 4\pi\sin\theta/\lambda$) from the XRD patterns for samples is useful to evaluate the size of the intermediate range order structure unit (Fig. 4.12). FSDP positions of the compressed samples show negative shift with increasing pressure and approach to that of silica glass, in which the medium range structure is mainly composed of six-membered rings of SiO_4 tetrahedra. These indicate that the intermediate range order structure of the shock compressed sample becomes larger than that of as-synthesized silica gel with increasing shock pressure.

On the other hand, Shimada et al. (2002) reported that the formation of small ring such as three-membered ring of SiO_4 tetrahedra in shock compressed silica glass at 26 GPa. The formation of small rings leads the densification of the structure of the shocked glass with positive shift of FSDP from S_1 = 1.5077 in original silica glass to 1.6465 in the shocked sample at 26 GPa, and this shock-induced small rings are reconstructed to larger ring by after shock temperature at above this shock pressure (Shimada et al., 2002). The formation of small ring structure may not occur in the compressed silica gel. The after shock temperature may be so high and relax the shock-induced densified structure in the sample compressed even at lower shock pressure.

4.4.2 Raman and infrared spectroscopic analyses

Raman spectra of shock compressed samples above 20.7 GPa show the increase of intensity of the broad band at $\nu < 480$ cm^{-1}. Kingma and Hemley (1999) reported that Raman spectra of some crystalline SiO_2 polymorphs show the band corresponding to larger ring structure of SiO_4 tetrahedra than four-membered ring in the frequency range of ν = 420-460 cm^{-1}. On the basis of their report, the development of the Raman band below ν = 480 cm^{-1} may indicate the formation of the larger ring such as six-membered

ring. The development of the band around ν = 450 cm^{-1} was also observed in the previous report for heat-treated silica gel (Bertouluzza et al., 1982; Kamiya and Nasu, 1998) and synthetic amorphous opal which has silica gel-like structure (Arasuna et al., 2013b). The references cited above indicated that the development and broadness of the band below ν = 480 cm^{-1} was due to the formation of Si-O-Si network structure by the dehydration and condensation of silianol and the upsizing of the intermediate structure. The upsizing reconstruction of intermediate structure of silica gel and synthetic opal started at 600-800 °C (see chapter 5). Moreover, with increasing shock pressure, the position of FTIR band corresponding to Si-O stretching shifts toward higher wavenumber by 13 cm^{-1}. This result indicates a shortening of the Si-O bond distance and implies the increase of mean Si-O-Si angle (Lasaga and Gibbs, 1988; Murray and Ching, 1989).

FTIR band attributed to Si-O-Si bending mode at around ν = 798 cm^{-1} may relate to the average Si-O-Si angle in the samples. The band position is almost constant with the shock pressure, whereas the results of FSDP and Raman analyses indicate the upsizing of intermediate structure of the compressed samples with increasing pressure. In next chapter, I will report on the structural change of synthetic opal by heat treatment. Synthetic opal shows the positive shift of the IR band at around ν = 800 cm^{-1} due to the release of water molecules by thermal treatment at above 400 °C. Above 800 °C, the intermediate structure of the heat-treated opal samples become larger than that of as-synthesized one, causing the negative shift of the IR band of Si-O-Si bending (see more chapter 5). In this study, TG analysis shows that the amount of water molecules and silanols in the sample compressed at 17.0 GPa is close to that of silica gel. Therefore, at lower pressure below 17.0 GPa, it is presumed that the high residual water content in the compressed sample leads the little positional change of the band of Si-O-Si bending. This is also supported by the distinct broad band around ν = 3500 cm^{-1} due to the water molecules and silanol in FTIR and Raman spectra for samples compressed below 17.0 GPa. At 20.7 -27.2 GPa, the decrease of water content may occur. However, the upsizing of the intermediate structure, formation of larger ring, in the compressed samples by after shock temperature may cancel out the shift of the band attributed to Si-O-Si bending.

Both the Raman and FTIR spectra of the compressed samples show that the Si-O stretching bands of silanol shifts toward lower frequency direction. The heat-treated

silica gel also shows the negative shift of the Raman band of silanol up to 600 °C (see chapter 5.4.1). The decrease of this band position in the compressed samples may relate to the dehydration and condensation of silanol by after shock temperature.

4.4.3 Water species and water behavior in silica gel under shock-wave compressions

TG result indicates that as-synthesized silica gel contains about 20 wt% of water. According to the report of Graetsch et al. (1985), the considerable weight loss (17.5 wt %) up to 160 °C may be responsible for the release of the adsorbed water molecules and the continuous weight loss of 4.7 wt% above 160 °C may largely depend on the dehydration of silanol groups. From the result of FTIR and Raman analyses, as-synthesized silica gel has a large number of water molecules and silanol groups. Both Raman and FTIR spectra of as-synthesized silica gel show distinct Q_3 band at around ν = 970 cm^{-1}. Furthermore, the Raman band of silanol at ν = 980 cm^{-1} has the weak tail to around ν = 900 cm^{-1}. Only Krol and Van Lierop (1984) assigned to this weak Raman band to Q_2, as called germinal silanol. In higher wavenumber region of both Raman and FTIR spectra of as-synthesized silica gel, the broad bands attributed to water molecule and silanol centered at ν = 3500 cm^{-1} are observed. By the deconvolution of this broad Raman band using a Gaussian peak fittings of IGOR pro 6.3 program, it was found that the broad band of as-synthesized silica gel contains at least five bands around ν = 3224, 3428, 3560, 3600 and 3651 cm^{-1} (Fig. 4.13). Based on the many previous reports, former two bands are attributed to OH stretching of water molecules. Although it is largely depends on the literature, later three Raman bands may be related to the silanol (Krol and Van Lierop, 1984; Walrafen and Samanta, 1978; Stone and Walrafen, 1982). However, it is difficult to decide the detailed assignment of later three bands.

Up to 20.7 GPa, Raman and infrared spectroscopic results indicate that almost water molecules and silanol remain. This is supported by TG analyses of the sample compressed at 17.0 GPa.

Above 20.7 GPa, Q_3 band is clearly observed in the Raman spectrum, although the weak Raman band at around 900 cm^{-1} disappears. According to the assignment of Krol and Van Lierop (1984), it is presumed that the germinal silanols are dehydrated and condensation by shock compression above 20.7 GPa. Above this pressure, the Raman

spectrum shows the drastic change. The Raman spectrum for the sample compressed at 27.2 GPa is also deconvoluted (Fig. 4.13). The specific band at around $\nu = 3598$ cm^{-1} in the compressed sample seems to be the same band at $\nu = 3592$ cm^{-1} in the Raman spectrum of as-synthesized silica gel (Fig. 4.13). Moreover, I suggest that the band at $\nu = 3666$ cm^{-1} corresponds to the band at $\nu = 3646$ cm^{-1} in the spectrum of as-synthesized silica gel. Davis and Tomozawa (1996) reported the IR band at around $\nu = 3608$ cm^{-1} in the water-bearing silica glass became intense during hydration, therefore they concluded that this band is due to the OH stretching of silanol which hydrogen bonded to the oxygen of neighboring water molecules. Moreover, on the basis of the report of Davis and Tomozawa (1996), the band around $\nu = 3559$ cm^{-1} and 3646 cm^{-1} may be responsible for the mutually hydrogen bonded silanol groups, and attributed to OH stretching of a proton donating silanol and a proton accepting silanol, respectively. In this study, the band at $\nu = 3592$ and 3646 cm^{-1} shift toward higher frequency by shock compression at 27.2 GPa (Fig. 4.13). Davis and Tomozawa (1996) also observed the band for the proton accepting silanol shifted by changing of the content of water molecules. The release of water molecules may make shortening of OH bonding of silanol groups, resulting in the positive shift of these bands.

From the deconvolution result for as-synthesized silica gel, the caluculated relative intensities of the bands corresponding to water molecules ($\nu = \sim 3450$ cm^{-1}) and silanol ($\nu = 3500$ $cm^{-1}\sim$) are about 82% and 18 %, respectively. However, in the sample compressed at 27.2 GPa, these relative intensities are about 65% and 35%. Moreover, obtained TG curve for sample compressed at 27.2 GPa reveals that the adsorbed water and silanol groups decrease to about 77 % and 42 %, respectively. These results indicate that water molecules release easily than silanol under shock compression.

FTIR result indicates the presence of mutually hydrogen bonded silanol groups in the sample after the compression at 30.9 GPa. ATR analysis is stronger tool for the detection of water than FTIR spectroscopy using KBr method, because ATR technique is free from influence of atmospheric water. ATR result reinforces the remaining of mutually hydrogen bonded silanol groups after shock compression at 30.9 GPa. Moreover, at this shock pressure, ATR result also indicates the compressed sample contains a small amount of water molecules.

Based on the above discussion, the water behavior in compressed samples may be explained as follows. Up to 17.0 GPa, water molecules are released easily, although

most silanol can remain after compressions. At the shock compression of 27.2 GPa, water molecules of 77 % are released, although the decrease ratio of silanol is only 42%. It indicates that the silanol endures the shock compression and the after shock temperature than water molecules. The residual silanol groups may be attributed to the mutually hydrogen bonded silanol group and the silanol hydrogen bonded to water molecules. After the compression at 30.9 GPa, the tiny amount of water molecules and the mutually hydrogen bonded silanol group can remain.

4.4.4 Structural evolution of silica gel by shock-wave compression

A considerable change of the structure in the silica gel by shock compression may occur above 20.7 GPa of shock pressure. At this shock pressure, germinal and single silanols may be dehydrated by the shock compression and the after shock temperature, resulting in the polymerization of Si-O-Si network. The results of FTIR and FSDP analyses clearly indicate that the intermediate structure of the compressed samples becomes larger than that of the as-synthesized one. Therefore, newly formed Si-O-Si network structure may contain the larger ring structure than four-membered ring.

In this study, the shock-induced small three-membered ring observed in the report of Okuno et al. (1999) is not detected in the compressed samples. The heat-treated silica gel shows that the reconstruction, upsizing, of the network structure may occur by thermal treatment at 600-800 °C and the thermal treatment at 800 °C may completely relax the three-membered ring structure (see more chapter 5). Therefore, the after shock temperature may be close to 800 °C even in the sample compressed at 20.7GPa. With increasing pressure above 20.7 GPa, the intermediate structure of the compressed samples becomes large and approaches to that of silica glass gradually.

However, some silanol groups and a tiny amount of water molecules may remain in the sample even after the shock compression at 30.9 GPa.

4.5 Conclusions

The study reported in this chapter reveals the structural changes of silica gel by shock compression and the behavior of water molecules and silanol groups during the

structural change.

Up to 17.0 GPa, almost water molecules and silanol in compressed samples can remain after shock compressions. The structure of the compressed samples changes significantly above the shock pressure of 20.7 GPa. A large amount of water molecules is released and some silanol, especially germinal silanol, are dehydrated. The dehydration and condensation of silanol groups form the new Si-O-Si network structure. At the same time, relatively high after shock temperature may relax the intermediate structure of compressed samples. Therefore, newly formed network structure may be formed by the six-membered ring of SiO_4 tetrahedra mainly. Based on the studies for heat-treated silica gel, after shock temperature may be close to 800 °C at 20.7 GPa.

Eventually, the intermediate structure of the compressed sample approaches to that of silica glass with increasing shock pressure. However, above 20.7 GPa, some silanol and tiny amount of water molecules can remain. The mutually hydrogen bonded silanol group and the silanol hydrogen bonded to water molecules could be present in the sample compressed at 27.2 GPa. After the compression at 30.9 GPa, the intermediate structure of the recovered sample is similar to that of silica glass, whereas some silanol groups and very small amount of water molecules may remain yet.

Table 4.1 the metal projectiles, velocities of projectile, and estimated shock pressures from projectile velocities

Metal projectile	Projectile velocity (km/s)	Shock pressure (GPa)
Al	0.88	10.5
Al	1.04	12.8
Cu	0.85	17.0
Cu	0.99	20.7
W	0.95	27.2
W	1.05	30.9

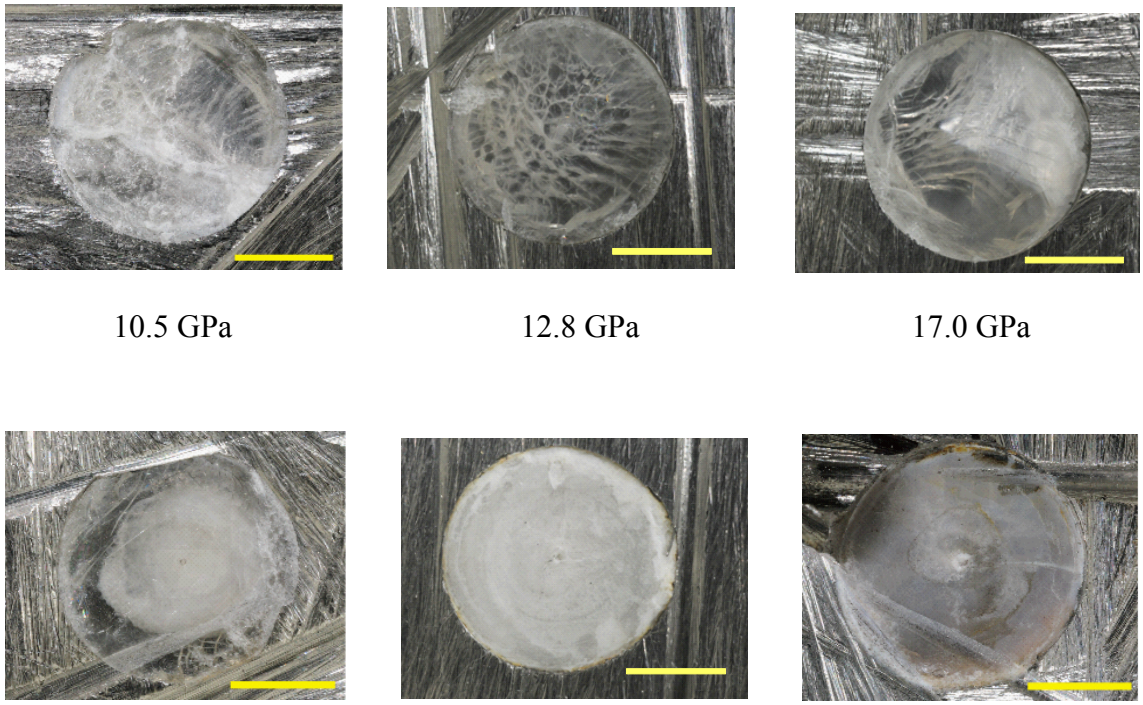

Fig. 4.1 The samples recovered after shock compression experiments. Scale bars are 5mm

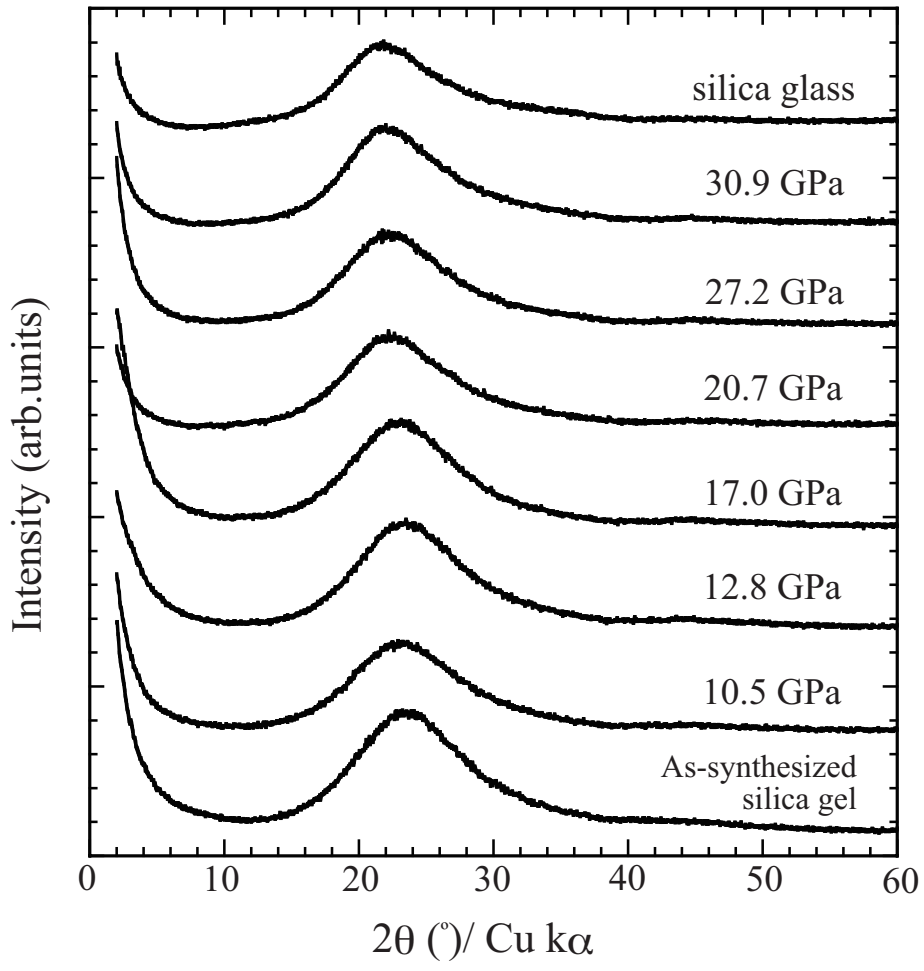

Fig. 4.2 X-ray diffraction patterns for the as-synthesized silica gel and samples recovered after the shock compressions. This figure was modified from Arasuna et al. (2016), © 2013 Springer, http://link.springer.com

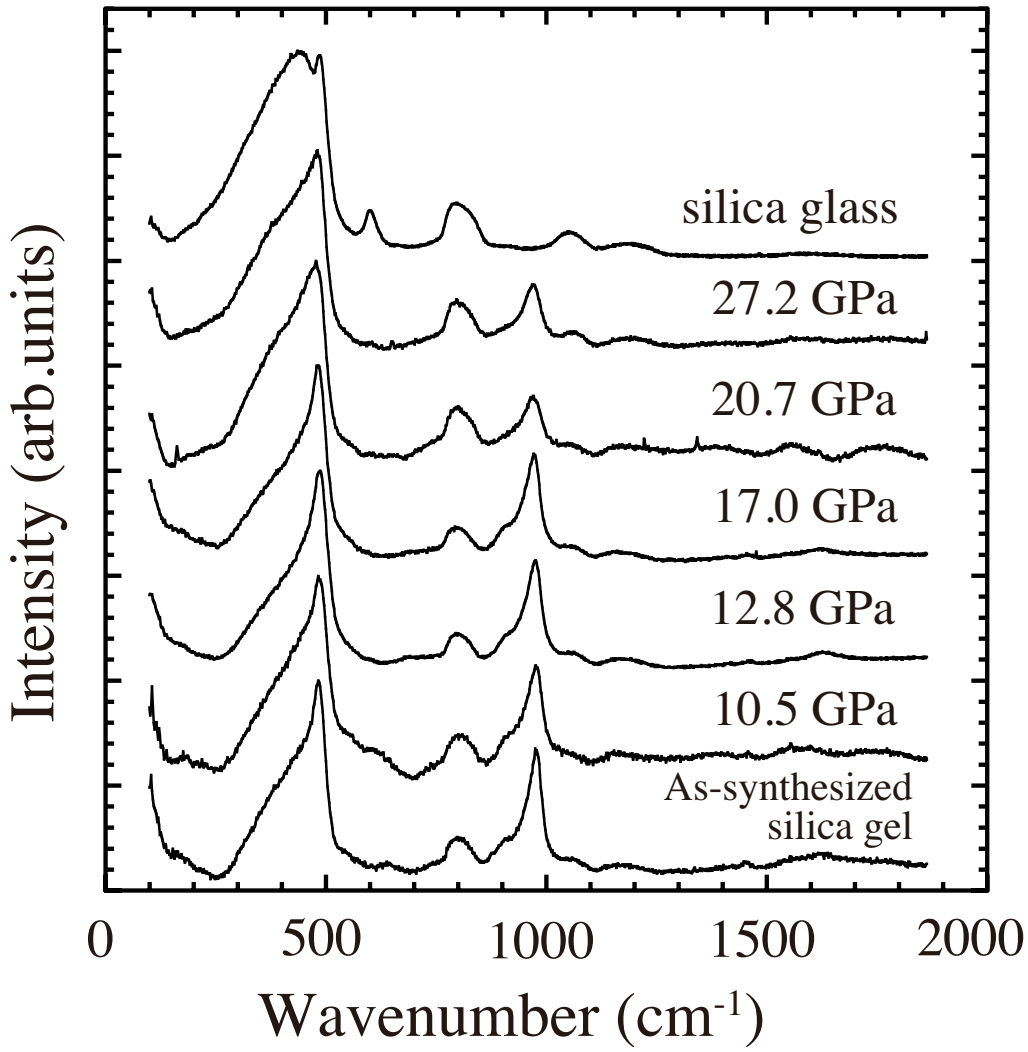

Fig. 4.3 Raman spectra (ν = 100-2000cm^{-1}) for as-synthesized silica gel and samples recovered after shock compressions. This figure was modified from Arasuna et al. (2016), © 2013 Springer, http://link.springer.com

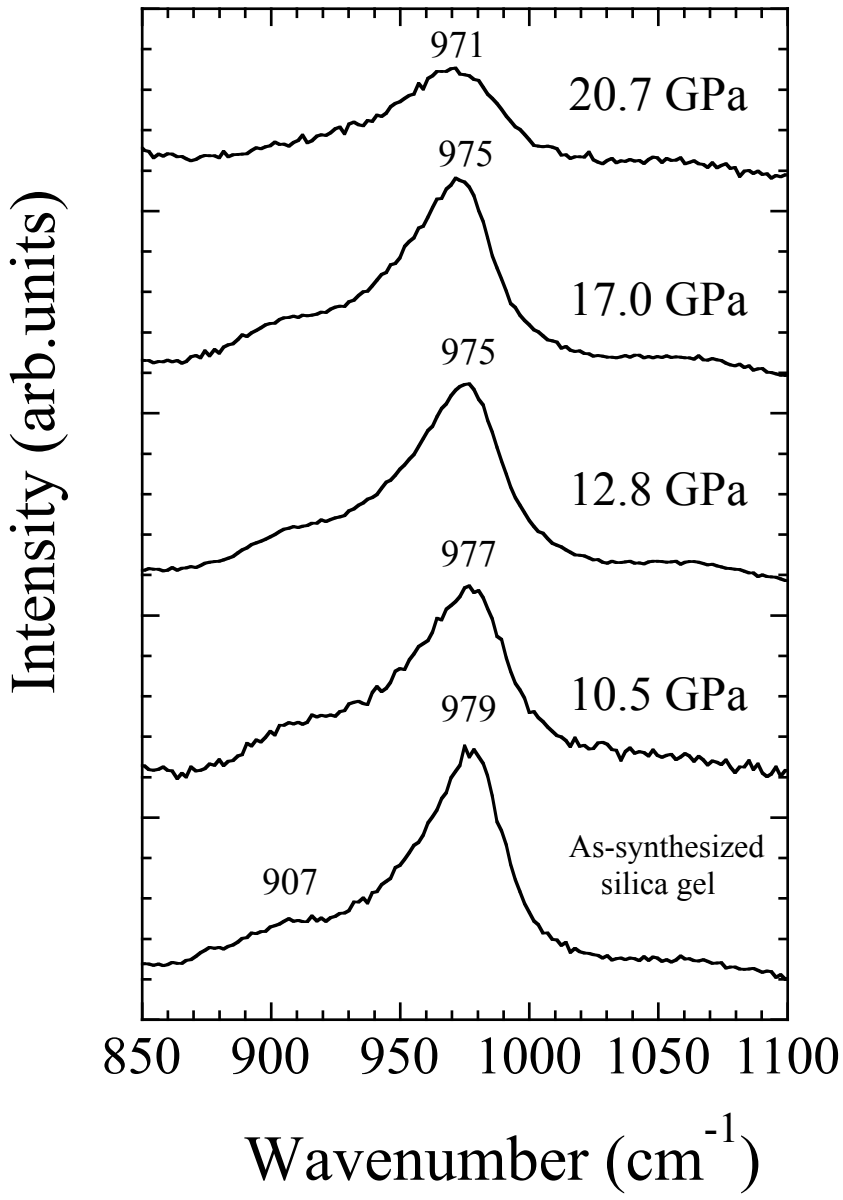

Fig. 4.4 Raman spectra (ν = 850-1000cm^{-1}) for as-synthesized silica gel and the samples recovered after shock compressions

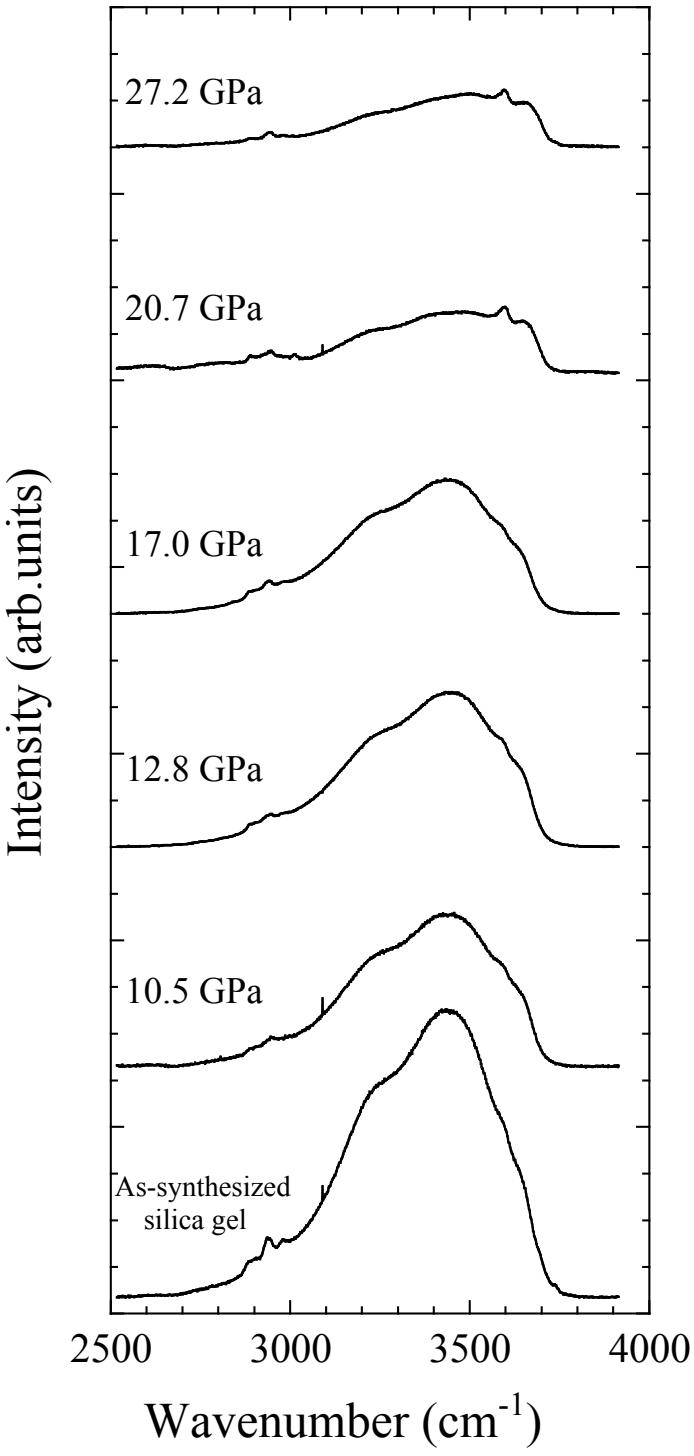

Fig. 4.5 Raman spectra (ν = 2500-4000cm^{-1}) for as-synthesized silica gel and the compressed samples. This figure was modified from Arasuna et al. (2016), © 2013 Springer, http://link.springer.com

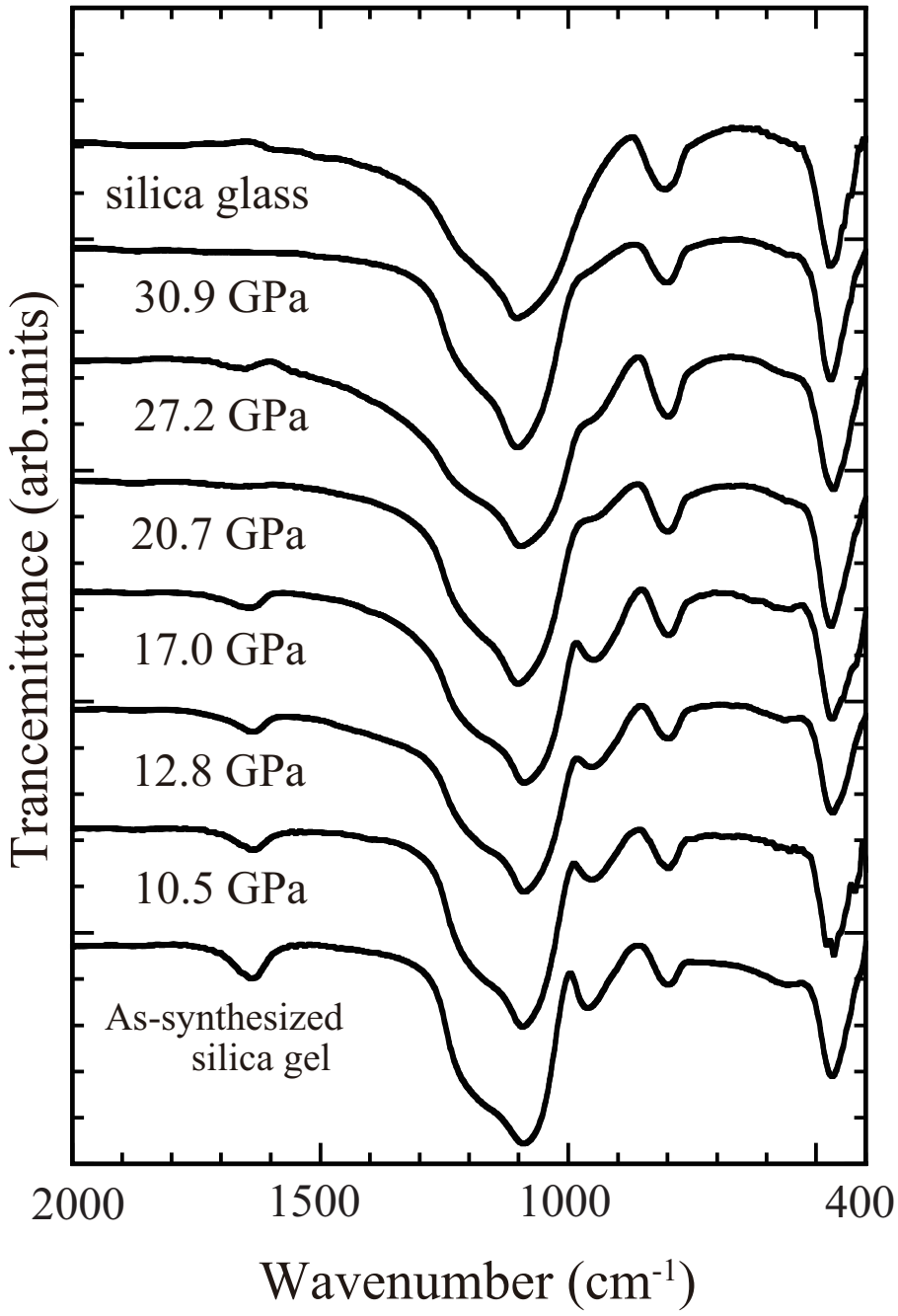

Fig. 4.6 FTIR spectra (ν = 400-2000cm^{-1}) for as-synthesized silica gel and the compressed samples. This figure was modified from Arasuna et al. (2016), © 2013 Springer, http://link.springer.com

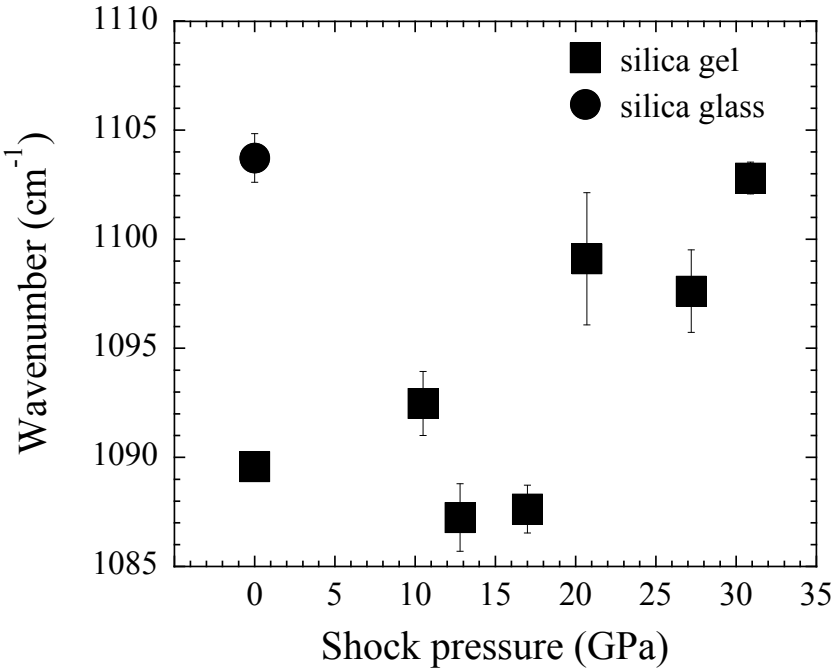

Fig. 4.7 The pressure variations of the band position of Si-O stretching mode

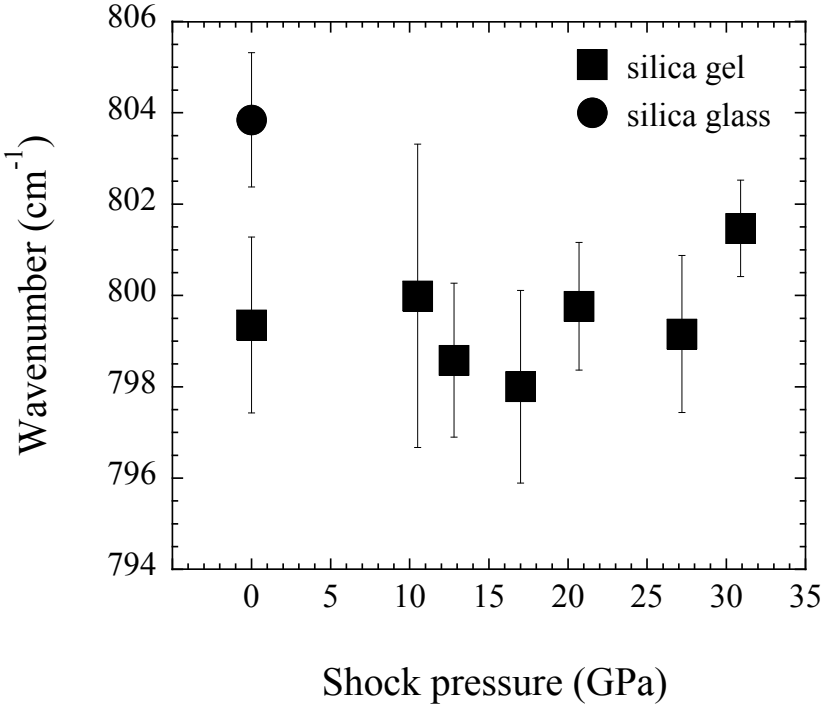

Fig. 4.8 The pressure variations of the band position of Si-O-Si bending mode

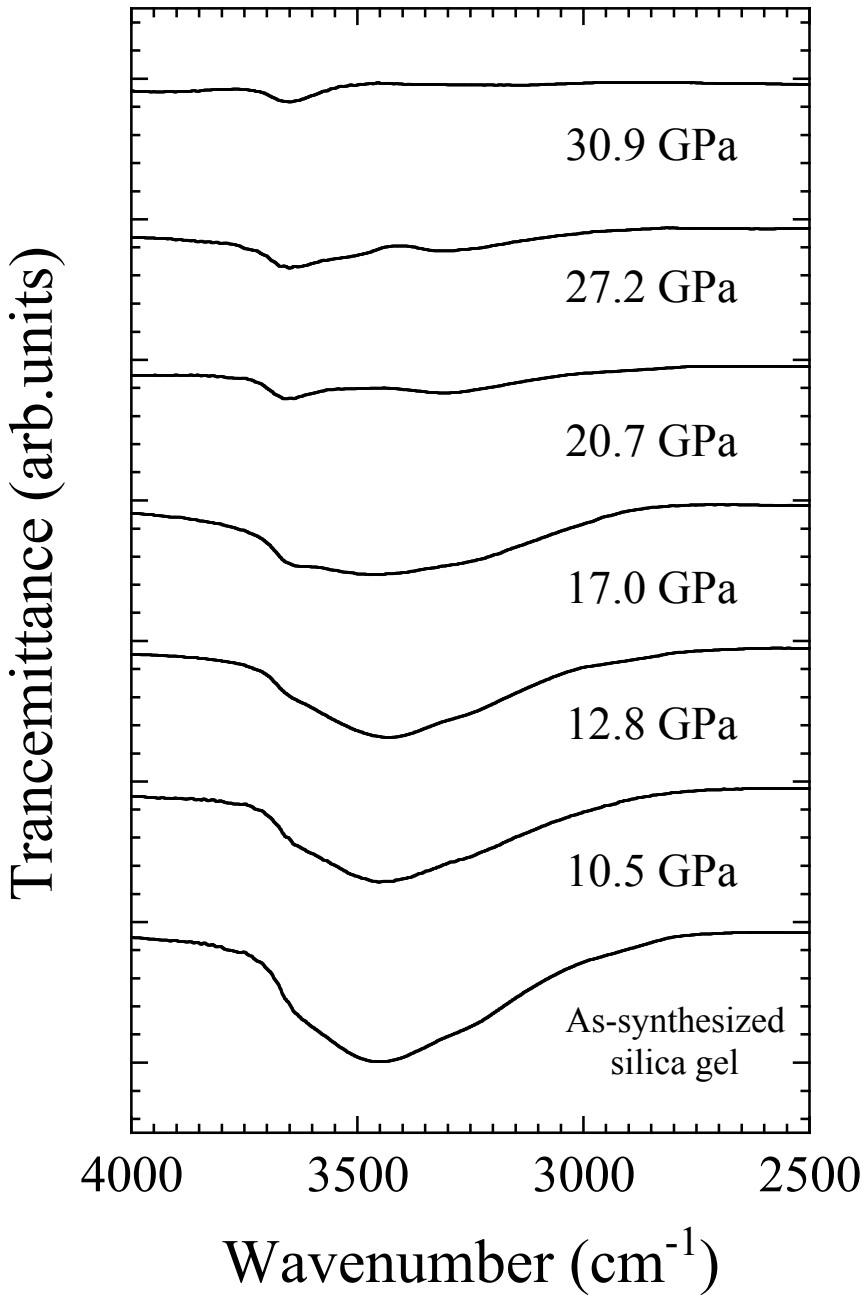

Fig. 4.9 FTIR spectra (ν = 2500-4000cm^{-1}) for as-synthesized silica gel and the compressed samples. This figure was modified from Arasuna et al. (2016), © 2013 Springer, http://link.springer.com

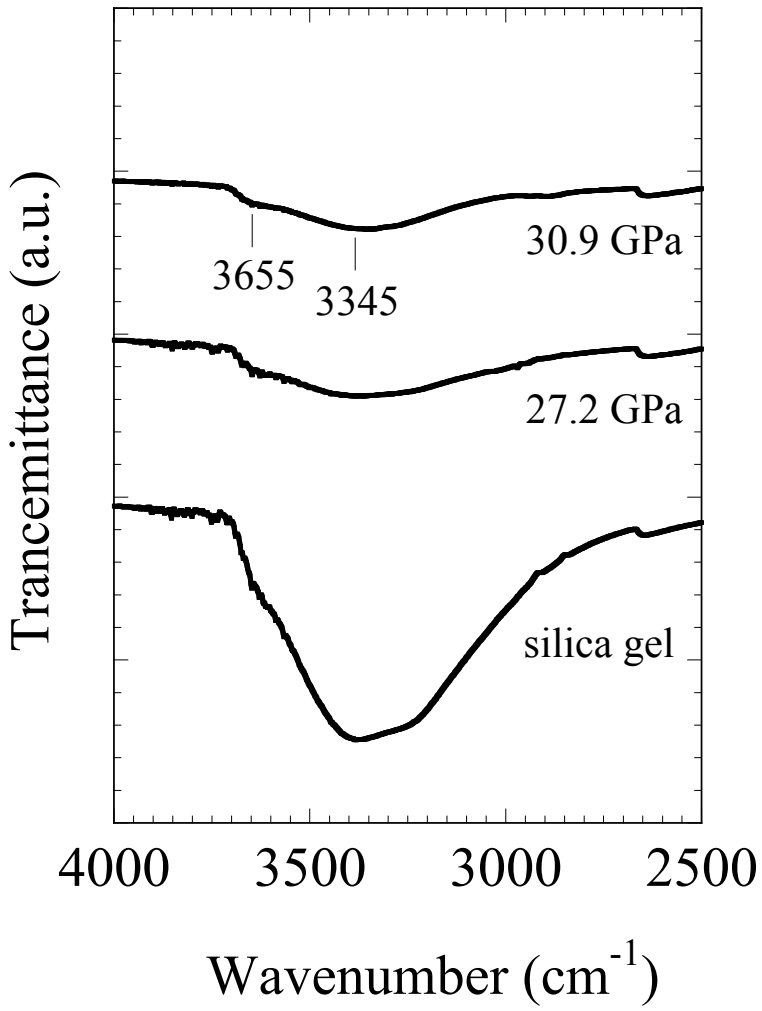

Fig. 4.10 ATR spectra (ν = 2500-4000cm^{-1}) for as-synthesized silica gel and the compressed samples. This figure was modified from Arasuna et al. (2016), © 2013 Springer, http://link.springer.com

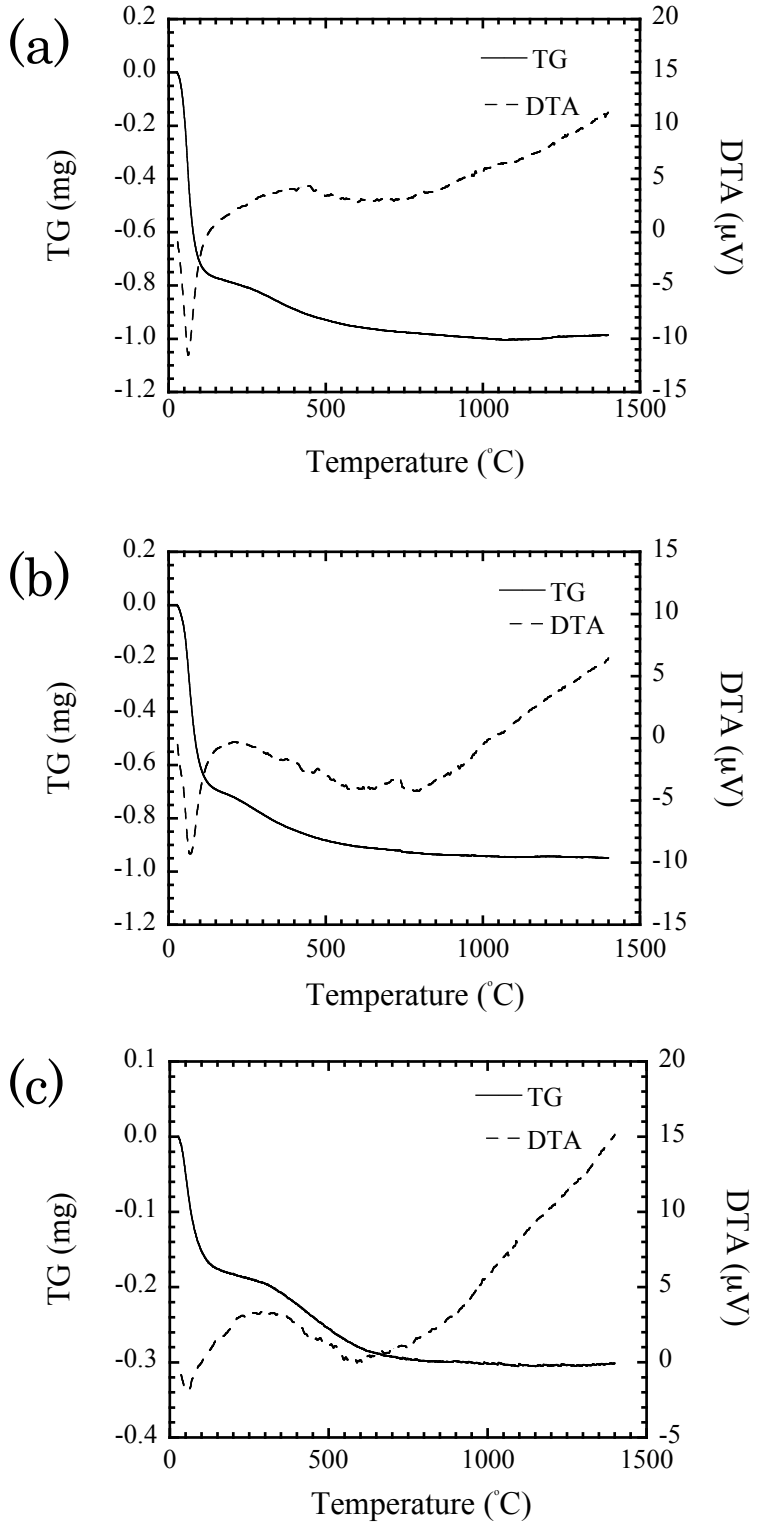

Fig. 4.11 TG-DTA curves for the (a) as-synthesized silica gel, (b) sample compressed at 17.0 GPa, and (c) sample compressed at 20.7 GPa. This figure was modified from Arasuna et al. (2016), © 2013 Springer, http://link.springer.com

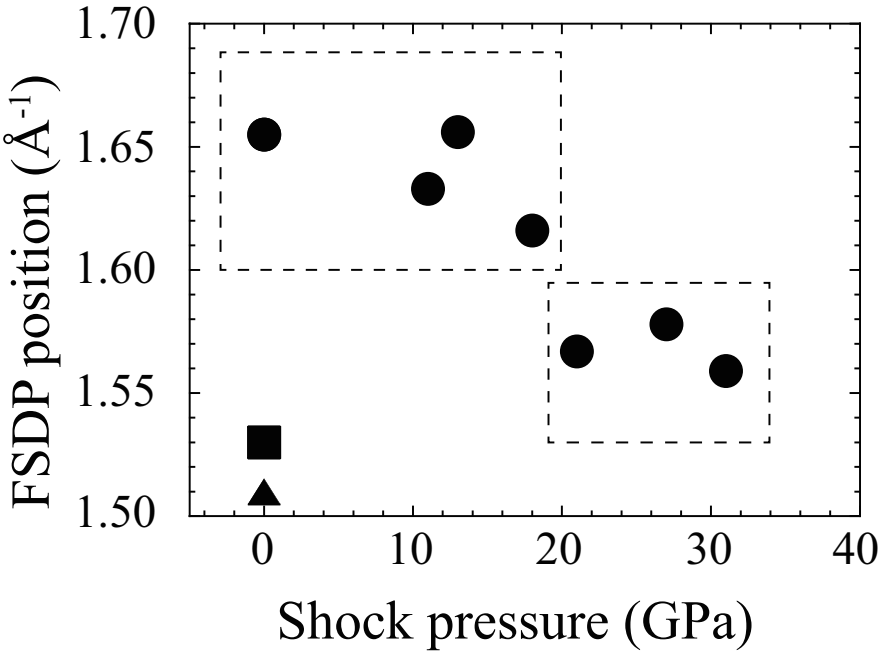

Fig. 4.12 FSDP position based on pressure variation. *Solid circle*, *triangle*, and *square* are silica gel, silica glass by Shimada et al. (2002), and silica glass used in this study. This figure was modified from Arasuna et al. (2016), © 2013 Springer, http://link.springer.com

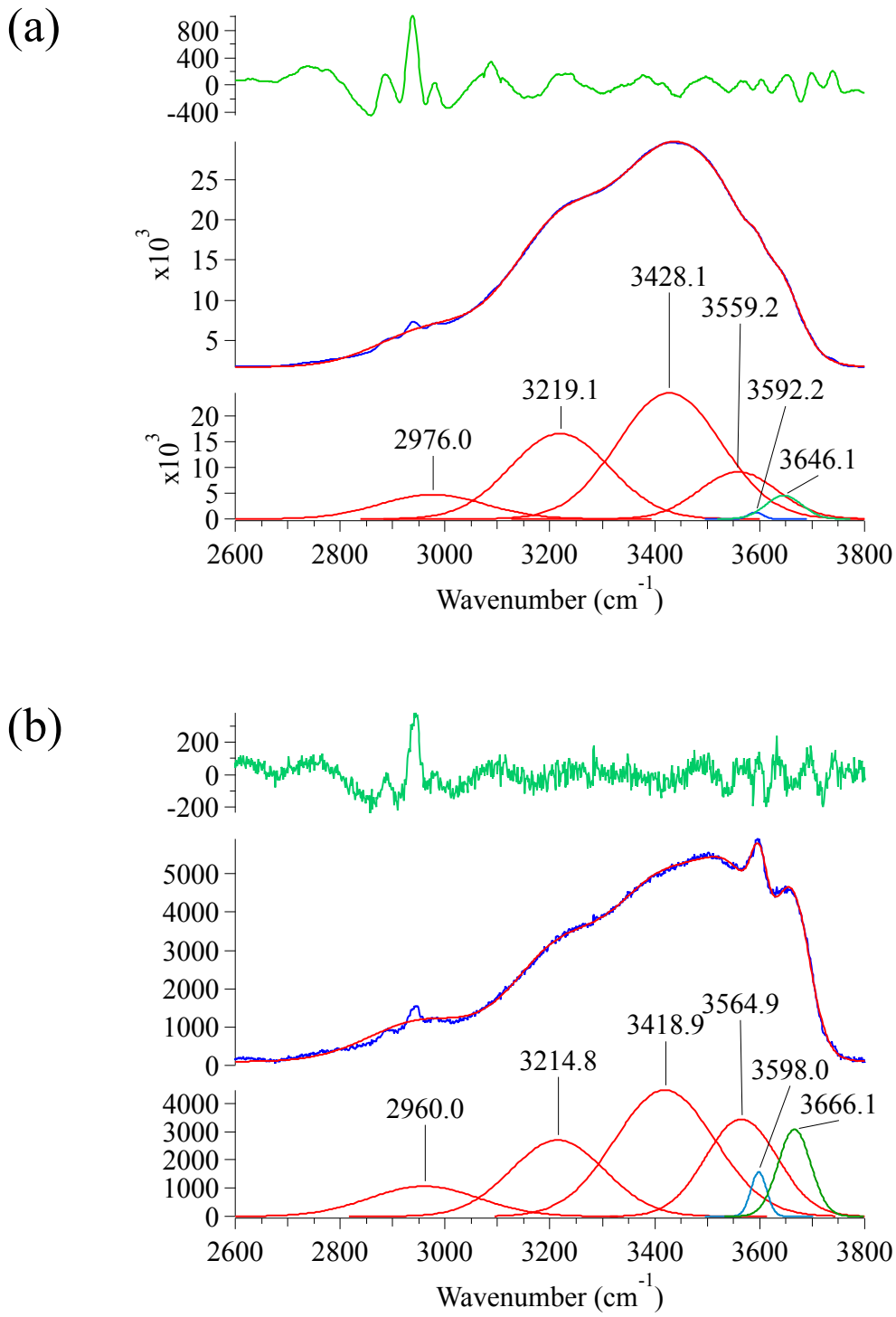

Fig. 4.13 Gaussian peak fittings results of the Raman spectra in the range of ν = 2600-3800 cm^{-1} for the (a) as-synthesized silica gel and (b) sample compressed at 27.2 GPa. This figure was modified from Arasuna et al. (2016), © 2013 Springer, http://link.springer.com

Chapter 5
Structural changes of synthetic opal and silica gel by heat treatment

5.1 Introduction

As mentioned in Chapter 1, opal is a one of typical hydrated amorphous silica minerals and classified into opal-C, opal-CT, and opal-A. Opal-A is further classified into opal-AN and opal-AG (Langer and Flörke, 1974). Opal-AN has fused SiO_2 glass-like network structure (Flörke, 1973). On the other hand, Opal-AG has a silica gel like structure (Langer and Flörke, 1974). Some of opal-AG are composed of close-packed aggregates of silica spheres with almost uniform diameter around ~ 400 nm, and has been regarded as a gemstone because of its splendid opalescence (Sanders, 1964). Silica gel is also composed of non-crystalline silica sphere aggregates, as found in opal-AG, although there is a large variety of arrangements and size distributions of the silica spheres.

Until now, several studies on heat-treated opals have been reported. Wahl et al. (1961) reported that opal-A crystallizes into cristobalite rapidly above 1000 °C by high temperature X-ray camera investigation. Jones and Segnit (1971) conducted DTA experiment for opal-A and XRD measurement for heat-treated opal-A, and suggested that opal-A crystallizes into a well-ordered cristobalite with a trace of tridymite-like stacking by heating at around 1300 °C. However, there are still unclear points about the intermediate structural change, mechanism of the crystallization to cristobalite, and dehydration behavior of opal by heat treatment.

On the other hand, many thermal experiments on silica gel have been also conducted. It is well known that the silica gel transforms to silica glass by heating above 800 °C (Bertouluzza et al., 1982; Brinker et al., 1986) and also crystallizes into a well-ordered cristobalite by heating above 900 °C (Whal et al., 1961). Kamiya and Nasu (1998) investigated the detailed intermediate structural change of heat-treated silica gel fibers and films based on NMR and FTIR spectroscopies, and XRD analysis. They revealed that a four-membered ring of SiO_4 tetrahedra reconstructed to a six-membered ring in the temperature range of 200–500 °C.

In the present study, the structural changes of synthetic non-crystalline opal and TEOS

derived silica gel by heat treatment are investigated using TG-DTA, SEM, XRD, FTIR and Raman spectroscopies. The findings from the heat experiments for heat-treated samples are compared with those of previous studies on heat-treated silica gels and natural opal-A, and the structural evolutions of synthetic non-crystalline opal and silica gel by heating are discussed in detail.

5.2 Experimental

5.2.1 TG-DTA measurement

TG-DTA measurements were performed using a Rigaku Thermo Plus 2 TG 8120 instrument. 10 mg samples of as-synthesized opal and silica gel were placed in a Pt pan. The sample then heated to 1400 °C at a heating rate of 10 °C min^{-1} in a nitrogen atmosphere.

5.2.2 Heat treatment of synthetic opal and silica gel

As-synthesized opals and silica gel were heated at the temperature listed in Table 5.1 for 1 h using an electric furnace. The heat-treated opals and silica gels were investigated using XRD measurement, FTIR and Raman spectroscopies. SEM observation was performed on the as-synthesized silica gel and opal and heat-treated synthetic opal.

5.2.3 SEM observations

SEM observations for as-synthesized opal and silica gel were conducted using HITACHI S-5200 at JAIST. SEM (JEOL JSM-5310) was used to observe the microstructures of the heat-treated synthetic opals. Samples were mounted on brass specimen supports and coated with gold. SEM observations were conducted with accelerating voltage in the range of 10–25 kV.

5.2.4 X-ray diffraction measurement

XRD measurements of the all samples were performed using an X-ray powder diffractometer (Rigaku RINT 2200) with Cu-Kα radiation. The θ-2θscanning technique was adopted with a scan speed of 0.5°/ min over the 2θ range of 2-60° for opal samples and with a scan step of 0.02° over the 2θ range of 2-60° for silica gel samples. The acceleration voltage and current used were 40 kV and 30 mA, respectively.

5.2.5 FTIR and Raman spectroscopies

FTIR absorption measurements were performed using Jasco FT/IR 610V with KBr micropellet method. FTIR spectra were recorded in the range of ν = 400-4000 cm^{-1} with a band path of 4 cm^{-1} for all samples.

Raman spectra for samples were recorded using a micro-Raman spectrometers (Horiba Jovin Yvon; Ramanor T-6400). The 514.5 nm line (green) of an Ar^{+} laser was used to excite Raman scattering. Raman light was collected in the backscattering geometry. Spectra were recorded in the range of ν = 100-1500 cm^{-1}. All observed Raman spectra were corrected for background.

5.3 Results

5.3.1 TG- DTA analysis

The TG and DTA curves for the as-synthesized opal and silica gel are present in figure 5.1. The TG curve of synthetic opal shows a large weight loss (9.5 wt%) up to 200 °C following a gradual weight loss (3.0 wt%) up to 700 °C. Moreover, a small continuous weight loss (1.0 wt%) is also observed in the range of 700-1400 °C. The total measured weight loss is about 13.5 wt%. Similarly, TG curve for as-synthesized silica gel shows a large weight loss (19.4 wt%) up to 200 °C and a gradual weight loss (3.3 wt%) up to 700 °C. Moreover, a small weight loss (0.1 wt%) is also observed in the range of 700-1400 °C. The total measured weight loss is about 22.8 wt%.

The DTA curves of as-synthesized opal and silica gel show broad endothermic bands

at about 60 °C and 80 °C, respectively. Exothermic reaction bands are also observed in DTA curves for both samples and observed at around 1260 °C in as-synthesized opal and at around 1230 °C in as-synthesized silica gel.

5.3.2 Heat-treated opals and their SEM observations

The changes in the opalescence of the heat-treated opals are shown in figures 5.2 a-c. Up to 1000°C, opals exhibit splendid opalescence, however those are slightly weaken with increasing temperature. A sample shows remarkable change in appearance by heat treatment at 1300 °C. The opalescence of the sample treated at 1300 °C completely disappears.

SEM observation indicates that the microstructure of as-synthesized opal consists of a regular stacking of amorphous silica spheres with diameters of approximately 400 nm (Fig. 5.3). SEM images of heat-treated opals are shown in figure 5.4 a-d. Increasing in temperature up to 1000°C, the regular arrangement of silica spheres is almost conserved, although partial disarray is sometimes observed. In contrast, above 800 °C, significant shrinkage of the silica spheres is observed. The radii of the silica spheres are reduced at shrinkage rates of approximately -11% at 800 °C, and -24% at 1000 °C. By heat treatment at 1300°C, the regular arrangement of silica spheres completely disappeared and a smooth surface becomes dominant.

5.3.3 X-ray diffraction analysis

The XRD pattern for the as-synthesized opal shows only a diffuse scattering maximum centered at $2\theta = 23.2°$ without crystalline peaks (Fig. 5.5). Therefore, the as-synthesized opal is classified as opal-A.

After heat treatment, the broad peak centered at $2\theta = 23.2°$ indicates a negative shift of about 1° with increasing temperature up to 1000 °C. Moreover, the XRD pattern of the opal heated at 1200 °C shows crystalline diffraction peaks of low-cristobalite phase. With increasing temperature up to 1400 °C, the peak intensities increase gradually. The diffraction pattern of opal heat-treated at 1400 °C shows other crystalline peaks at about $2\theta = 21$ and 28° (asterisks in Fig. 5.5) of the low-tridymite phase.

On the other hand, the intensity of small angle scattering around $2\theta = 2°$ decreases by

about 15% at 400 °C and abrupt reduction of the intensity occurred above 1000 °C. The intensity is roughly constant above 1200 °C, though new peaks of low-cristobalite and low-tridymite appear at 1200 °C and 1400 °C, respectively.

On the other hand, XRD patterns for as-synthesized and heat-treated silica gel are shown in figure 5.6. The XRD pattern for the as-synthesized silica gel indicates only a diffuse scattering maximum centered at $2\theta = 23.4°$. Similar to heat-treated opals, the scattering maximum centered at $2\theta = 23.4°$ shows a negative shift of about 1.7° with increasing temperature up to 1000 °C. A small angle scattering around $2\theta = 2°$ becomes less intense with increasing temperature and the intensity decreases by about 90 % at 1000 °C.

5.3.4 Infrared spectroscopic analysis

Figure 5.7 shows FTIR spectra (ν = 400-2500 cm^{-1}) for as-synthesized and the heat-treated synthetic opals. The spectrum of as-synthesized opal shows bands at ν = 470, 800, and 1100 cm^{-1}. These bands can be attributed to the Si-O-Si rocking, Si-O-Si bending, and Si-O anti-symmetric stretching vibration mode, respectively (Handke and Mozgawa, 1993). The band at around ν = 950 cm^{-1} may be attributed to Si-O stretching vibration of silanol groups (Inoue et al., 2010). The band at ν =1640 cm^{-1} can be attributed to the H-O-H bending mode of molecular water (Benesi and Jones, 1959).

Figure 5.8 shows FTIR spectra for the as-synthesized and heat-treated opals in the range of ν = 2000-4000 cm^{-1}. The FTIR spectrum for the as-synthesized opal has a broad band in the frequency range of ν = 2900-3700 cm^{-1}. This broad band may be composed of the O-H stretching bands of molecular water and silanol (Orcel et al., 1986; Davis and Tomozawa, 1996). The spectrum has a shoulder at ν = 3650 cm^{-1}, whereas it is difficult for the assignment of this shoulder. However, this shoulder may be related with the presence of silanol (Graetsch et al., 1985; Orcel et al., 1986; Graetsch, 1994). All bands of molecular water and silanol almost disappear after heat treatment at 600 °C.

On the other hand, FTIR spectra in the range of ν = 400-2500 cm^{-1} for as-synthesized and heat-treated silica gel are shown in figure 5.9. Similar to synthetic opal, FTIR spectrum for as-synthesized silica gel has the bands at around ν = 470, 800, 960, 1090, and 1650 cm^{-1}. The assignments of these bands are coincident with those of as-synthetic

opal. The bands of silanol at around ν = 960 cm^{-1} and the water molecule at around ν = 1650 cm^{-1} remain after the heat treatment up to 600 °C, though these bands becomes less intense and the silanol band becomes a shoulder. By heat treatment at 800 °C, these bands are disappeared completely.

FTIR spectra for the as-synthesized opal indicate that the position of the band around ν = 800 cm^{-1} shifts toward a higher wavenumber by heat treatment above 400 °C (Fig. 5.10). The band position is maintained up to 800 °C, although the standard deviation of the band position at 800 °C is large. This band shifts toward a lower wavenumber above 1000 °C. On the other hand, heat-treated silica gels show the smaller positive shift of the band at around ν = 800 cm^{-1} than heat-treated opals.

Both FTIR spectra for heat-treated opal and silica gel show a new weak band at around ν = 620 cm^{-1} after heat treatment above 1200 °C. This band may be attributed to the band of low-cristobalite (Etchepare et al., 1978).

5.3.5 Raman spectroscopic analysis

Raman spectra for the as-synthesized and heat-treated opals are present in figure 5.11. The Raman spectrum for the as-synthesized opal has a weak broad band centered at ν = 450 cm^{-1} and a sharper band at ν = 483 cm^{-1}. Previous studies reported that the former band may be attributed to a symmetrical Si-O-Si stretching mode, and the latter band is due to the oxygen-breathing mode of the four-membered ring of the SiO_4 tetrahedra, denoted as the D_1 band (Galeener, 1982a and b; Galeener and Geissberger, 1983; Sharma et al., 1984). Generally, the D_1 band may be not clear in the Raman spectrum for natural opal-A (Smallwood et al., 1997; Ostrooumov et al., 1999). Raman spectra for the as-synthesized and heat-treated silica gel are shown in figure 5.12. Similar to the as-synthesized opal, the Raman spectrum of as-synthesized silica gel has the broad band of symmetrical Si-O-Si stretching mode and D_1 band clearly.

Heat-treated Opal and silica gel show a similar characteristic. With increasing temperature, the D_1 band becomes much less intense, whereas the broad band (ν < 480 cm^{-1}) becomes prominent. For the sample heat-treated above 800 °C, the band centered at ν = 450 cm^{-1} becomes significantly broader, though this band in the Raman spectrum for the heat treated-silica gel at 600 °C has already broadened. Above these temperature, the spectra for opal and silica gel approach to that of silica glass.

In both Raman spectra for silica gel and opal treated above 400 °C, a new band at ν = 590 cm^{-1} is observed. This band may be due to the oxygen-breathing mode of the three-membered ring of the SiO_4, denoted as D_2 band (Sharma et al., 1981; Galeener, 1982a and b). The intensity of the D_2 band in Raman spectra for both samples may become intense and sharp with the heat treatment temperature up to 800 °C, whereas this band in the heat-treated silica gels is weaker than that of heat-treated opals. After heat treatment at 1000 °C, the band becomes weaker.

Raman spectra of the as-synthesized opal and silica gel have bands attributed to the silanol at ν = 950 and 976 cm^{-1}, respectively (Stolen and Walrafen, 1976; Murray and Greytak, 1979). For Raman spectra for heat-treated silica gels, the band of silanol show 10 cm^{-1} negative shift with increasing temperature up to 600 °C. Interestingly, this positive shift is not observed in the Raman spectra for heat-treated opals. The band of silanol disappears entirely at 800 °C. The spectra for the opal and silica gel treated at 1300 °C are similar to that of low-cristobalite (Bates, 1972; Kingma and Hemley, 1994).

5.4 Discussion

5.4.1 Water of as-synthesized opal and dehydration behavior of synthetic opal and silica gel

The results of TG-DTA and FTIR analysis for as-synthesized opal suggest that it contains molecular water and silanol groups. Similarly, water molecules and silanol groups also present in silica gel and natural opal-A (Langer and Flörke, 1974).

As I noted in before chapters, based on the report by Graetsch et al. (1985), the contents of silanol and molecular water in as-synthesized opal were roughly estimated from the results of TG–DTA. TG analysis for as-synthesized opal indicates a 9.5 wt% weight loss up to 200 °C, a 3.0 wt% weight loss from 200 to 700 °C, which may be attributed to molecular water, surface silanols, respectively. Above 700 °C, small weight loss (1.0 wt%) is observed. It may be related with the silanol located in the structural site, although the more discussion is required for the elucidation of this weight loss. According to the result of TG measurement for silica gel, the content of

water molecule and silano groups is also estimated as follow. The content of water molecule and surface and internal silanol is about 19.4, 3.3, and 0.1 wt%, respectively.

The ratio of molecular water to silanols is 0.42 in as-synthesized opal. Comparing with the contents for natural opal-AG (0.18: Langer and Flörke, 1974), the synthetic opal contains considerable amount of silanol than natural opal. The total water content in as-synthesized silica gel is much higher than as-synthesized opal. Especially, the water molecule dehydrated by heat treatment below 200 °C in silica gel sample is about 10 % higher than that of opal. However, the content of surface silanol in silica gel is close to that of opal.

The IR band at ν = 950 cm^{-1} observed for as-synthesized opal (Fig. 5.7) may be attributed to Si-OH. This band was also observed in silica gel, but was not distinct in natural opal-A (Graetsch et al., 1994). This may suggest that the feature of water in synthetic opal is similar to that of silica gel, and implies that the proportion of the network structure in synthetic opal and silica gel may be much smaller than that in natural opal due to the bond-termination by OH groups. The total water content for as-synthesized silica gel estimated from the TG result is higher than that of opal, though the dehydration behaviors of synthetic opal and silica gel are basically similar as discussed in the following.

From the result of TG analyses for as-synthesized opal and silica gel, a significant amount of molecular water adsorbed at the sample surface is lost by heating at about 200 °C. The DTA curves of the as-synthesized opal and silica gel have a broad endothermic peak at 60-80 °C, which is attributed to the great loss of water molecules. The result of TG analyses for these samples indicate that all molecular water and almost surface silanol groups have been lost by heating up to 700 °C.

On the other hand, the results of Raman and FTIR analyses show that the both as-synthesized opal and silica gel lose the water molecules and silanol by heat treatment at 800 °C. Therefore, it is considered that the dehydration and condensation of silanol groups may lead to the formation of new Si-O-Si linkages. This is supported by the formation of the D_2 band and the development of the broad band at ν = 450 cm^{-1} in the Raman spectra for opal and silica gel heat-treated at 400–600 °C. In the Raman spectra for heat-treated silica gel, the band of silanol at around ν = 976 cm^{-1} shows the negative shift with heating up to 600 °C, although the Raman spectra of opals show the negligible change of this band position. A further experiment and discussion is

necessary, but the dehydration of silanol by heat treatment may be related with the shift of the band of silanol.

5.4.2 Temperature variation of the SEM image

The SEM image of as-synthesized opal displays a regular three-dimensional stacking of amorphous silica spheres and the diameter of the spheres is approximately 400nm (Fig. 5.3). According to Sanders (1964), this stacking structure may be responsible for the opalescence. Up to 1000°C, the regular stacking of the silica spheres seems still to be kept. However, increasing in temperature, silica spheres begin to shrink. The shrink rate seems not to be constant. Heating up to 600°C cause only a small shrinkage of silica sphere, so that it seems that the spheres still contact each other. However, the sample treated at 800°C has shown separation of each silica sphere. These results may indicate that dehydration of silanole groups is responsible for shrinkage of silica spheres in synthetic opal. Although shrinkage of the silica spheres occurred with increasing temperature, the regular arrangement of the spheres remained up to 1000 °C, so that opalescence was still observed, even after heat treatment at 1000 °C. The smooth surface of the opal treated at 1300 °C indicated complete melting of the regular arrangement of silica spheres and consequent loss of the opalescence.

Natural opal has secondary structure as well as silica gel, so that the amorphous silica spheres of opal are agglomerated particle of a tiny silica sphere with the diameter of 10-20 nm (Jones and Segnit, 1969; Langer and Flörke, 1974). The intensity of the peak at $2\theta = 2°$ in the XRD pattern of synthetic opal and silica gel may be related to the presences of the tiny silica spheres. The reduction in the intensity above 1000 °C may be due to the loss of the secondary structure of synthetic opal and silica gel.

5.4.3 Temperature variations of FSDP position in XRD patterns

Analysis of the FSDP positions in XRD patterns is useful to evaluate the size of the intermediate order structure as already described in chapter 3, 4. Figure 5.13 shows the temperature variations of the FSDP positions for as-synthesized opal and silica gel. The FSDP position for as-synthesized opal (S_1 = 1.64 $Å^{-1}$) is very close to that of silica gel

(S_1 = 1.65 Å^{-1}). Consequently, it is presumed that the intermediate range structure of as-synthesized opal is similar to that of silica gel and may be mainly composed of four-membered ring of SiO_4 tetrahedra. This is also supported by the strong and distinct D_1 band in Raman spectrum for as-synthesized opal. The FSDP positions for synthetic opal and silica gel show the similar temperature variation. The FSDP position for synthetic opal and silica gel are constant up to 400 °C, indicating that the average network structures for opal and silica gel still maintain a four-membered ring structure up to this temperature. The FSDP positions of both opal and silica gel gradually shift toward smaller *S* above 400 °C and approach that of silica glass (S_1 = 1.51 Å^{-1}, Shimada et al., 2002) by heat treatment at 1000 °C. These indicate that the intermediate range structures of opal and silica gel may be undergone the thermal reconstruction and may be mainly composed of six-membered rings by thermal treatment at 1000 °C. This structural evolution may be also concerned with the dehydration of silanol in samples by heat treatment up to 800 °C.

5.4.4 IR and Raman spectroscopic analyses

The Raman spectra between as-synthesized opal and silica gel have similar characteristics such as the presence of strong D_1 band and silanol. These may indicate that the structure of as-prepared opal is similar to that of silica gel. The synthetic opal and silica gel show the similar spectral change by heat treatment. At 400 °C, D_1 band becomes less intense in both Raman spectra for opal and silica gel, and the D_2 band appears. These spectral changes are developed up to 800 °C. Previous reports for heat-treated silica gel show the formation of three-membered rings due to dehydration reactions of adjacent surface silanols (Humbert et al., 1992; Brinker et al., 1986). Therefore, also in this study, the structural evolutions such as D_2 band formation for samples treated up to 800 °C may be due to dehydration of surface silanol by heat treatment. However, the D_2 band in the Raman spectrum for silica gel is slightly weaker than that of opal, although the content of surface silanol in silica gel is similar to that of opal. This reason will be discussed later.

In the Raman spectra for heat-treated opals, the intensity of the Raman band at around ν = 450 cm^{-1} due to the symmetric Si-O-Si stretching vibration increases and reaches a clear maximum above 600 °C. The band also becomes broad with heat treatment at

800 °C, indicating the polymerization of the network structure by the dehydration of silanol. Moreover, the upsizing of the intermediate structure by thermal effect may start at this temperature. In the Raman spectra for silica gels, similar changes of bands below ν = 480 cm^{-1} are observed. However, the broadening of bands below ν = 480 cm^{-1} may develop more rapidly (at 600 °C) than that of heat-treated opals. Both D_1 and D_2 bands become less intense with heat treatment at 1000 °C for heat-treated opal and silica gel. These observations may indicate that the intermediate structure of both samples treated at 1000 °C approach the silica glass-like network structure with a wide range Si-O-Si angle distribution and a small content of three- and four-membered rings.

In FTIR spectra for heat-treated opals, the band at ν = 800 cm^{-1} attributed to the Si-O-Si bending vibration shows the positive shift about 11 cm^{-1} after heat treatment at 400 °C. This may be related to a decrease of the Si-O-Si angle due to the loss of the water molecules and the formation of three-membered rings with the dehydration of surface silanols as indicated by the Raman spectra. This IR band shows a large positional deviation at 800 °C and shift to lower wavenumber above 1000 °C, which may indicate the formation of a network structure with a wide range Si-O-Si angle distribution. This result corresponds to the development of the Raman band around ν = 450 cm^{-1} attributed to the Si-O-Si symmetric stretching mode. The IR band position observed after heat treatment at 1000 °C is similar to that of silica glass (ν = 803 cm^{-1}). On the other hand, the band at ν = 799 cm^{-1} in the heat-treated silica gels show only small positive shift to ν = 802 cm^{-1} after heat treatment at 400 °C. Raman and FTIR results for silica gels show that the complete dehydration of water may occur at slightly higher temperature than opal. Besides, the TG result for the silica gel shows that the silica gel includes water molecules in a lot of 10 % than opal. Moreover, the result of Raman spectra shows that the reconstruction of the network structure, which is upsizing of intermediate structure may occur rapidly in the heat-treated silica gels than that of opal. These may induce the formation of the weak Raman band of three-membered ring and the small shift of the band of the Si-O-Si bending mode for the treated silica gels up to 1000 °C.

For opal and silica gel sample, the reconstruction of the network structure to a six-membered ring predominant structure starts by heat treatment above 800 °C and 600 °C, respectively. Moreover, the Raman spectra show a decrease in the intensity of the D_1 and D_2 bands after the heat treatment at 1000 °C, which indicates the structure is

very close to that of silica glass. The structural change derived from the FTIR and Raman spectra is consistent with the change of the FSDP positions with temperature.

For synthetic opal and silica gel treated at 1000 °C, FTIR spectra shows the broad band attributed to the Si-O stretching mode shift towards to higher wavenumber by 20 and 17 cm^{-1}, respectively. The lengthening of this band with increasing temperature may indicate the increase of mean Si-O-Si angle (Lasaga and Gibbs, 1988; Murray and Ching, 1989). Therefore, the increase in the mean Si-O-Si angle may be owing to thermal reconstruction of the network structure. This interpretation is consistent with the Raman spectra, FSDP of XRD measurements and the position of the IR band at ν = 800 cm^{-1}.

5.4.5 Structural change of the amorphous phase and crystallization to cristobalite

The XRD, IR, and Raman results indicate that synthetic opal and silica gel begin to crystallize to low-cristobalite by thermal treatment at 1200-1300 °C. The exothermic reaction at 1200–1300 °C in the DTA curve for as-synthesized opal and silica gel may be caused by rapid crystallization to well-ordered cristobalite, in accordance with the report by Jones and Segnit (1971). Moreover, for the XRD patterns of opals treated above 1200 °C, the intensity of the cristobalite phase increased with increasing of the treatment temperature to 1400 °C.

The stable phase of SiO_2 in 870 - 1470°C is high-tridymite, and low-cristobalite is a metastable phase (Sosman, 1955). Opal and silica gel samples directly transform to low-cristobalite according to the Ostwald's step rule. Because the energy gap between amorphous phase and low-cristobalite is smaller than that between amorphous and β-tridymite phase. This temperature region (around 1200°C) is stabilized phase of high-tridymite, however, according to the Ostwald's step rule, low-cristobalite that is the metastable phase is crystallize in this temperature.

5.5 Conclusions

The structural evolutions of synthetic opal and silica gel by heat-treatment can be

summarized as follows. Synthetic opal is considered to consist mainly of the four-membered ring as similar to silica gel. A large quantity of water molecules and silanol groups is contained in the spherical structure units of opal.

However, the water content of as-synthesized opal is smaller than that of silica gel.

For both opal and silica gel, heat treatment up to 400 °C results in the dehydration for a large number of surface silanols and polymerization to form new Si-O-Si linkages as three-membered rings. However, the quantity of the three-membered ring in the heat-treated silica gel may be lower than opal. It may be related with the rapid thermal reconstruction in the heat-treated silica gel. By the heat treatment up to 800 °C, water molecules in synthetic opal and silica gel are lost, silanols are completely dehydrated, and the formation of the network is developed. This network structure contains a widely distribution of Si-O-Si angle like silica glass, although relatively small ring as three and four member ring is still abundant. By heat treatment above 1000 °C, the structures of opal and silica gel approach that of silica glass, of which the intermediate structure contains a large amount of six-membered ring. In addition, the amount of small rings decreases. This structural change may be due to thermal reconstruction of the network structure. The result in this study suggests that the synthetic opal may require higher temperature to reconstruct the network structure than that of silica gel. This discussion is consistent with results of the previous report by Kamiya and Nasu (1998). The distinct formation of three-membered ring by dehydration of surface silanol in the treated opal is origin of the higher reconstruction temperature of opal.

Above 1300 °C, the structures of opal and silica gel changes to that of low-cristobalite completely. However, minor evidence of low-tridymite stacking is observed at 1400 °C in heat-treated opal.

synthetic opal	silica gel
160	-
400	400
600	600
800	800
1000	1000
1100	-
1200	-
1300	1300
1400	-

Table 5.1 The temperature of heat treatment for opal and silica gel. Each sample treated for 1 hr

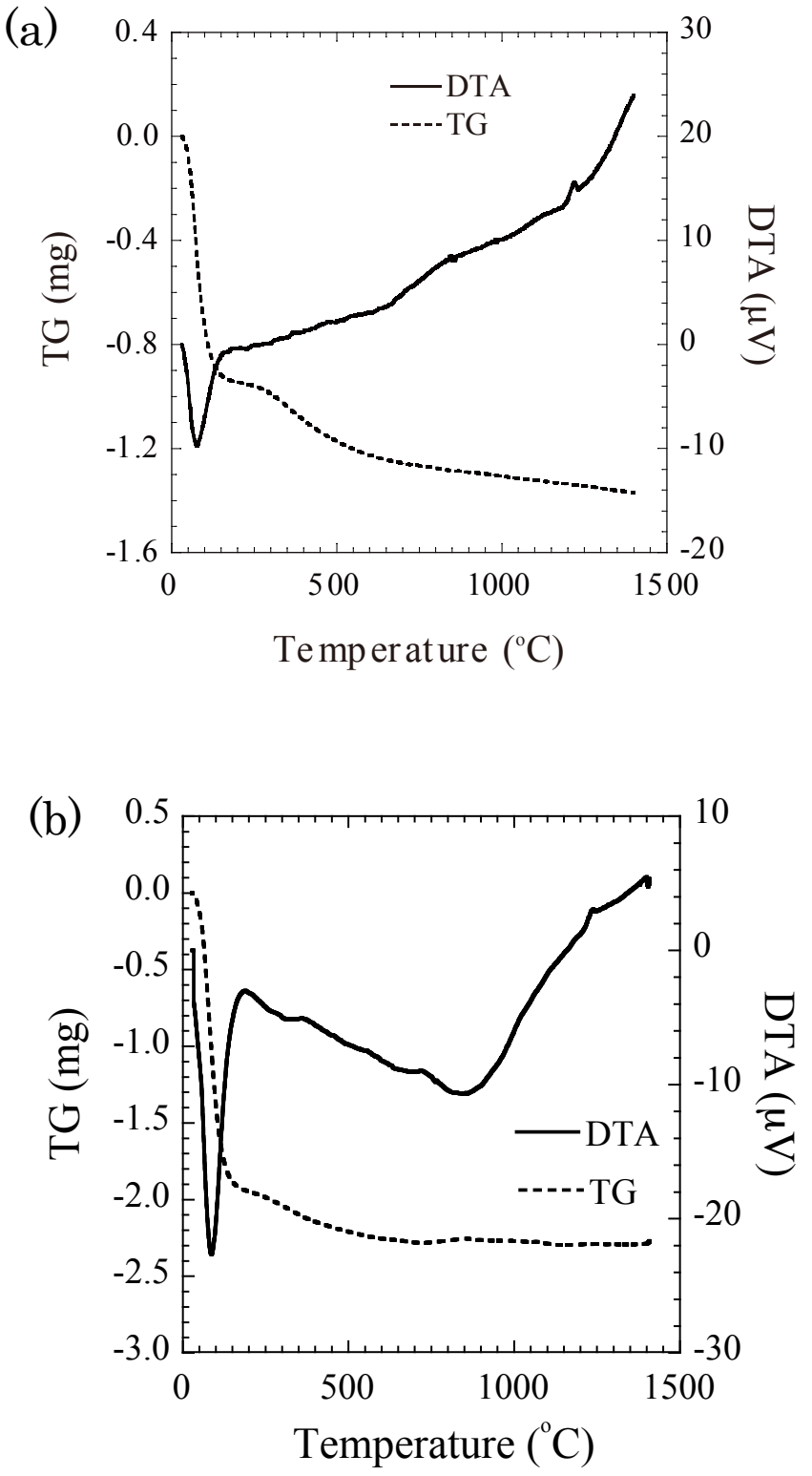

Fig. 5.1 DTA and TG curves for the (a) as-synthesized opal and (b) silica gel. Fig 5.1 (a) is from Arasuna et al. (2013b), © 2013 Springer, http://link.springer.com/

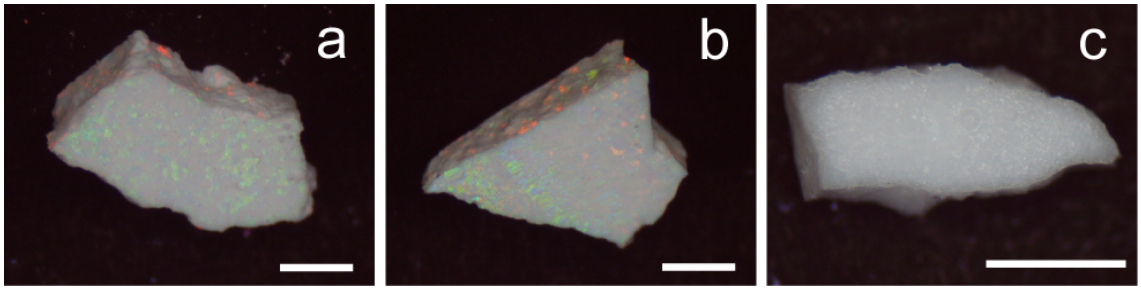

Fig. 5.2 Opalescence changes of heat-treated opals at (a) 600 °C, (b) 1000 °C, and (c) 1300 °C. Scale bars are 1mm. This figure is from Arasuna et al. (2013b), © 2013 Springer, http://link.springer.com

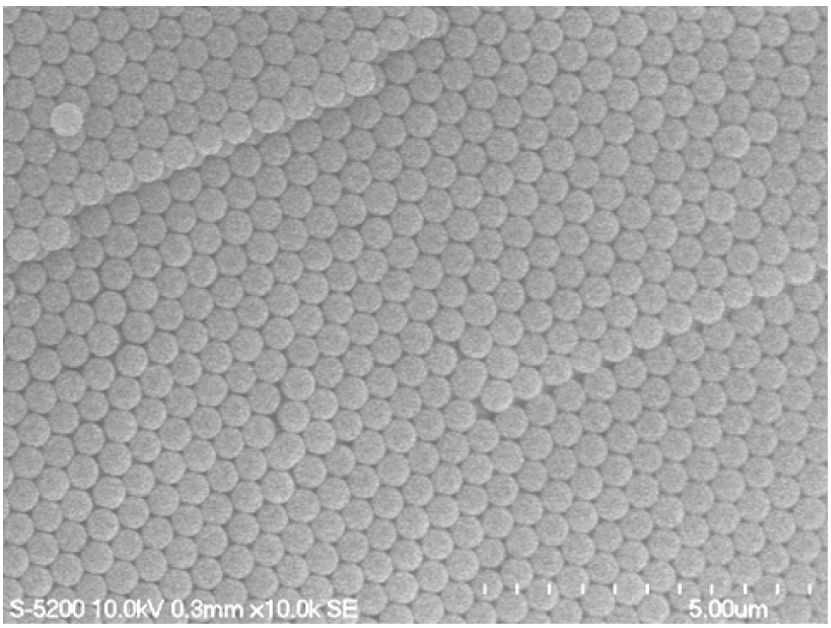

Fig. 5.3 SEM image for as-synthesized opal. This figure is from Arasuna et al. (2013b), © 2013 Springer, http://link.springer.com

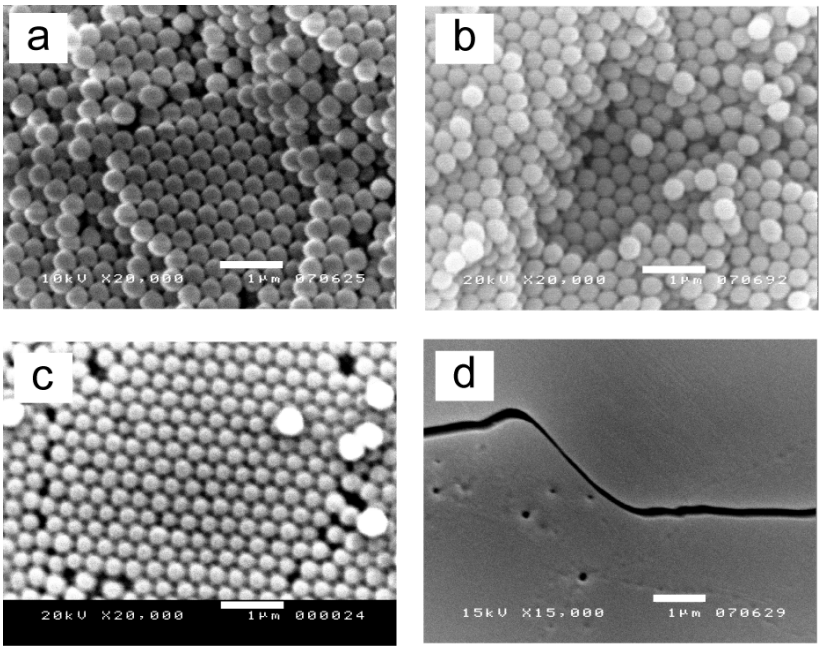

Fig. 5.4 SEM micrographs of heat-treated opals at (a) 600 °C, (b) 800 °C, (c) 1000 °C and, (d) 1300 °C. Scale bars are 1µm. This figure is from Arasuna et al. (2013b), © 2013 Springer, http://link.springer.com

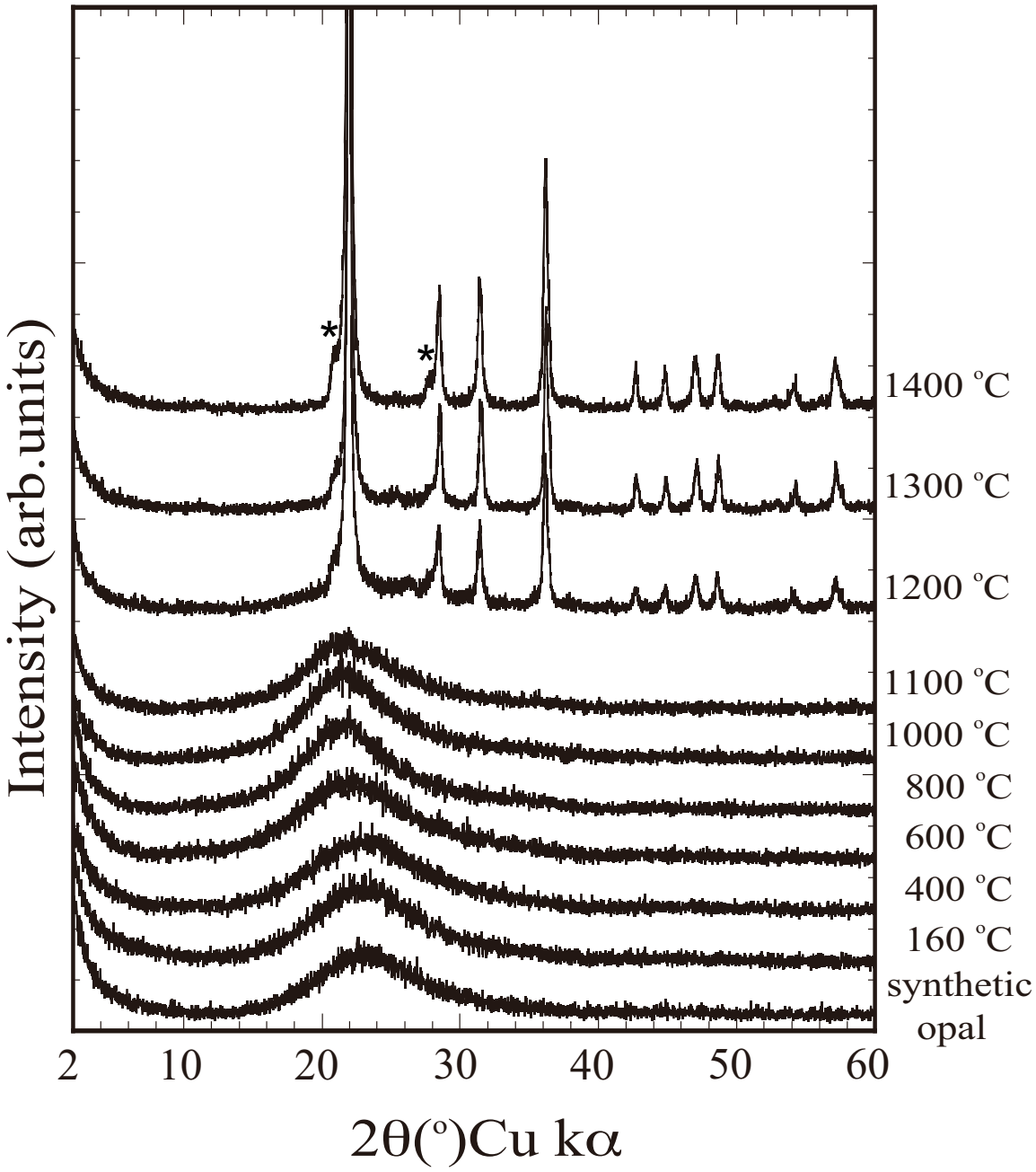

Fig. 5.5 XRD patterns of as-synthesized and heat-treated synthetic opals. The asterisks at around 2θ = 21 and 28° correspond to the low-tridymite phase. This figure is from Arasuna et al. (2013b), © 2013 Springer, http://link.springer.com

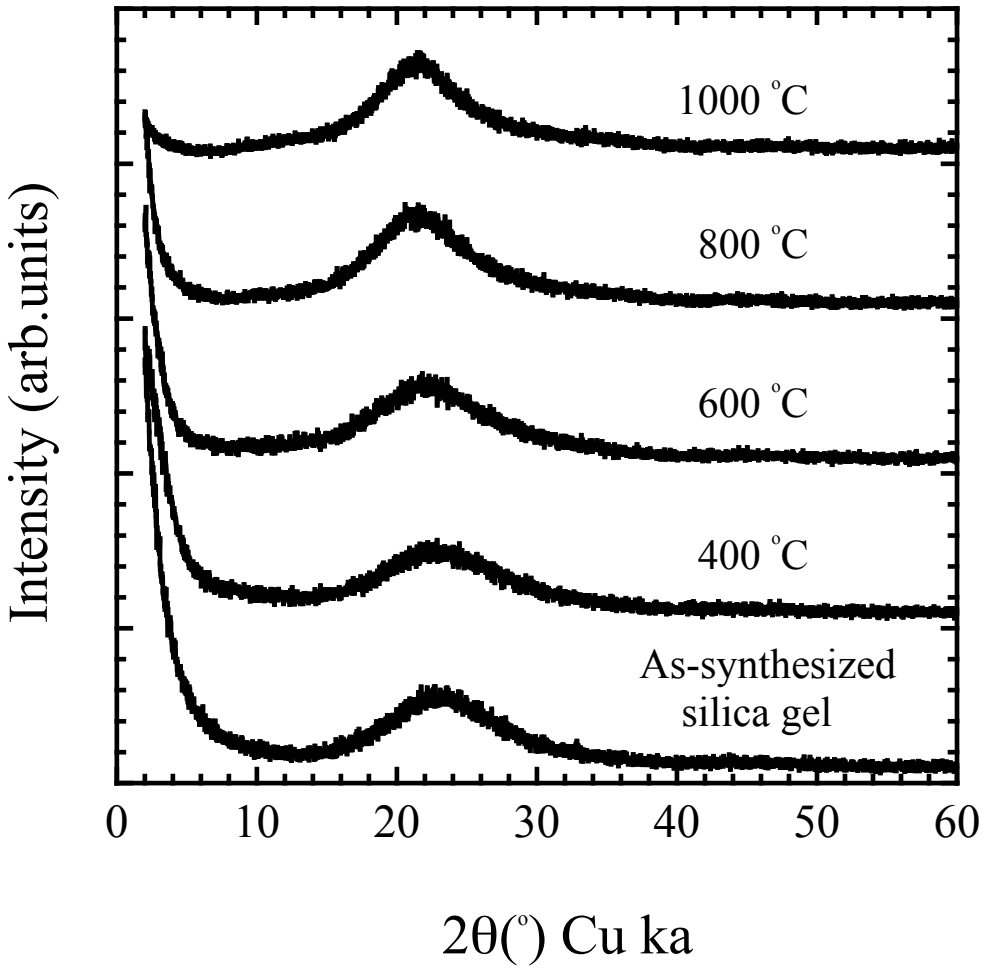

Fig. 5.6 XRD patterns for as-synthesized and heat-treated silica gel

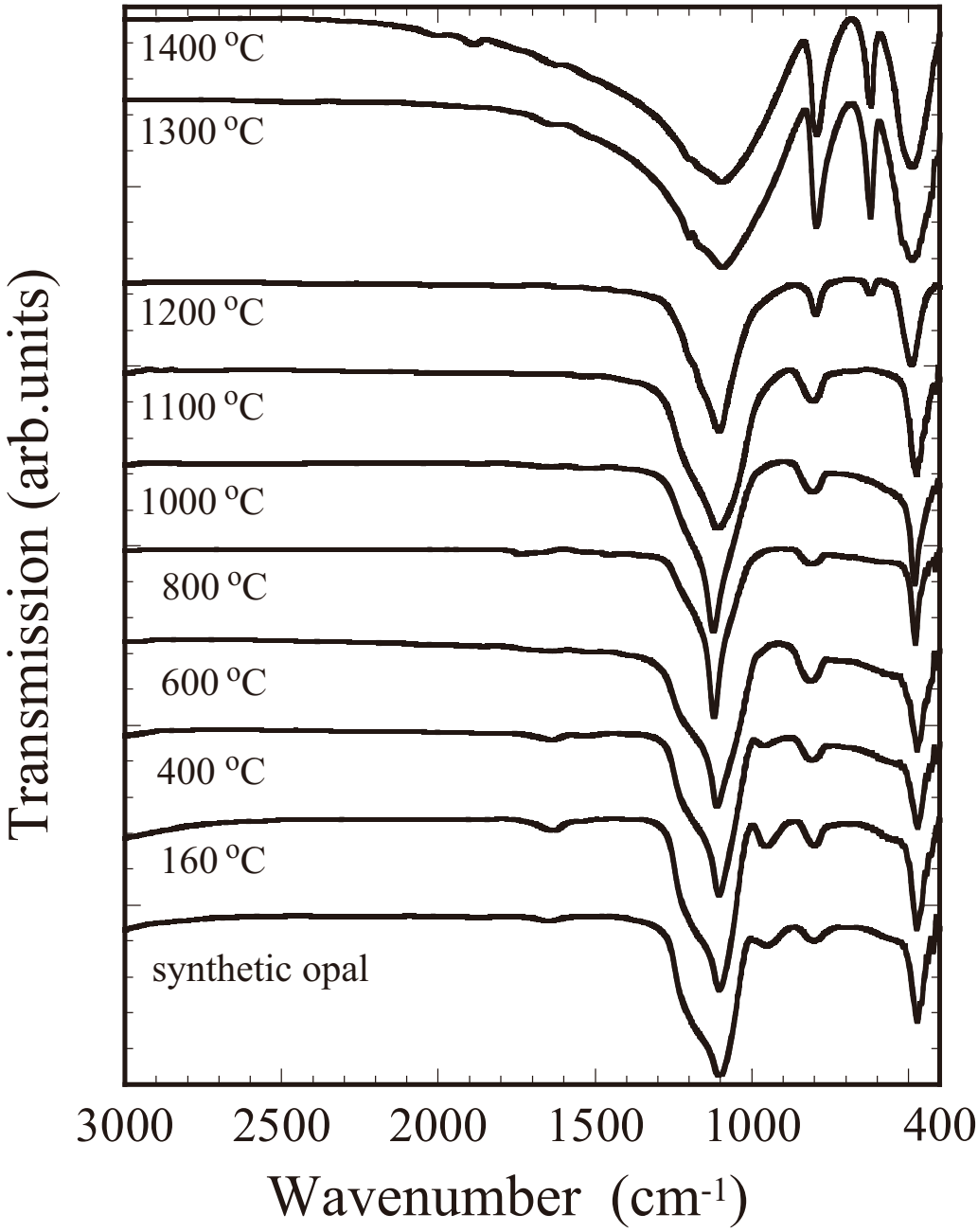

Fig. 5.7 FTIR spectra for as-synthesized and heat-treated synthetic opals (ν = 400-2500 cm^{-1}). This figure is from Arasuna et al. (2013b), © 2013 Springer, http://link.springer.com

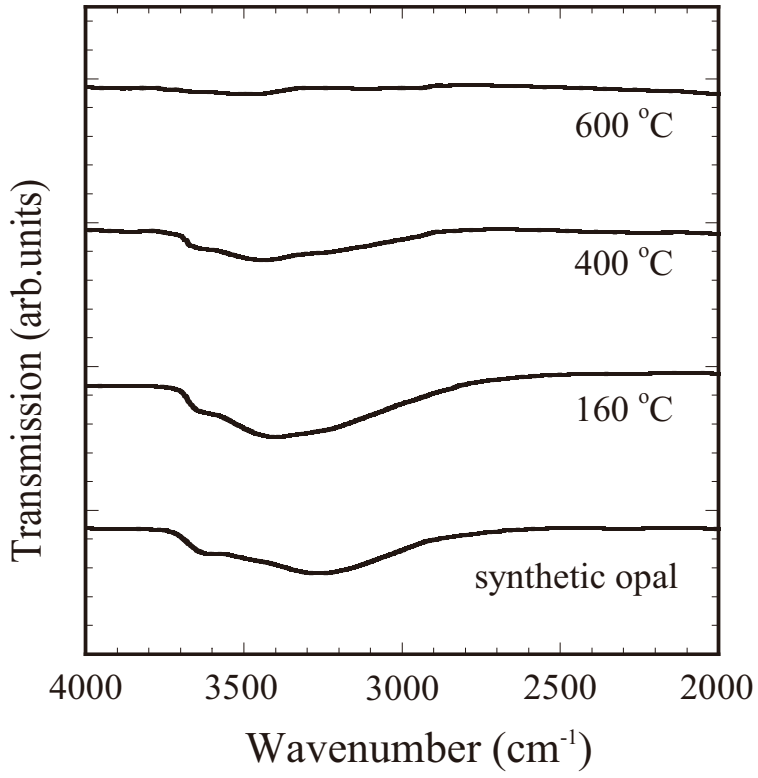

Fig. 5.8 FTIR spectra for as-synthesized and heat-treated synthetic opals (ν = 2000-4000 cm^{-1}). This figure is from Arasuna et al. (2013b), © 2013 Springer, http://link.springer.com

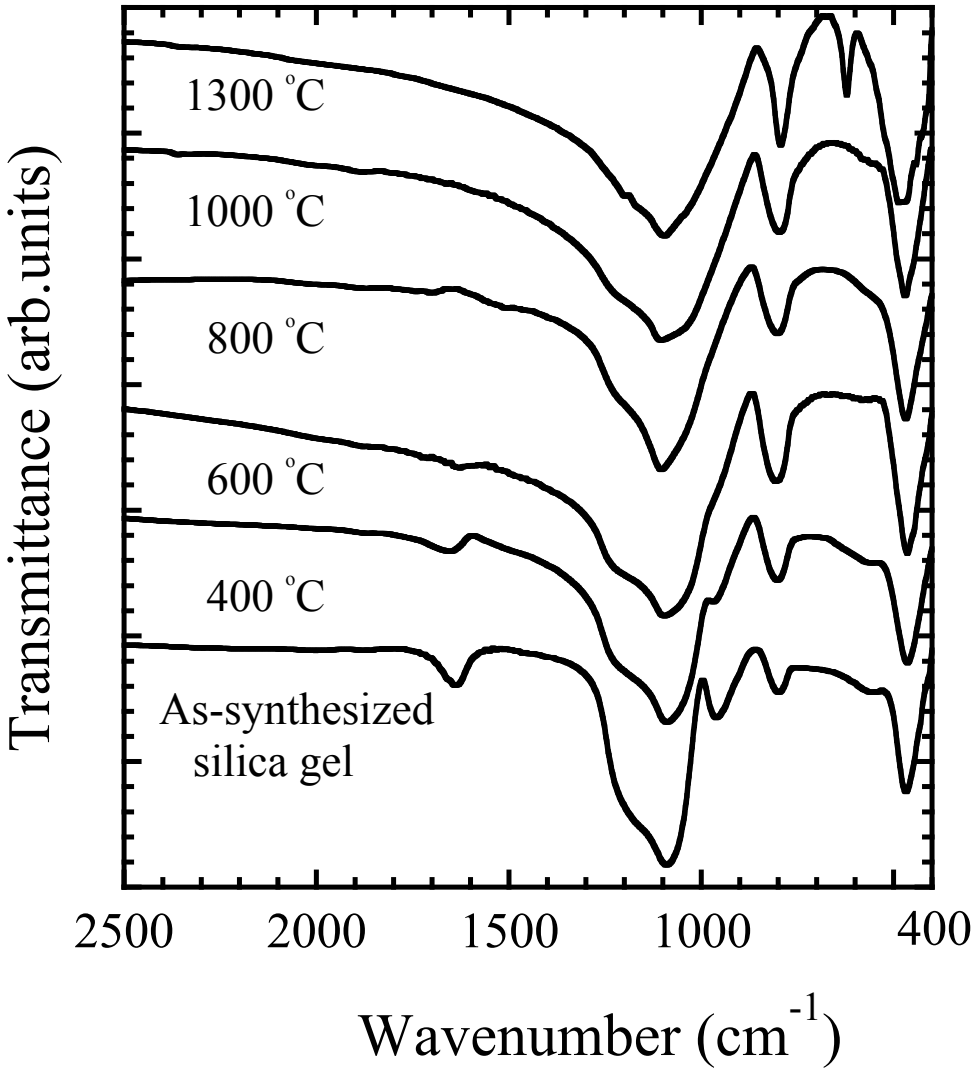

Fig. 5.9 FTIR spectra for as-synthesized and heat-treated silica gels (ν = 400-2500 cm^{-1})

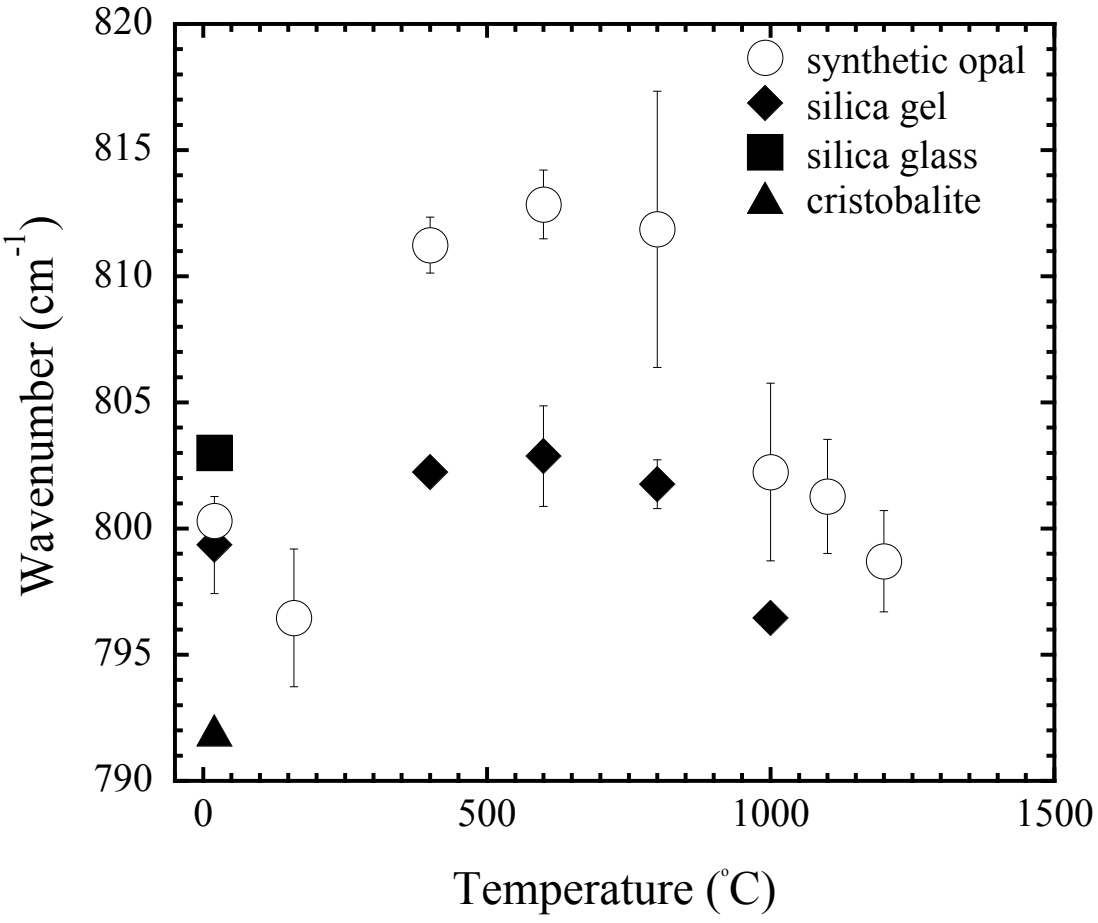

Fig. 5.10 Variations of the Si-O-Si bending mode with heat treatment temperature. This figure was modified from Arasuna et al. (2013b), © 2013 Springer, http://link.springer.com

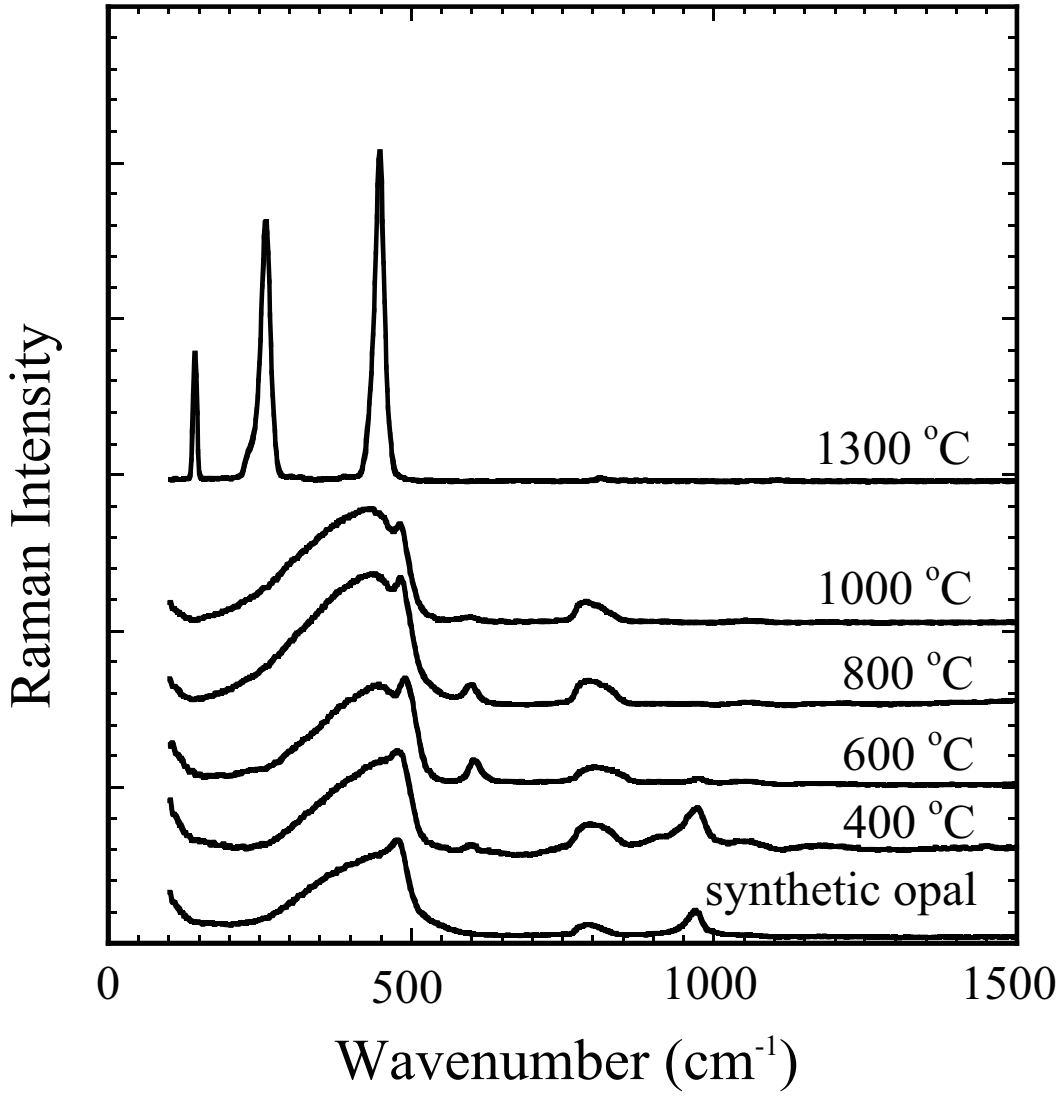

Fig. 5.11 Raman spectra for as-synthesized and heat-treated synthetic opals. This figure is from Arasuna et al. (2013b), © 2013 Springer, http://link.springer.com

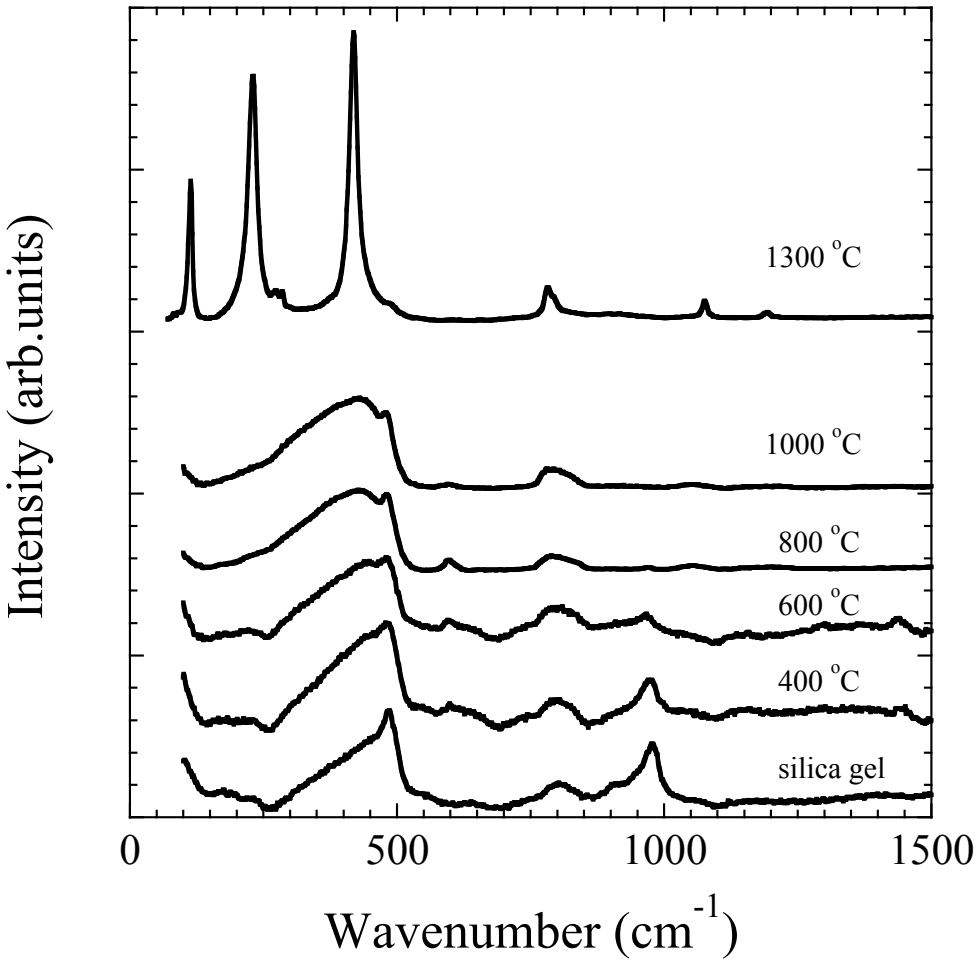

Fig. 5.12 Raman spectra for as-synthesized and heat-treated silica gels

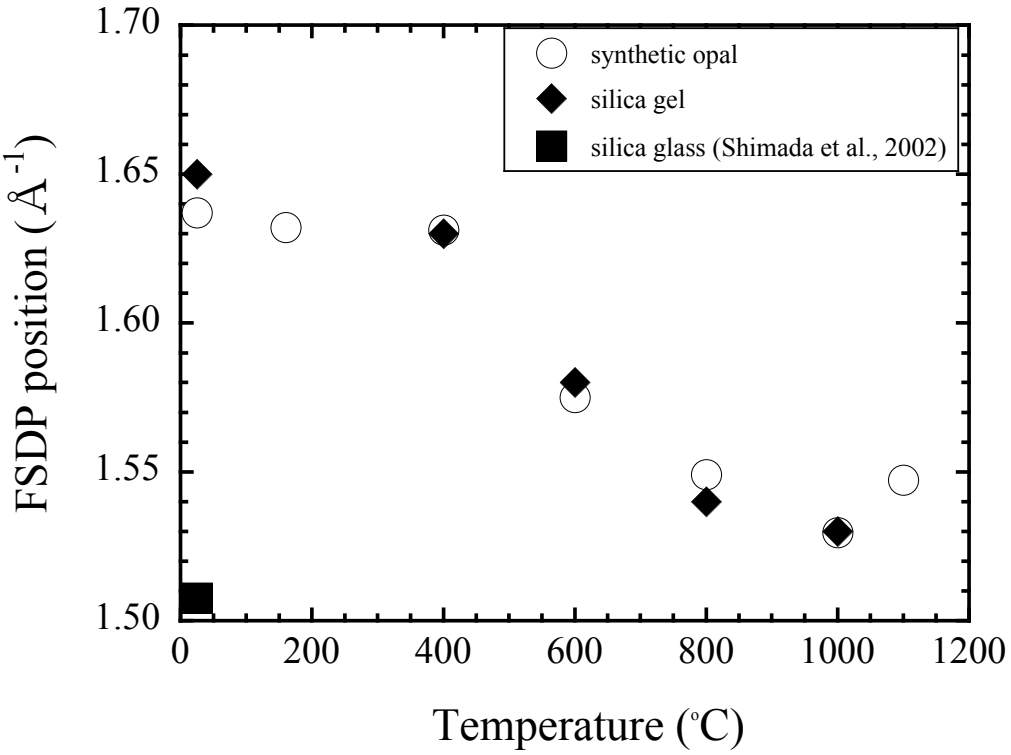

Fig. 5.13 Variations of the FSDP positions with heat treatment temperature. This figure is modified from Arasuna et al. (2013b), © 2013 Springer, http://link.springer.com

Chapter 6
General conclusion

6.1 The water behavior in hydrous amorphous silica materials under high pressure and temperature

Silica gel and synthetic opal include a great number of water molecules and silanol groups in the structure, though the volume of water in the silica gel is much greater than synthetic opal.

Under the static compression of silica gel up to 10 GPa at 25ºC, the adsorbed water molecules at the surface are released easily, though most of silanols remain in the structure. Obvious presence of the Q_3 silanol in these materials is observed in their FTIR, Raman, and NMR spectra. Moreover, ^{29}Si MAS NMR indicates that the most of Q_3 species are left in the structure. It is not clear, but Q_2 is also likely to be left. These indicate clearly that the silanol groups are not dehydrated by compressions up to 10 GPa at 25ºC. However, under the compressions at 100 °C and 2 GPa, the dehydration of silanol occurs easily. Thus, the temperature, even if it is not so high, strongly contributes to the dehydration of silanol than pressure. On the other hand, the dehydration and condensation of silanol form the new Si-O-Si network in their structures. Moreover, depending on the pressure and temperature, newly formed network structure has various ring structures of SiO_4 tetrahedra as summarized in next section. Therefore, the dehydration of silanol has a great influence on the structure.

In the subducition zone, temperature should be higher than the experimental condition in this study. The static compression for sample shows the pressure may not give the influence on the dehydration of silanol. Therefore, on the basis of the result of the thermal experiment, the silanol may be left to the region with temperature about 800 °C in the subduction zone.

In the shock-wave experiments, the water molecules of silica gel and synthetic opal decrease gradually, although their silanol may not be dehydrated until 17.0 GPa. Therefore, it could be concluded that the water molecules are released easily than silanol under the shock compression. This conclusion is similar to the result of the static compression for silica gel. Above 20.7 GPa of shock pressure, the considerable amount of water molecules may be released and about half of silanol are dehydrated. However,

the Raman spectra of the sample compressed at above 20.7 GPa show the presence of specific silanol clearly. Two types of remaining silanol are presumed from the results of Raman spectroscopic analysis; mutually hydrogen bonded silnols and silanol which has hydrogen bond to neighboring water molecule.

However, nearly half of silanols are dehydrated above 20.7 GPa. It is considered that relatively high after shock temperature influenced strongly to the dehydration of silanol.

On the other hand, tiny amount of water molecules and the silanol remain even after the shock compression at 30.7 GPa. In conclusion, the water in the comet may endure the shock compression and the high after shock temperature and may be carried to the surface of the earth.

6.2 The structural change of hydrous amorphous silica materials under high pressure and temperature

The hydrous amorphous silica material containing the silanol in its structure, such as silica gel and synthetic opal, has less polymerized silica network structure. This structural feature may induce the drastic structural change in contrast to that of fully polymerized amorphous material such as silica glass under relatively low temperature and pressure.

Under the compression at 5 GPa and room temperature, the buckling (compaction) of the network structure occurs easily, because the less polymerized structure of silica gel and opal must be variable than fully polymerized one. Furthermore, this less polymerized structure may lead the irreversible structural change even under the compression at 5 GPa and room temperature.

On the other hand, the network structure of silica gel is ordered under the compression at 2 GPa at 100 °C to form the ordered four- and six-membered rings of SiO_4 tetrahedra. Under the compression at 5 GPa and 100 °C, only ordered four-membered rings are formed, resulting in the crystallization to coesite. Izutani (2003) reported that silica glass crystallizes to quartz under 5.0 GPa at 500 °C, although the stable pressure and temperature region for quartz is lower than coesite. In contrast with this report, the silica gel sample shows the crystallization to coesite at lower pressure and temperature. It is thus considered that the less polymerized network structure with silanols may easily transform to the structure of thermal equilibrium state.

Moreover, the dehydration and polymerization of silianol in the buckling network structure under the compression may be conducive to the formation of the ordered small ring, such as four-membered ring. These may allow the easy crystallization of silica gel by compression at relatively low temperature and short duration. The presence of silanol gives a great influence on the structural change of hydrous amorphous silica. As I noted in chapter 5, thermal treatment can only induce the dehydration and condensation of silanol. Consequently, the structural change of the silica gel is affect by the after shock temperature rather than pressure. These results indicate that the external skeleton of diatom can also crystallize to high-pressure phase, such as coesite, in the subduction zone under relatively low temperature and pressure condition.

On the other hand, for the precise study of the structural change of minerals in subduction zone, strain and strain rate should be also considered. It will be discussed in my future work.

In the shock-wave experiments for silica gel, high after shock temperature gives a considerable influence on the network structure of silica gel. Unlike the static compression experiments under room temperature, the intermediate range structure of silica gel approaches to that of silica glass including the larger rings (>six-membered ring) in the network structure. The four-membered ring of SiO_4 tetrahedra in the recovered samples may be relaxed to larger ring such as six-membered ring by high after shock temperature.

The thermal experiments for the synthetic opal and silica gel support this presumption. By the thermal treatment at 600-800 °C, upsizing of the intermediate structure of the samples are observed. It indicates that the structure of samples approaches to that of silica glass. Therefore, in the shock-wave experiments for silica gel, the after shock temperature may be significantly high (>600 °C) even at 20.7 GPa.

Comparing with the result of the static compression, the structure in the recovered sample after shock compressions does not show the crystallization. It is considered that the atomic diffusion is necessary for phase transition. However, in the shock wave experiment adopted in this study, the calculated duration time for shock pressure is around 10^{-7}s. Moreover, the duration time of after shock temperature may be several or several tens minutes and temperature decreases gradually. These short duration times of shock pressure and after shock temperature may not enough for the atomic diffusion. Therefore, the recovered sample after the shock compression could not transform to

high pressure phase.

Acknowledgements

The author expresses a greatest gratitude to Prof. M. Okuno of Kanazawa University for his kind instruction and variable advices. The author also thanks to Dr. H. Okudera of Kanazawa University for preparation of the synthetic opal and silica gel, and for the valuable advices and suggestions.

The author wishes to express thanks to Prof. S. Arai and Dr. T. Mizukami of Kanazawa University for Raman spectra measurements and their valuable advices. The author expresses her thanks to Prof. M. Akaogi of Gakushuin University for carrying out the static compression using multi anvil apparatus and for providing synthesized coesite sample. The author also thanks to Dr. Y. Shirako and Ms. T. Yokoyama for carrying out the static compression using multi anvil apparatus. The author is thankful to Dr. X. Xue of Institute for study of the Earth's interior of Okayama University for carrying out NMR measurements and for her valuable suggestions and advices. The author is grateful to Prof. T. Mashimo and Dr. L. Chen of Kumamoto University for carrying out the shock-wave experiments. The study of shock-wave compression was supported by G-COE program of Kumamoto University (GCOE-JS2012-9). The author also wishes to express the thanks to Dr. M. Koyano of Japan Advanced Institute of science and technology for carrying out Raman spectra measurements for synthetic opal. The author also thanks to Mr. N. Ito of Japan Advanced Institute of Science and Technology for his help on SEM measurements. A part of this work was conducted in Kyoto-Advanced Nanotechnology Network, supported by "Nanotechnology Network" of the Ministry of Education, Culture, Sports, Science and Technology, Japan. Finally, this work was supported by Grant-Aid for JSPS Fellow Grant Number 255624.

References

Arasuna A, Okuno M, Mizukami T, Akaogi M, Yokoyama T, Okudera H, Arai S (2013a) The role of water in coesite crystallization from silica gel. *Eur. J. Mineral.*, 25, 791-796

Arasuna A, Okuno M, Okudera H, Mizukami T, Arai S, Katayama S, Koyano M, Ito M (2013b) Structural changes of synthetic opal by heat treatment. *Phys. Chem. Minerals.,* 40, 747-755

Arasuna A, Okuno M, Chen L, Mashimo T, Okudera H, Mizukami T, Arai S (2016) Shock-wave compression of silica gel as a model material for comets. *Phys. Chem. Minerals.,* 43, 493-502,

Bates JB (1972) Raman spectra of α and β cristobalite. *J. Chem. Phys.,* 57, 4042-4047

Benesi HA, Jones AC (1959) An infrared study of the water–silica gel system. *J. Phys. Chem.,* 63, 179-182

Bergna HE (2006) Colloid chemistry of silica: An overview. in ‘‘Colloidal silica fundamentals and applications’’, Bergna HE, Roberts WO ed. Taylor and Francis, 9-35

Bertoluzza A, Fagnano C, Morelli MA, Gottardi V, Guglielmi M (1982) Raman and infrared spectra on silica gel evolving toward glass. *J. Non-Cryst. Solid.,* 48, 117-128

Brinker CJ, Tallant DR, Roth EP, Ashley CS (1986) Sol-Gel Transition in simple silicates -Structural studies during densification. *J. Non-Cryst. Solids.,* 82, 117-126

Coes L (1953) A new dense crystalline silica. *Science*, 118, 131-132.

Costa TMH, Gallas MR, Benvenutti EV, de Jomada JAH (1997) Infrared and thermogravimetric study of high pressure consolidation in alkoxide silica gel powders. *J. Non-Cryst. Solids.,* 220, 195-201

Davis KM, Tomozawa M (1996) An infrared spectroscopic study of water-related species in silica glasses. *J. Non-Cryst. Solids.,* 201, 177-198

DeCarli PS, Jamieson JC (1959) Formation of n amorphous form of quartz under shock conditions. *J. Chem. Phys*., 3, 1675-1676

Elsila JE, Glavin DP, Dworkin JP (2009) Cometary glycine detected in samples returned by Stardust. *Meteor. Planet. Sci.,* 44, 1323-1330

Etchepare J, Merian M, Kaplan P (1978) Vibrational normal modes of SiO_2. II. Cristobalite and tridymite. *J. Chem. Phys.,* 68, 1531–1537

Flörke OW (1973) The genesis of Hyalite. *Neues. Jahrb. Mineral. Mh.*, 2, 82-89

Galeener FL (1982a) Planar rings in vitreous silica. *J. Non-Cryst. Solids.,* 49, 53-62

Galeener FL (1982b) Planar rings in glasses. *Solid. State. Commun.,* 44, 1037-1040

Galeener FL, Geissberger AF (1983) Vibrational dynamics in ^{30}Si-substituted vitreous SiO_2. *Phys. Rev. B,* 27, 6199-6204

Gendron-Badou A, Coradin T, Maquet J, Frhilich F, Livage J (2003) Spectroscopic characterization of biogenic silica. *J. Non-Cryst. Solids.,* 316, 331-337

Gratz AJ, DeLoach LD, Clough TM, Nellis WJ (1993) Shock amorphization of cristobalite. *Science,* 259, 663-666

Graetsch H, Flörke OW, Miehe G (1985) The Nature of Water in Chalcedony and Opal-C from Brazilian Agate Geodes. *Phys. Chem. Minerals.,*12, 300-306

Graetsch H, Gies H, Topalović I (1994) NMR, XRD and IR study on microcrystalline opals. *Phys. Chem. Minerals.,* 21, 166-175

Graetsch H (1994) Structural characteristics of opaline and microcrystalline silica minerals. *Rev. Mineral.,* 29, 209-232

Greenberg JM (1998) Making a comet nucleus. *Astron. Astrophys.,* 330, 375-380

Handke M, Mozgawa W (1993) Vibrational spectroscopy of the amorphous silicates. *Vib. Spectrosc.,* 5, 75–84

Hemley RJ*,* Mao HK, Bell PM, Mysen BO (1986) Raman spectroscopy of SiO_2 glass at high pressure. *Phys. Rev. Lett.,* 57, 747-750

Hemley RJ, Prewitt CT, Kingma KJ (1994) High-pressure behavior of silica. *Rev. Mineral.,* 29, 41-81

Hench LL, West JK (1990) The Sol-Gel Process. *Chem. Rev.,* 90, 33-72

Humbert B, Burneau A, Gallas JP, Lavalley JC (1992) Origin of the Raman bands, D_1 and D_2, in high surface area and vitreous silicas. *J. Non-Cryst. Solids.,* 143, 75-83

Innocenzi P (2003) Infrared spectroscopy sol-gel derived silica-based films: a

spectra-microstructure overview. *J. Non-Cryst. Solids.,* 316, 309-319

Inoue A, Okuno M, Okudera H, Mashimo T, Omurzak E, Katayama S, Koyano M (2010) Shock compression of synthetic opal. *J. Phys.: Conf. Ser.,* 215, 012147, 1-5

Izutani K (2003) Structural changes of GeO_2-SiO_2 glasses and agate by shock compression. Master thesis of Kanazawa University

Jones JB, Segnit ER (1969) Water in sphere-type opal. *Min. Mag.,* 37, 357-361

Jones JB, Segnit ER (1971) The nature of Opal I. nomenclature and constituent phases. *J. Geol. Soc. Aust.,* 18, 57-68

Kamiya K, Sakka S (1980) TiO_2-SiO_2 glasses prepared from metal alkoxides. *J. Materials. Science.,* 15, 2937-2939

Kamiya K, Nasu H (1998) Structural and thermal change of alkoxy-derived silica gel fibers and films. *Ceram. Trans.,* 81, 21-28

Kamiya K, Oka A, Nasu H, Hashimoto T (2000) Comparative study of structure of silica gels from different sources. *J. Sol-Gel. Sci. Technol.,* 19, 495-499

Kato M, Sawamoto H, Kumazawa M, Wada N (1975) Synthesis of coesite from ultra fine particles. *Jpn. J. Appl. Phys.,* 14, 181-183

Kingma K, Hemley RJ (1994) Raman spectroscopic study of microcrystalline silica. *Am. Mineral.,* 79, 269-273

Koch-Müller M, Fei Y, Hauri E, Liu Z (2001) Location and quantitative analysis of OH in coesite. *Phys. Chem. Minerals.,* 28, 693-705

Krol DM, Van Lierop JG (1984) Raman study of the water adsorption on monolithic silica gels. *J. Non-Cryst. Solids.,* 68, 163-166

Langer K, Flörke OW (1974) Near infrared absorption spectra (4000-9000 cm^{-1}) of opals and the role of "water" in these SiO_2 n H_2Ominerals. *Fortschr. Miner.,* 52, 17-51

Lasaga AC, Gibbs GV (1988) Quantum mechanical potential surfaces and calculations on minerals and molecular clusters I. STO-3G and 6-31G results. *Phys. Chem. Minerals.,* 16, 29-41

Lippincott ER, Van Valkenburg A, Weir CE, Bunting EN (1958) Infrared studies on

polymorphs of silicon dioxide and germanium dioxide, *J. Res. Natl. Bur. Stand.,* 61, 61-78

Mashimo T, Ozaki S, Nagayama K (1984) Keyed-powder gun for the oblique-impact shick study of solids in several 10s of GPa region. *Rev. Sci. Inst.,* 55, 226-230

Matson DW, Sharma SK, Philpotts JA (1986) Raman spectra of some tectosilicates and of glasses along the orthoclase-anorthitea and nepheline-anorthite joins. *Am. Mineral.,* 71, 694-704

McMillan P (1984) Structural studies of silicate glasses and melts - applications and limitations of Raman spectroscopy. *Am. Mineral.,* 69, 622-644

McMillan PF, Wolf GH (1995) Vibrational spectroscopy of silicate liquids. *Rev. Mineral. Geochem.,* 32, 247-315

Miehe G, Graetsch H (1992) Crystal structure of moganite: A new structure type for silica. *Eur. J. Mineral.,* 4, 693-706

Murray CA, Greytak TJ (1979) Intrinsic surface phonons in amorphous silica. *Phys. Rev. B,* 20, 3368-3387

Murray RA, Ching WY (1989) Electronic- and vibrational-structure calculation in models of the compressed SiO_2 glass systems. *Phys. Rev. B,* 39, 1320-1331

Naka S, Inagaki M, Kameyama T, Suwa K (1974): The effect of water on the crystal growth of coesite. *J. Cryst. Grow.,* 24-25, 614-616

Okudera H, Hozumi A (2003) The formation and growth mechanisms of silica thin film and spherical particles through the Stöber process. *Thin. Solid. Films.,* 434, 62-68

Okuno M, Reynard B, Shimada Y, Syono Y, Willaime C (1999) A Raman spectroscopic study of shock-wave densification of vitreous silica. *Phys. Chem. Minerals.,* 26, 304-311

Orcel G, Phalippou J, Hench LL (1986) Structural changes of silica xerogels during low temperature dehydration. *J. Non-Cryst. Solids.,* 88, 114-130

Orcel G, Hench LL, Artaki I, Jonas J, Zerda TW (1988) Effect on formamide additive on the chemistry of silica sol-gels II: Gel structure. *J. Non-Cryst. Solids.,* 105, 223-231

Ostrooumov M, Eritsch E, Lasnier B, Lerfrant S (1999) Spectres Raman des opals:

aspect diagnostique et aide à la classification. *Eur. J. Mineral.,* 11, 899-908

Sanders JV (1964) Colour of Precious Opal. *Nature,* 204, 1151-1153

Sharma SK, Mammone JF, Nicol MF (1981) Raman investigations of ring configurations in vitreous silica. *Nature,* 292, 140-141

Sharma SK, Matson DW, Philpotts JA, Roush TL (1984) Raman study of the structure of glasses along the join SiO_2-GeO_2. *J. Non-Cryst. Solids.,* 68, 99-114

Shimada Y, Okuno M, Syono Y, Kikuchi M, Fukuoka K, Ishizawa N (2002) An X-ray diffraction study of shock-wave-densified SiO_2 glasses. *Phys. Chem. Minerals.,* 29, 233-239

Shimoda K, Okuno M, Syono Y, Kikuchi M, Fukuoka K, Koyano M, Katayama S (2004) Structural evolutions of an obsidian and its fused glass by shock-wave compression. *Phys. Chem. Minerals.,* 31, 1-11

Smallwood AG, Thomas PS, Ray AS (1997) Characterisation of sedimentary opals by Fourier transform Raman spectroscopy. *Spectrochim. Acta. A,* 53, 2341-2345

Sosman RB (1955) New and old phase diagram of silica. *Trans. Br. Ceram. Soc.,* 54, 655-670

Stöber W, Fink A, Bohn E (1968) Controlled growth of monodisperse silica spheres in the micron size range. *J. Colloid. Inter. Sci.,* 26, 62-69

Stöffler D (1994) Shock metamorphism of quartz in nature and experiment: I. Basic observation and theory. *Meteoritics.,* 29, 55-181

Stolen RH, Walrafen GE (1976) Water and its relation to broken bond defects in fused silica. *J. Chem. Phys.,* 64, 2623-2631

Stone J, Walrafen GE (1982) Overtone vibrations of OH groups in fused optical fibers. *J. Chem. Phys.,* 76, 1712-1722

Takabatake K (2000) Vitrification of albite crystal and structure change of albite glass by shock-wave compression. Master thesis of Kanazawa Univ.

Tan CZ, Arndt J (1999) X-ray diffraction of densified silica glass. *J. Non-Cryst. Soilds.,* 249, 47-50

Tattevin H, Syono Y, Kikuchi M, Kusuba K, Velde B (1990) Shock deformation of α-quartz: Laboratry experiments and TEM investigations. *Eur. J. Mineral.,* 2, 227-234

Wahl FM, Grim RE, Graf B (1961) Phase transformations in silica as examined by

continuous X-ray diffraction. *Am. Mineral.,* 46, 196-208

Walrafen GE, Samanta SR (1978) Infrared absorbance spectra and interactions involving OH groups in fused silica. *J. Chem. Phys.,* 69, 493-495

Walrafen GE, Krishnan PN (1981) Raman spectrum of pressure compacted fused silica. *J. Chem. Phys.,* 74, 5328-5330

Whipple FL (1950) A comet model. I. The acceleration of comet Encke. *Ap. J.,* 111, 375-394

Whipple FL (1951) A comet model. II. Physical relations for comets and meteors. *Ap. J.*, 121, 750-770

Williams Q, Hemley RJ, Kruger MB, Jeanloz R (1993) High-Pressure Infrared Spectra of α-Quartz, Coesite, Stishovite and Silica Glass. *J. Geophys. Res.,* 98, 22157-22170

Xue X, Kanzaki M (2007) High-pressure δ-AlOOH phases and isostructural hydroxides/oxhydroxides: New structural insights from high-resolution ^{1}H and ^{27}Al NMR. *J. Phys. Chem. B*, 111, 13156-13166

Zhang GQ, Xu DP, Song GX, Xue YF, Li L, Wang DY, Su WH (2009) Effect of Si-OH on the transformation of amorphous SiO_2 to coesite. *J. Alloys. Comp.,* 476, L4-L7